NATIONAL AERONAUTICS AND SPACE ADMINISTRATION

Technical Memorandum 33-491

Proceedings of the Fourth Annual Conference on Effects of Lithium Doping on Silicon Solar Cells

Held at the Jet Propulsion Laboratory
Pasadena, California
April 29, 1971

Edited by
P. A. Berman

JET PROPULSION LABORATORY
CALIFORNIA INSTITUTE OF TECHNOLOGY
PASADENA, CALIFORNIA

September 15, 1971

NATIONAL AERONAUTICS AND SPACE ADMINISTRATION

Technical Memorandum 33-491

Proceedings of the Fourth Annual Conference on Effects of Lithium Doping on Silicon Solar Cells

Held at the Jet Propulsion Laboratory
Pasadena, California
April 29, 1971

Edited by
P. A. Berman

JET PROPULSION LABORATORY
CALIFORNIA INSTITUTE OF TECHNOLOGY
PASADENA, CALIFORNIA

September 15, 1971

Prepared Under Contract No. NAS 7-100
National Aeronautics and Space Administration

Page intentionally left blank

PREFACE

The purpose of this conference was to provide a forum for an in-depth review and discussion of the results of investigations being carried out by various organizations under NASA/JPL sponsorship as part of the Solar Cell Research and Development Program. Participating organizations included cell manufacturers and university and industrial research laboratories. Because of the relevance of this program to activities outside JPL, members of the aerospace industry involved in the space effort were invited to attend the conference in addition to representatives of NASA, JPL, and JPL contractor organizations.

LIST OF ATTENDEES

ANSPAUGH, B.
Jet Propulsion Laboratory, Pasadena, Calif.

ARNDT, R.
COMSAT, Washington, D. C.

BRANDHORST, H. W.
Lewis Research Center, Cleveland, Ohio.

BRIGGS, D. C.
Philco Ford Corp., Palo Alto, Calif.

BRIGLIO, A.
Jet Propulsion Laboratory, Pasadena, Calif.

BRUCKER, G.
RCA Astro Electronics Division of RCA, Princeton, N. J.

CARTER, J. R.
TRW Systems, Redondo Beach, Calif.

COHN, E. M.
NASA Headquarters, Washington, D. C.

COLEMAN, W. J.
North American Rockwell, Downey, Calif.

CURTIS, O.
Northrup Corporate Laboratories, Hawthorne, Calif.

DeANGELIS, H.
Air Force Cambridge Research Laboratories, Bedford, Mass.

DOWNING, R. G.
TRW Systems, Redondo Beach, Calif.

DRESSELHAUS, M.
Massachusetts Institute of Technology, Department of Electrical Engineering, Cambridge, Mass.

FAITH, T.
RCA Astro Electronics Division of RCA, Princeton, N. J.

GIVEN, R.
Lockheed Missiles and Space Co., San Jose, Calif.

GOLDSMITH, J.
Jet Propulsion Laboratory, Pasadena, Calif.

HARNE, W. E.
The Boeing Co., Seattle, Wash.

ILES, P. A.
Centralab Semiconductor Division of Globe Union, Inc., El Monte, Calif.

JOHNSON, E. S.
University of Southern California, Los Angeles, Calif.

JOSLYN, D.
Aerospace Corp., Los Angeles, Calif.

KIRKPATRICK, A.
Ion Physics Corp., Burlington, Mass.

KRULL, W.
Lockheed Georgia Co., Marietta, Ga.

LEADON, R. E.
Gulf Radiation Technology Division of Gulf Energy and Environmental Systems Co., San Diego, Calif.

LUFT, W.
TRW Systems, Redondo Beach, Calif.

NABER, J. A.
Gulf Radiation Technology Division of Gulf Energy and Environmental Systems Co., San Diego, Calif.

PATTERSON, R.
Jet Propulsion Laboratory, Pasadena, Calif.

PASSENHEIM, B.
Gulf Radiation Technology Division of Gulf Energy and Environmental Systems Co., San Diego, Calif.

PAYNE, P.
Heliotek Division of Textron, Inc., Sylmar, Calif.

PRICE, W. E.
Jet Propulsion Laboratory, Pasadena, Calif.

RALPH, E. L.
Heliotek Division of Textron, Inc., Sylmar, Calif.

RAUSCHENBACH, H. S.
TRW Systems

REYNARD, D. L.
Philco-Ford Corp., Palo Alto, Calif.

SARGENT, G. A.
University of Kentucky, Department of Metallurgical Engineering and Materials Science, Lexington, Ky.

SPRY, R.
Wright Patterson Air Force Base, Ohio

SROUR, J.
Northrup Corporate Laboratories, Hawthorne, Calif.

STANNARD, J. E.
Naval Research Laboratory, Washington, D. C.

STATLER, B. L.
Naval Research Laboratory, Washington, D. C.

STOFEL, E.
Aerospace Corp., Los Angeles, Calif.

TSANG, J. C.
Massachusetts Institute of Technology, Cambridge, Mass.

WEINGART, J.
Jet Propulsion Laboratory, Pasadena, Calif.

FOREWORD

The results of the investigations carried out during the past year represent the most significant achievements attained thus far with respect to the lithium-doped solar cell program. Lithium-doped solar cells fabricated from oxygen-lean and oxygen-rich silicon have been obtained with average initial efficiencies of 11.9% at air mass zero and 28°C, as compared to state-of-the-art N/P cells fabricated from 10 Ω-cm silicon with average efficiencies of 11.3% under similar conditions. Improvements in cell-processing techniques have made possible the fabrication of large-area lithium-doped cells. Excellent progress has been made in quantitative predictions of post-irradiation lithium-doped cell characteristics as a function of cell design by means of capacitance-voltage measurements, and this information has been used to achieve further improvements in cell design. Specifically, analysis of irradiated lithium-doped cells has shown that the recovery characteristics can be very well predicted by the lithium density gradient near the junction and that very good cell-to-cell reproducibility of lithium density gradient can be obtained with reduced lithium distribution time schedules. Low-flux real-time irradiation tests have shown, for the first time, that lithium-doped solar cells can exhibit power levels higher than those state-of-the-art N/P cells in space environments. This is very encouraging, since the cells studied in these latter experiments were, of necessity, cells fabricated about one year ago. Since that time, significant improvements in lithium-doped solar cell design have been achieved, and it is expected that more recent cells would present an even greater advantage than observed here. Also, tests recently conducted with 28-MeV electron irradiation indicate a very marked advantage of lithium-doped cells over state-of-the-art N/P cells for radiation which results in cluster defects.

The advancements made during this year with respect to lithium-doped cell development have clearly shown the power of the interdisciplinary approach which was adopted throughout the life of the program. Problems such as cell instability, low efficiency, poor process control, unpredictability of recovery characteristics, variations in recovery rate, cell size limitations, etc., that at one time appeared to be all but insoluble, appear to be rapidly falling by the wayside. These problems could not have been solved without the involvement of the multi-expert team represented by the organizations participating at this conference. Each organization isolated the problems with respect to its own area of expertise, and the resultant body of information was coordinated and distributed to the other organizations. It is strongly felt that such an approach is applicable to many other programs (e.g., application of space technology to the economic generation of terrestrial power by means of solar energy conversion) and should prove to be of immense value in the majority of cases.

ACKNOWLEDGMENTS

The conference chairman would like to acknowledge the support of NASA and JPL with respect to the investigations reported here. He would also like to express his particular appreciation to all the organizations and personnel who have diligently and conscientiously performed the work described at this conference, and who have contributed to this program with significant personal involvement.

CONTENTS

N72-10053

SOME MAJOR RESULTS OF THE FOURTH ANNUAL CONFERENCE ON EFFECTS OF LITHIUM DOPING ON SILICON SOLAR CELLS

P. A. Berman
Conference Chairman

I. INTRODUCTION

The conference was held at the Jet Propulsion Laboratory in Pasadena, Calif., on April 29, 1971. Attendees were members of the photovoltaic community interested in the radiation hardening of solar cells and personnel involved in research on lithium-doped silicon cells sponsored by NASA/JPL. A large body of information was presented, and a summary of all the significant points is not feasible. Some of the points that will be of interest to the majority of readers are summarized.

II. SUMMARY OF RESULTS

Lithium-doped silicon solar cells having dimensions as large as 12 cm^2 are now possible, due to significantly improved boron-diffusion techniques, which stress the cells far less than techniques used previously. A large increase was observed in the short-circuit current measured in tungsten (long wavelength) light for cells that were fabricated using the improved diffusion techniques as compared with previous cells, indicating a preservation of minority carrier diffusion length in the base region of the former cells. Sintering (at about 600°C) of the contacts of lithium-doped cells fabricated from Lopex silicon resulted in large increases in maximum power (of between 1 and 4 mW), mostly due to an open-circuit voltage improvement, over non-sintered cells. Efficiencies as high as 12.8% were observed, with the average efficiency being about 11.9%. The sample is small, but the efficiency is significantly higher than the average efficiency of 10 Ω-cm N/P cells (state-of-the-art) which is about 11.3 to 11.5%.

Measurements of the lithium surface concentration in silicon as a function of lithium diffusion time indicated the occurrence of a peak in surface concentration. The occurrence of lower lithium concentrations for longer diffusion times is indicative of diffusion from a limited source. The peak occurred more rapidly and was of greater magnitude as the diffusion temperature was increased.

The uniformity of solar cells fabricated with the addition of a redistribution cycle was more difficult to control than that of cells fabricated using a single-cycle lithium distribution. Also, longer lithium distribution cycles gave rise to larger cell-to-cell variations in lithium concentration gradient and open-circuit voltage.

The use of ion implantation has provided additional flexibility in lithium solar cell design. Ion implantation was used to implant an N^+ region at the back face of the cell and to implant lithium through the N^+ layer. In this way, the amount of lithium introduced prior to lithium distribution (which is still accomplished by diffusion at 300 to 400°C) can be precisely controlled, and the ratio of electrically active lithium after distribution to the amount of lithium initially present in the cell can be determined. The presence of the N^+ region at the back surface was found to inhibit loss of lithium after lithium distribution by a factor of ten over the loss observed in samples without the N^+ region. Very good post-irradiation recovery has been obtained on ion-implanted cells fabricated in this manner, with recovered powers being greater than that of state-of-the-art N/P cells.

In highly lithium-doped float zone (low oxygen content) silicon the carrier removal reached equilibrium shortly after irradiation. In lightly lithium-doped float-zone silicon and highly lithium-doped crucible silicon, carrier removal reached equilibrium approximately one to two years after irradiation. A close pair vacancy-interstitial model applies quite well to lithium-doped crucible-grown silicon, but not as well for lithium-doped float-zone silicon.

For a given fluence, the lithium-doped solar cell short-circuit current appears to be a linear function of the logarithm of the lithium density gradient as measured with the capacitance-voltage technique and a linear function of the logarithm of minority carrier diffusion length.

The damage coefficient of lithium-containing cells immediately after irradiation appears to be a function of the fluence and exhibits a square root dependence on the lithium density gradient. Time to half-recovery is linearly dependent on the logarithm of the lithium density gradient as is the dependence of the recovered open-circuit voltage.

Long lithium-diffusion times resulted in large variations in lithium density gradients (differences as large as a factor of 24) while shorter diffusion times yielded very small variations of lithium

density gradients (within a factor of 2). This indicates that one can tightly control post-irradiation recovery rates by proper control of the lithium distribution schedules.

Investigation of cells with various amounts of lithium coverage on the back prior to distribution (50, 80, and 100% coverage) indicated that the recovery of the 80 and 100% coverage cells were similar to one another while the 50%-coverage cells recovered more slowly and less completely. The rate and extent of recovery was directly related to the lithium concentration near the junction. These results indicate that careful control of the area coverage of the lithium prior to lithium introduction is not critical to the cell recovery characteristics.

It was postulated that the fact that the time to half-recovery appears to increase with increasing irradiation fluence might actually be a result of annealing that occurs during the irradiation (higher fluences generally require longer irradiation times), so that the damage measured after bombardment does not represent the actual total damage, and the apparent half-recovery time is longer than the actual half-recovery time. If the time to half-recovery does not increase with increasing fluence, this would simplify the description of the annealing kinetics.

It was observed that carrier removal rates increase with increasing lithium concentration and hence with distance from the P-N junction. That is, the amount of lithium which reacts with a radiation-induced defect during the recovery stage is proportional to the amount of lithium available for interaction with the defect, indicating that the defect can nucleate precipitation of large numbers of lithium atoms if they are present in the vicinity of the defect. For example, the change in lithium concentration at 5 μm from the junction was observed to be five times as great as the A-center (oxygen-vacancy defect) concentration at that depth. Furthermore, in lithium-containing cells fabricated from float-zone silicon, the carrier removal rate was found to decrease with increasing fluence, again indicating a defect-lithium interaction dependent upon the number of available lithium atoms per defect. This indicates that the model used in the past, which simply assumed that two lithium donors were removed for each annealed damage center, must be modified.

Annealing of 90% of the radiation damage was observed in lithium-doped silicon after isothermal and isochronal anneals of samples irradiated with fission neutrons and with high energy (30 MeV) electrons. Samples with high lithium concentration exhibited degradation coefficients immediately after electron irradiation which were greater than those of samples that did not contain lithium. The post-irradiation characteristics lend themselves to interpretation by a two-defect model, one defect controlling the minority carrier lifetime τ at low temperatures and the other controlling τ at higher temperatures. The annealing appears to be a first-order process, characterized by an activation energy and an atomic frequency factor.

From electron spin resonance measurements it was inferred that lithium inhibited the production of oxygen-vacancy radiation defect centers and that the centers annealed at 350 K rather than in the 600 K range observed for non-lithium-treated samples. In contrast, the production of phosphorus-vacancy radiation defects did not appear to be influenced by the presence of lithium. The radiation-induced divacancy, as observed by means of infrared spectroscopy, appeared to have an introduction rate in lithium-doped silicon similar to that observed in non-lithium-doped silicon, but in the lithium-doped silicon annealing of the divacancy proceeded much more rapidly. As the absorption band associated with the divacancy decreased through annealing, two new absorption bands appeared, indicating the formation of a new defect which is probably influenced by the association with lithium.

Hall measurements performed at 4 K allowed separate determination of donor and acceptor concentration in silicon. Electron-irradiated lithium-doped silicon exhibited a defect level located 0.14 eV below the conduction band. It is postulated that this defect may be a vacancy-oxygen defect (A-center) associated with another impurity such as an additional oxygen or carbon atom. It was inferred that lithium interacted much more strongly with the oxygen-vacancy defect than with the phosphorus-vacancy defect and that as many as four lithium atoms may be involved in the annealing of radiation-induced defect centers. Annealing was observed to result in the disappearance of acceptor levels in irradiated lithium-containing samples but not in irradiated samples containing phosphorus but no lithium. Also, the carrier concentration of irradiated lithium-containing samples was observed to decrease at room temperature while the carrier concentration of irradiated non-lithium-containing samples remained constant.

Electron microscopy of neutron irradiated lithium and non-lithium-containing solar cells was performed using a surface replication technique. The density and diameters of the radiation-induced disordered regions were obtained as a function of lithium doping and neutron fluence. It was found that the number of disordered regions observed by this technique increased with increasing fluence and increasing lithium density. The diameter of the disordered regions, however, were found to decrease with increasing fluence and with increasing lithium concentration. At a specific fluence, the total volume of the disordered regions appears to be relatively constant with respect to lithium density, increasing lithium densities resulting in more numerous, but smaller-diameter, disordered regions. The defect density of the lithium-containing cells did not appear to change with annealing temperatures up to 1200°C, while the defect density of the non-lithium-containing samples did change. Electron transmission microscopy of the lithium- and non-lithium-containing cells indicated evidence of precipitate formation in both cell types.

Low flux irradiations obtained using a Co^{60} source indicated a 4% superiority in maximum power of lithium-doped cells fabricated from crucible-grown silicon over N/P (non-lithium containing) 10 Ω-cm silicon cells after a cumulative dose of approximately 5×10^{14} equivalent 1-MeV electrons/cm^2 (100 days exposure) at a temperature of 60°C. Similar lithium-containing

cells irradiated at a temperature of 30°C were inferior to N/P cells at this fluence level. Similar groups of cells were also irradiated by means of a Van de Graaf generator to a fluence of 5×10^{14} 1-MeV electrons/cm^2 and allowed to anneal at 30 and 60°C. The same percentage superiority of the lithium-containing cells over the N/P cells was observed for the 60°C anneal as was observed for the cells exposed to the Co^{60} irradiation at this temperature. This indicates that the use of accelerated irradiation tests are valid for determining the relative radiation resistance of lithium-doped cells with respect to N/P cells.

Two low flux experiments have also been carried out using a Sr^{90} source for a time period of about six months (total fluence equivalent to about three years in synchronous orbit). The lithium-containing cells in these experiments represented the best cells obtainable about one year ago, but not the best cells presently being fabricated. For the cells maintained at temperatures of 50°C and above, lithium-doped cells fabricated from crucible-grown silicon exhibited maximum powers which were relatively constant over the life of the test and about 8% higher than non-lithium-containing N/P cells. In one of the experiments the cells were post-irradiation annealed at the test temperature with no significant changes in power output being observed. This indicated that the cells were annealed as well as they could be during the test; that is, maximum annealing of radiation-induced damage was occurring during the test.

There appeared to be no additional radiation protection afforded by 1-mil integral shields for the low flux environment studied. One of the experiments indicated that the maximum power of unilluminated cells was consistently about 4% higher than that of illuminated cells, while the other experiment was inconclusive with respect to this phenomenon. If the results of the former experiment are accurate, this would indicate that the results of most solar cell irradiation tests (i.e., not only lithium-doped cell tests), which are performed with the cells in an unloaded unilluminated condition, may significantly underestimate the amount of damage to the solar cell maximum power.

Lithium-doped solar cells fabricated from low oxygen content silicon appear to have optimum annealing characteristics at a temperature of about 20°C, while lithium-doped solar cells fabricated from crucible-grown (oxygen-rich) silicon appear to be superior for temperatures of 50°C and above, for the conditions studied in these low flux experiments.

Irradiation of lithium-doped cells fabricated from crucible-grown silicon by 28-MeV electrons to fluences of 5×10^{14} and 5×10^{15} e/cm^2 exhibited recovered short-circuit currents 100% higher than similarly irradiated state-of-the-art N/P cells. This is consistent with previous investigations using neutron irradiation, since in both cases considerable cluster damage occurs. All results obtained thus far strongly indicate that lithium is extremely efficient in reducing the detrimental effects of radiation-induced defect clusters on the cell electrical characteristics. This means that for environments consisting of high energy electrons, protons, or neutrons, lithium-doped solar cells should be vastly superior to state-of-the-art N/P solar cells.

N72-10054

LITHIUM-DOPED SOLAR CELLS FOR SPACE USE

P. Payne and E. L. Ralph
Heliotek Division of Textron, Inc.
Sylmar, Calif.

I. INTRODUCTION

This paper summarizes the lithium-doped solar cell research and development carried out by Heliotek over the past nine months under JPL Contract 952547, Part II. The work performed can be separated into two basic areas: (1) experimental work aimed at the improvement of cell processes and efficiencies, and (2) demonstration of these improvements by the fabrication and statistical analyses of quantities of various lithium-doped solar cell types.

Over the past several years the lithium-doped solar cell has progressed from a laboratory curiosity, because of its unusual radiation damage recovery characteristics, to a high-efficiency radiation-resistant solar cell. Although significant improvements are still being made and a better understanding of the device has been achieved, it is a good time to stop and evaluate the state-of-the-art. Some important factors are:

(1) Lithium-doped solar cells have been made that have exhibited higher power outputs than conventional N/P solar cells after irradiation to a fluence of $>10^{15}$ 1-MeV electrons per cm^2.

(2) Lithium-doped cells have recently been made with very high efficiencies that are substantially higher than N/P cells.

(3) The size of lithium-doped cells have been increased from 1 × 2 cm to 2 × 2 cm and even 2 × 6 cm as the result of the elimination of the boron diffusion stresses.

These factors indicate that the lithium-doped solar cell basically meets or exceeds the electrical and radiation resistance characteristics of conventional N/P solar cells and improvements with lithium cells are still being made. The logical step to be made next is the pilot production of these cells, so that questions of cost, reproducibility, reliability, and space worthiness can be answered.

This paper summarizes the work that has been done in the past nine months in respect to lithium cell power output, cell thickness, large area cells, integrity of cell contacts and types of experimental cells prepared for radiation tests.

II. SUMMARY OF PREVIOUS DEVELOPMENT EFFORTS

The lithium-doped P/N solar cell has gone through distinct development stages over the past four years, with each stage showing a definite improvement in initial and post-irradiation recovered efficiencies.

During the initial work (1966 to 1967) float-zone silicon was used. Lithium diffusion times ranged from 5 to 120 min, and diffusion temperatures ranged from 350 to 500°C. The concentration gradients in the silicon slice were very steep, causing lithium cell instability, as exhibited by shelf-life degradation and redegradation after post-irradiation recovery. In order to reduce this gradient, redistribution cycles (removal of the excess lithium from the cell surface and further heating of the cell to move the lithium deeper into the slice) ranging from 30 to 120 min were used. Redistribution cycles produced higher output cells

with little change in the recovery characteristics. Table 1 shows typical air mass zero (AMO) electrical output values for cells diffused 5 and 90 min and the change in output after 60- and 120-min redistributions.

Discovery in 1967 of the recovery capabilities of lithium-doped solar cells fabricated from crucible grown (C. G.) silicon led to extensive investigation in this area. The higher oxygen concentration C. G. lithium cells exhibited retarded room temperature post-irradiation recovery; however, recovery rates equivalent to those obtained with low oxygen concentration lithium cells were observed when the cell temperature was raised to 60 or 100°C. Cell stability, both shelf-life and after radiation recovery, which was poor for some float-zone lithium cells, was not a problem with C. G. lithium-doped solar cells. In June 1969 the output of C. G. lithium cells was typically about 2 mW higher (28. 3 versus 26. 5 mW) than similarly doped float-zone lithium cells.

The next stage of development was the investigation of lower lithium diffusion temperatures. Eight-hour diffusions at 325°C were performed and typical C. G. lithium cell efficiencies were approximately 2 mW higher (30. 0 versus 28. 3 mW) than C. G. lithium cells that were diffused 90 min and redistributed 60 min at 425°C. The outputs of these cells after being irradiated with 1-MeV electrons to a level of 3×10^{15} e/cm^2 were 11 to 20% higher than the 19. 5 mW average output of 10 Ω-cm N/P cells.

These improvements in lithium cell characteristics were made independently of other processes in the fabrication procedure. They were primarily due to changes in lithium diffusion parameters. In order to further improve cell output, develop procedures which could be used in production and show capability of meeting basic requirements for space quality cells, investigation in areas such as the boron diffusion, method of lithium application, and contact quality has been done.

III. BORON DIFFUSION INVESTIGATION

The objective of the boron diffusion investigation has been to develop a boron diffusion process which could be used to diffuse large quantities (≥100 blanks per diffusion) of stress-free high-efficiency cells. BCl_3 has been the diffusion source most commonly used in fabricating lithium-doped solar cells. This diffusion source was optimized for fabrication of P/N cells (432-μm thick 1 × 2 cm C. G. silicon blanks) early in the 1960's. This process had a very serious limitation in that it could not be used for fabricating thin cells or cells of a 2 × 2 cm size or larger without a significant amount of bowing due to stresses introduced during the diffusion. Therefore, two methods for reducing the stresses generated during boron diffusion were investigated: (1) a modification of the standard BCl_3 diffusion, involving reduction of the boron deposition time, and (2) use of BCl_3 with O_2.

The BCl_3 diffusion, as it had been used over the years, consisted of an 8-min warmup time, an 8-min boron deposition time and a 10-min diffusion time. During the boron deposition the BCl_3 reacts with the silicon; the silicon is etched and a heavy deposit of boron silicides (Ref. 1) is left on the cell surface. This etch reaction and buildup of boron silicides had previously been shown to be influenced by cell position on the boat during diffusion, with the cells first exposed to the BCl_3 flow showing the greatest amount of silicon etched, the highest frequency of bowing, and the lowest output. In an experiment to determine whether the stresses could be reduced by reduction of the boron deposition time, the boron deposition time was varied from 8 min down to 2 min. Both lapped and etched blanks were included in the experiment. It was found that the etched blanks (350 μm thick) were more susceptible to bowing than the lapped blanks (also 350 μm thick), i. e., etched cells (1 × 2 cm, 350 μm thick) were bowed after using an 8-min boron deposition time, whereas lapped cells were not. Reduction of the boron deposition time to 2 to 5 min reduced this heavy boron layer and produced unbowed cells. By using a 2-min boron deposition time 150 μm thick 2 × 6 cm blanks were then successfully diffused with no bowing. Typically, 8-min diffusions have produced bowed 2 × 2 and 2 × 6 cm cells (250 μm thick) with the radius of curvature being as small as 8. 5 cm. The absence of bowing of the large area cells achieved with a 2-min boron deposition time indicated that the stresses were reduced considerably.

The other process modification investigated for reduced stresses was BCl_3 with O_2. Just as with the previously described diffusion, an 8-min warmup time was used. The O_2 was introduced into the BCl_3 gas just before the gas flow entered the diffusion tube. The BCl_3 reacted with the O_2 to produce B_2O_3, which deposited on the cells as a glass layer. This glass layer and the subsequent diffusion did not bow the cells.

Since low-stress cells were produced with both processes discussed above, the two processes were compared to determine which resulted in the best cell electrical output. Two groups of 100 cells were fabricated using the two different processes. The silicon blanks used were 300 to 380 μm thick with a resistivity of 0. 2 to 1. 2 Ω-cm. These were P/N cells with no lithium present. Etched rather than lapped blanks were used since, unlike the standard BCl_3 diffusion, neither of these diffusion processes etch sufficient silicon to remove the crystal surface damage present on a lapped blank. As shown in Fig. 1, the AMO output of cells diffused in BCl_3 (no O_2) with a 2-min deposition time, averages 3 to 4 mW higher than the output of the cells diffused in BCl_3 with O_2. The lower output of the cells diffused with O_2 was primarily due to lower open-circuit voltage and higher series resistance. The average open-circuit voltage of the cells diffused with O_2 was 590 mV, whereas the open-circuit voltage of cells diffused without O_2 was 615 mV. The series resistance of cells from each group was measured. The series resistance of the cells diffused with O_2 was typically around 0. 8 Ω, whereas for the cells diffused with no O_2 the series resistance was around 0. 3 Ω. Table 2 summarizes the electrical data on these two groups of cells.

At the present time, although neither of these two diffusions discussed can be used for diffusion of one hundred cells or more per diffusion, the BCl_3 diffusion with a short deposition time and without O_2 produces the best combination of low stress and high efficiency.

IV. EFFECT OF BORON DIFFUSION PARAMETERS ON IMPROVEMENTS IN LITHIUM CELL OUTPUT

Once reduced stresses were obtained on P/N cells by reducing the boron deposition time, the effects of this process change on lithium cell output were investigated. Experimental lithium diffusions were performed using 20 Ω-cm Lopex silicon material with both 2- and 8-min boron deposition times. Both groups were placed in the same lithium diffusion. The electrical characteristics of these cells are summarized in Table 3. The short-circuit current of the lithium cells subjected to the 2-min boron deposition averaged 11 mA higher when measured in a 100 mW/cm^2 tungsten light source and 6 mA higher when measured in a solar simulator (AMO) than lithium cells subjected to an 8-min boron deposition time. Figures 2 and 3 show the short-circuit current distribution obtained in the two light sources for the two groups of cells (20 cells per group). These distributions show that the 2-min boron deposition results not only in higher, but more uniform, short-circuit currents.

In addition to the higher short-circuit currents obtained for lithium cells subjected to a 2-min boron diffusion, open-circuit voltages (measured at 25°C) as high as 615 mV were obtained; the highest open-circuit voltage observed for cells diffused with an 8-min boron deposition was 595 mV. The higher short-circuit currents and open-circuit voltages led to Lopex lithium cell AMO outputs ranging from 27.6 to 31.7 mW, rather than 23.6 to 28.8 mW as was obtained when an 8-min boron deposition was used.

Sintering of the contacted cell was investigated to determine its effect upon the curve factor, which for some cells was below 0.70. Sintering consisted of a heat treatment at 605°C for 6 min in an H_2 atmosphere. In most cases the sintering improved the curve factor slightly; in addition the AMO short-circuit current of lithium cells subjected to a 2-min boron deposition time increased 3 to 5 mA with sintering. Typically improvements of 10 to 25 mV in open-circuit voltage were also observed. These improvements in curve factor, open-circuit voltage, and short-circuit current resulted in AMO outputs 1 to 4 mW higher than the unsintered cell output. Figure 4 shows I-V curves of a typical cell before and after sintering. The open-circuit voltage increased by 25 mW (600 to 625 mV); the short-circuit current increased by 3 mA (71.5 to 74.5 mA); the curve factor increased from 0.706 to 0.721; and the output increased by 3.3 mW (30.3 to 33.6 mW).

In fabricating Lopex lithium cells for Lot 11 the following lithium diffusion schedules were used: (1) 3 h at 340°C, (2) 7 h at 340°C, (3) 3 h at 360°C, and (4) 7 h at 360°C. Figure 5 shows the distributions in maximum power (after sintering) for the different groups of Lopex lithium cells. The various lithium diffusion parameters produced similar AMO outputs with the outputs for all the groups ranging from 29 to 34 mW. This is equivalent to an AMO efficiency range of 10.9 to 12.8%. The median efficiency is 11.9%. These efficiencies are the highest obtained on lithium cells thus far and are comparable to high-quality conventional N/P cells.

In Fig. 6 the Lopex cells which make up each group in Fig. 5 are treated as a single group and the AMO output is compared to a typical AMO output distribution of conventional 10 Ω-cm N/P cells. The lithium cell output is 3 to 10% higher than the N/P cell output. Even if, for some reason, the sintering step is eliminated from the process, the lithium cell outputs are in the same range as the 10 Ω-cm N/P cells. Figure 7 compares I-V characteristic curves of a typical 10 Ω-cm N/P cell, and a typical lithium cell from this group of 105 lithium cells. These curves show that the high lithium-doped cell output is due to short-circuit currents as high as 10 Ω-cm N/P cell currents and higher open-circuit voltages.

Not only has the BCl_3 diffusion with a 2-min boron deposition resulted in improved lithium cell output, but it has also made it possible to fabricate 2 × 2 and 2 × 6 cm lithium cells. Figure 8 shows various sized lithium cells which have been fabricated. Sample cells, 2 × 2 cm and 2 × 6 cm, which were fabricated from 20 Ω-cm crucible grown silicon and lithium diffused 8 h at 325°C exhibited efficiencies ranging from 10.3 to 11.3%.

V. CONTACT QUALITY

In order to evaluate Ti-Ag contact integrity, lithium-doped P/N cells were subjected to humidity and peel testing.

The humidity test consisted of exposing lithium cells with soldered contacts to 30 days of 90% relative humidity at 45°C. The cells were measured at 25°C in 100 mW/cm^2 tungsten light source before and after thirty days of humidity exposure. The cells exhibited 2.5 to 3.5% short-circuit current degradation, 0 to 2% current degradation at 450 mV, and no open-circuit voltage degradation. Peel tests were performed on these same cells after humidity exposure. The test consisted of soldering wires to both front and back contacts and pulling at a 90-deg angle to the cell surface until contact failure. The ten samples all exhibited peel strengths of 500 to 1000 g for both front and back contacts.

A tape peel test is also used to test contact integrity on unsoldered cells. Scotch brand adhesive no. 810 is applied to both front and back surfaces of the cells. If the contacts are weak, they will peel off with the tape. This test is used on all lithium cells fabricated and the failure level is less than 5%.

VI. CONCLUSIONS

Lithium-doped P/N solar cells meet the basic requirements of solar cells for space use. The efficiencies of the Lopex lithium cells which range from 10.5 to 12.8% are equal to or better than C.G. lithium cell and 10 Ω-cm N/P cell efficiencies. Reduction in the stresses introduced during boron diffusion has eliminated cell size restrictions and both 2 × 2 and 2 × 6 cm lithium-doped cells have been fabricated. The Ti-Ag contacts which are tested 100% with a tape peel test, and pull tested and humidity tested on a sample basis are comparable to the Ti-Ag contacts on N/P cells.

ACKNOWLEDGEMENT

The authors wish to thank P. Berman of JPL for his technical coordination, and JPL for support of the program under Contract No. 952547, Part II.

References

1. Powell, C. F., Campbell, I. E., and Gonser, B. W., Vapor Plating, p. 107. John Wiley & Sons, New York, 1955.

Table 1. Output of lithium-doped P/N solar cells

Diffusion temperature, °C	Diffusion time, min	Redistribution time, min	P_{max}, mW
425	5	–	25.8 to 27.3
425	5	60	29.2 to 29.4
425	5	120	30.4 to 30.6
425	90	–	25.5 to 27.0
425	90	60	26.7 to 27.6
425	90	120	28.3 to 29.3

Table 2. Electrical characteristics of 1 Ω-cm P/N cells (no lithium)

Description	BCl_3 (no O_2) 2-min deposition range (median)	BCl_3 (with O_2) range (median)
AMO output, mW	28 to 33 (30.5)	25 to 28 (26.9)
V_{oc}, mV	600 to 625 (615)	570 to 600 (590)
Series resistance, Ω	0.2 to 0.5 (0.3)	0.4 to 1.0 (0.8)

Table 3. Electrical characteristics of lithium-doped P/N cells 2-min versus 8-min boron deposition (20 cells per group)

Parameter	Boron deposition range (median)	
	2 min	8 min
I_{sc}, mA[a]	63.5 to 66.0 (65.0)	48.0 to 59.0 (51.0)
I_{sc} (AMO), mA	69.0 to 71.0 (70.4)	60.0 to 66.0 (63.7)
$(V_{oc})^b$, mV	571 to 612 (595)	552 to 595 (578)
Output (AMO), mW	27.6 to 31.7 (29.5)	23.6 to 28.8 (26.5)

[a]Measured in a tungsten light source at an intensity of 100 mW/cm^2.

[b]Measured at 25°C.

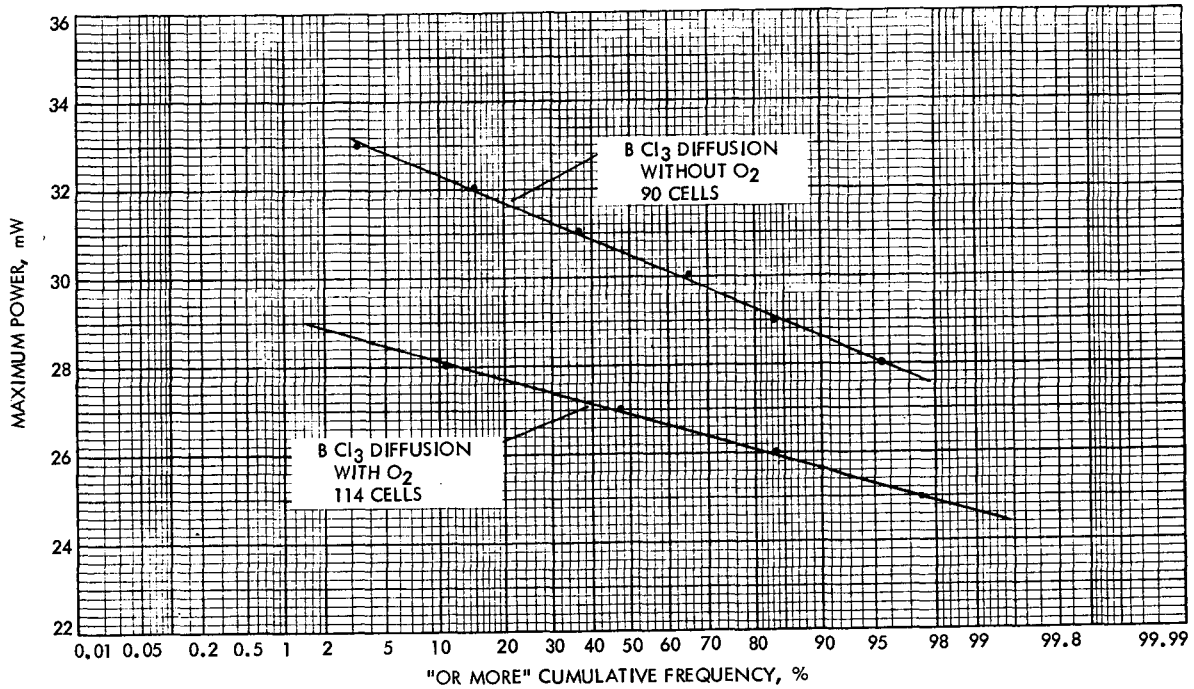

Fig. 1. Maximum power distributions for 1 Ω-cm P/N cells diffused with two different boron diffusion techniques (measured at 25°C in solar simulator at 140 mW/cm^2 intensity)

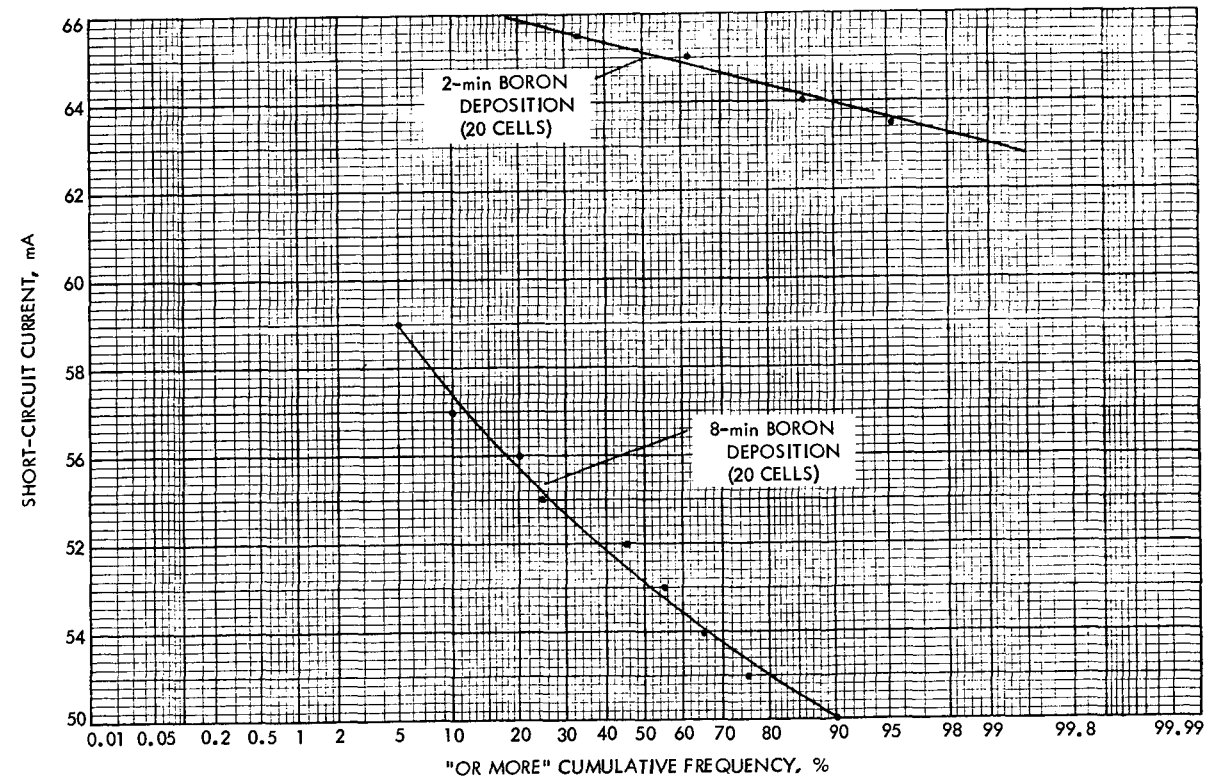

Fig. 2. Comparison of short-circuit current of lithium cells as a function of boron deposition time (measured at 25°C in a tungsten light source at 100 mW/cm^2 intensity)

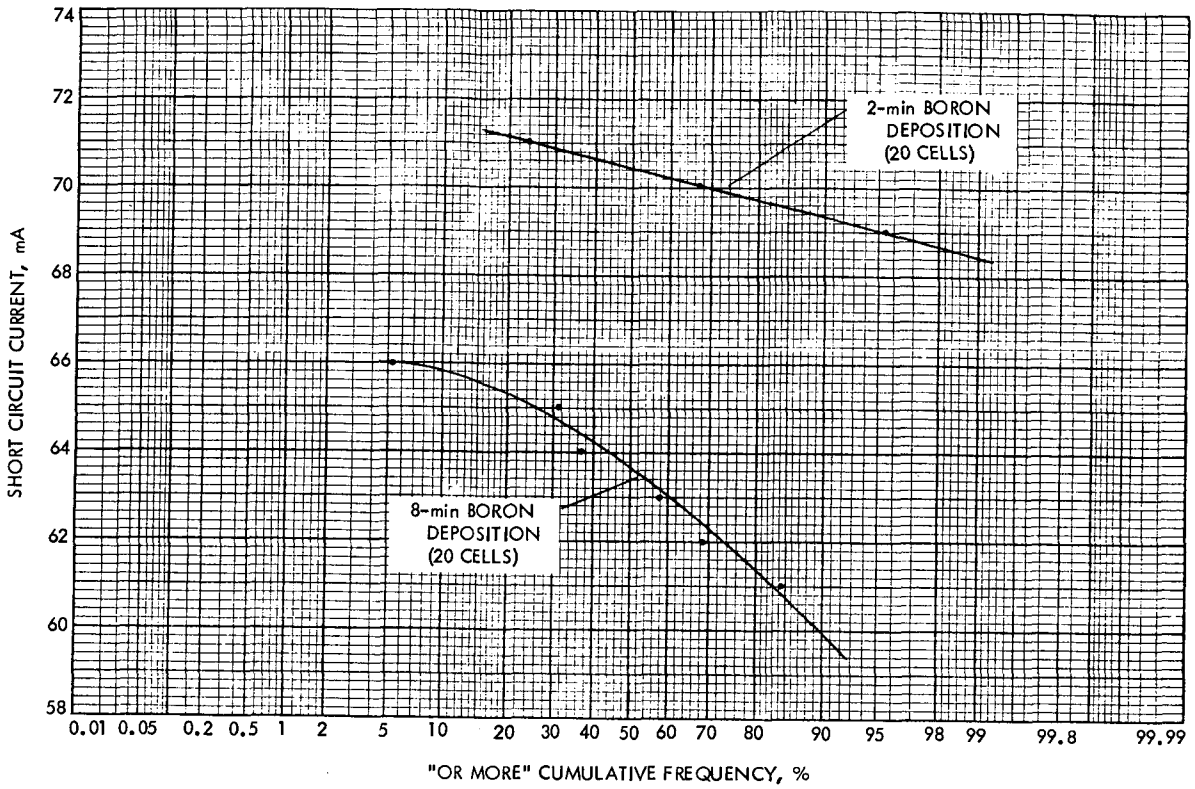

Fig. 3. Comparison of short-circuit current of lithium cells as a function of boron deposition time (measured at 25°C in solar simulator at 140 mW/cm^2 intensity)

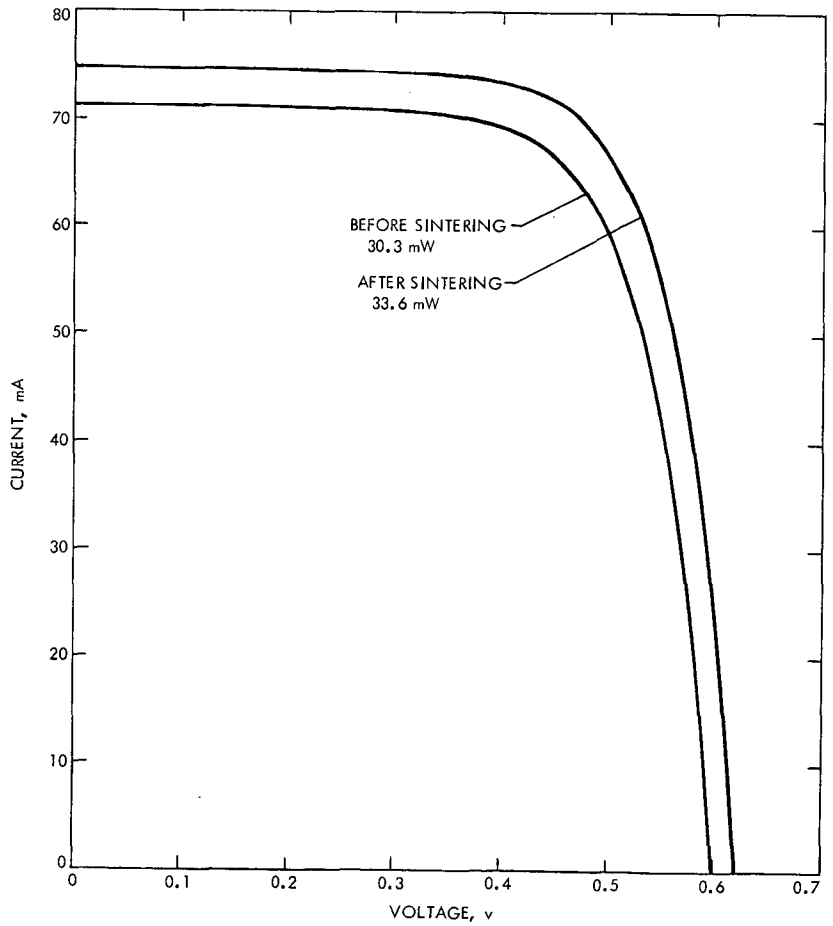

Fig. 4. I-V characteristics curves of a typical lithium cell before and after sintering (measured at 25°C in solar simulator at 140 mW/cm^2 intensity)

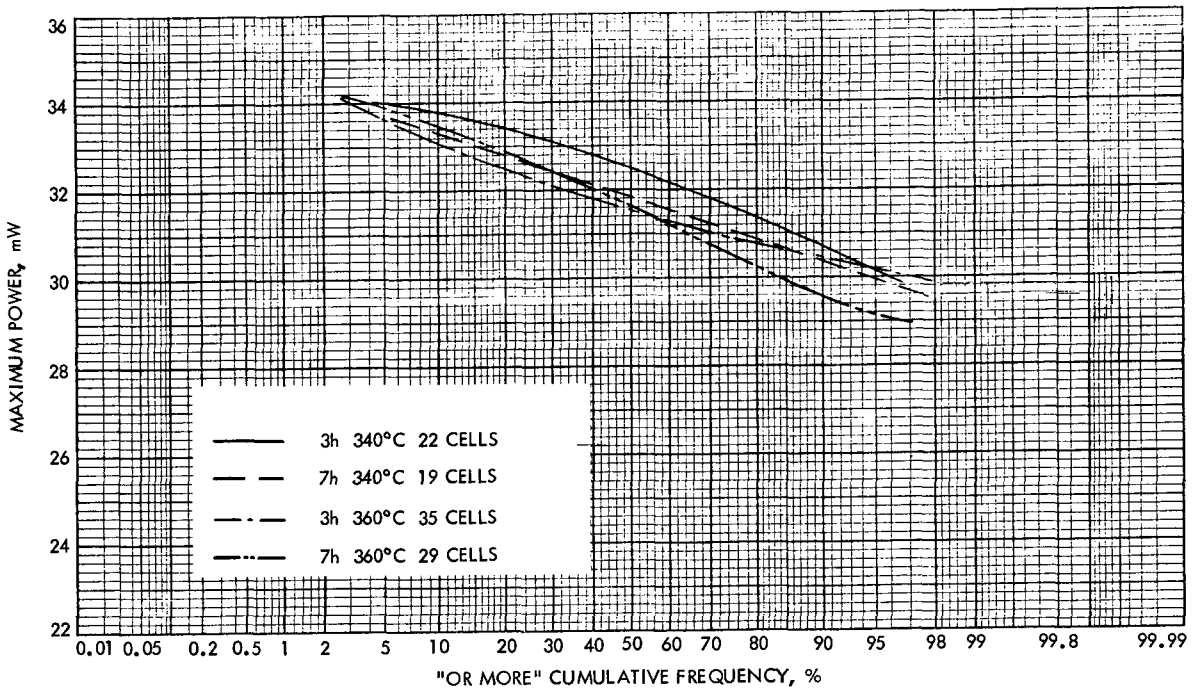

Fig. 5. Maximum power distributions of Lopex lithium fabricated for Lot 11 (measured at 25°C in solar simulator at 140 mW/cm^2 intensity)

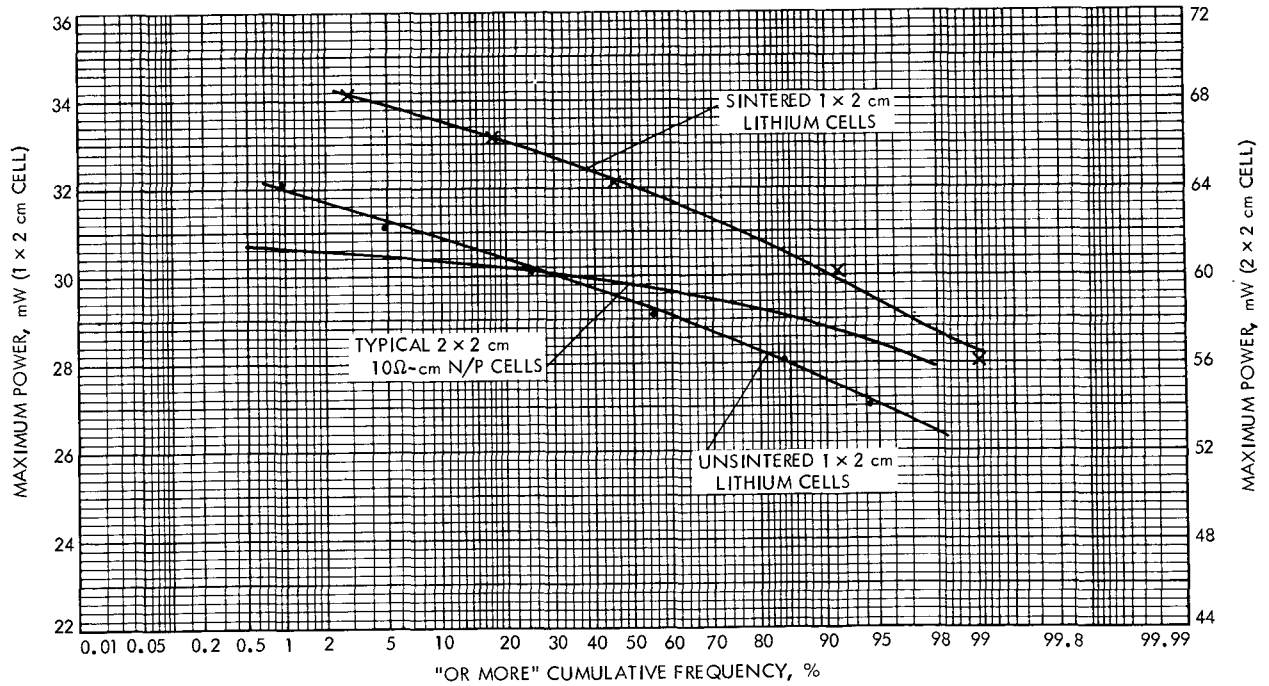

Fig. 6. Comparison of sintered and unsintered Lopex lithium cell output distributions to a typical 10 Ω-cm N/P cell output distribution (measured at 25°C in solar simulator at 140 mW/cm^2 intensity)

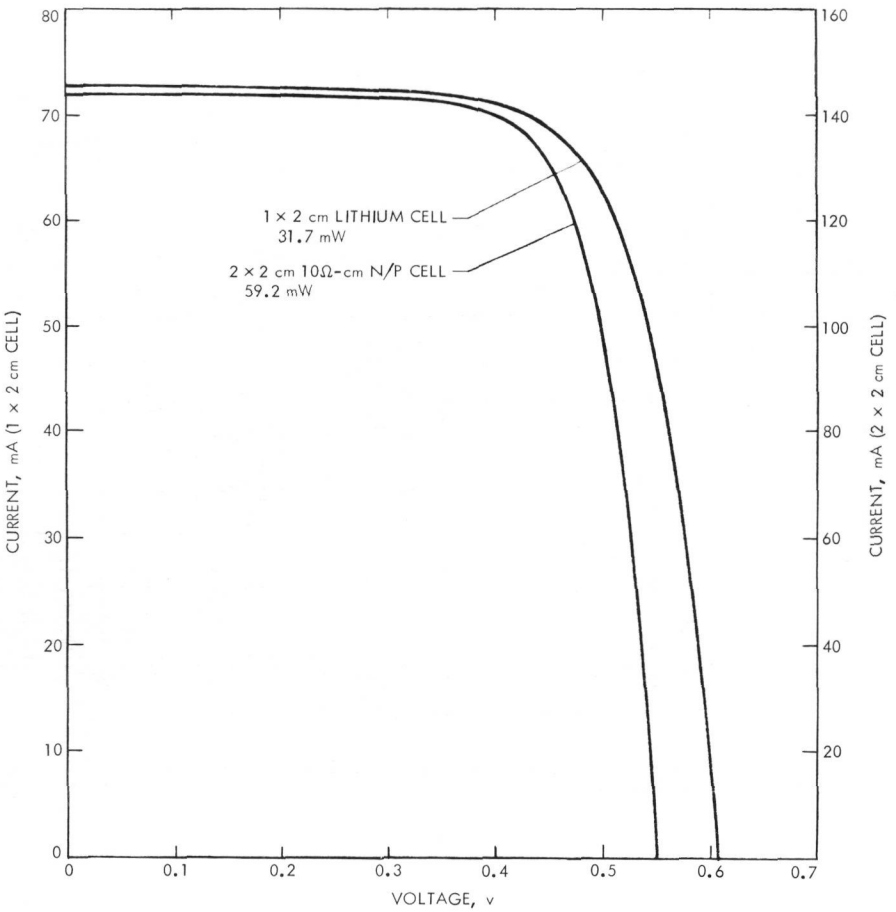

Fig. 7. Typical 10 Ω-cm N/P cell versus typical Lopex lithium cell (measured at 25°C in solar simulator at 140 mW/cm^2 intensity)

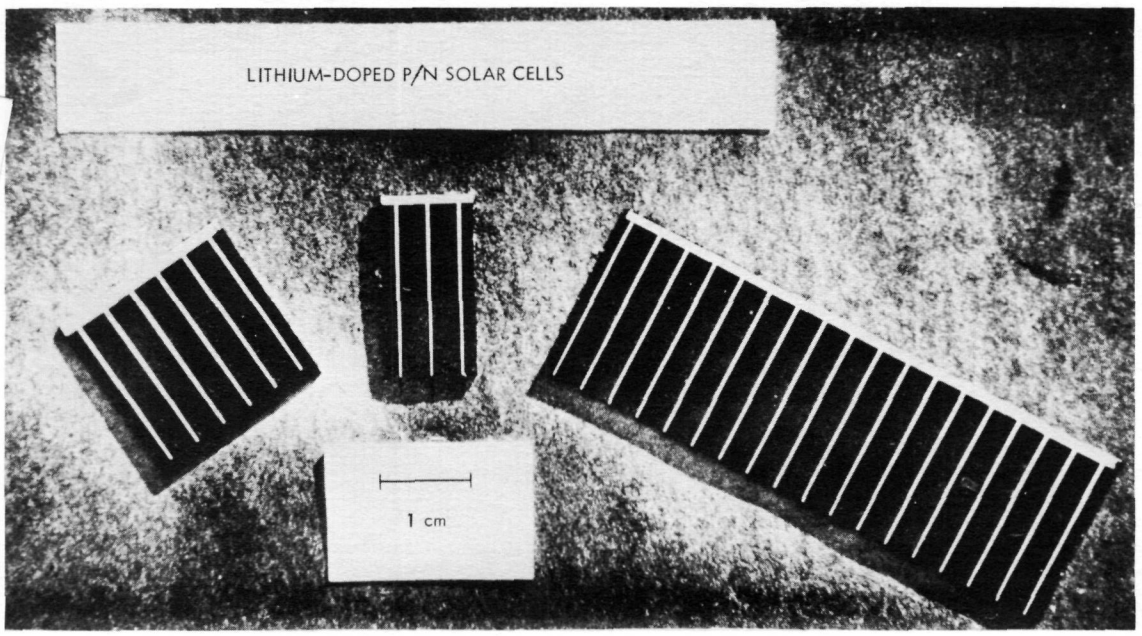

Fig. 8. Various size lithium cells fabricated by Heliotek

N72-10055

DEVELOPMENT AND FABRICATION OF LITHIUM-DOPED SOLAR CELLS

P. A. Iles
Centralab Semiconductor
Globe-Union Inc., El Monte, Calif.

I. INTRODUCTION

This paper outlines the progress made in the past year in the understanding and performance of lithium-doped solar cells.

II. SURVEY OF 1970 PRESENTATION

In the corresponding presentation a year ago (Ref. 1), the following achievements were reported:

(1) Improved boron diffusion methods, especially the use of reduced tack-on boron trichloride cycles, were developed. These methods had led to improved output from cells, especially when oxygen-lean silicon was used. Thus, the full capability of the several forms of silicon crystal growth was available for exploring a wide range of possible recovery times and degrees of cell stability.

(2) The lithium diffusion cycles used were predominantly with a single time cycle and with diffusion temperatures below 425°C, extending as low as 325°C.

(3) The cell output resulting from the combination of these boron and lithium diffusion methods was higher, as shown in Figs. 1 and 2, where the cumulative power distributions for JPL shipments C-11 and C-12 are shown.

(4) The lithium distribution throughout the cells was better understood by combining resistance probing, which gave the donor concentration in the bulk of the cell with capacitance-voltage analysis. This analysis explored the donor concentration very close to the PN junction. The distributions resulting from five different lithium diffusion schedules are given in Fig. 3 (bulk distribution) and Fig. 4 (distribution near the PN junction).

III. SURVEY OF WORK SINCE 1970

The work reported here has extended the results summarized in the foregoing in the following areas:

A. Cell Fabrication Sequence

The main fabrication steps required for cell fabrication (silicon growth, cutting, surface preparation, boron diffusion, lithium diffusion, contact application, coating application) have considerable interactions. Also the order of the fabrication processes can affect cell performance, often to a greater extent than anticipated. To illustrate the effects of the order, if contacts are applied to the front (boron diffused) P^+ surface before lithium diffusion, fairly severe heating cycles can be used to sinter the contacts. However, both these front contacts (and the antireflective coating, if present) can be attacked by lithium during its application and the diffusion cycle unless the lithium source is sufficiently diluted.

On the other hand, if the lithium is diffused first, there is no attack of the front contact and coating, and in addition, the P^+ layer can be

protected from possible interaction with the lithium. However, the range of sintering cycles available is now restricted to those which do not cause appreciable disturbance of the lithium concentration in the cell. Evaluation work reported by RCA (Ref. 2) showed good correlation between cell recovery time after irradiation, and the lithium concentration gradient near the PN junction. Thus, it is particularly important that the sintering cycles do not change this lithium gradient significantly.

Work in the past year has shown that it is possible to apply contacts and coating after lithium diffusion to obtain good electrical output and satisfactory contact adhesion by sintering for short times at temperatures less than the lithium diffusion temperature.

The effect of more severe sinter cycles on the lithium distribution is also being investigated quantitively.

B. Lithium Application

The paint-on lithium method provided well-controlled groups of cells (e.g., Figs. 1 and 2) despite apparent disadvantages in lack of uniformity. However, for consistency in larger scale fabrication of cells, vacuum evaporation of lithium metal was reevaluated. This reevaluation was prompted by several changes of cell design, all reducing some of the previous difficulties found with lithium evaporation. These favorable design changes included the need for less lithium in the cells than in previous years, and the use of lower lithium diffusion temperatures. Also the altered sequence described in the foregoing Subsection A, with contacts and coating applied last, allowed protection of the front cell surface during the lithium diffusion. Many of the cell groups prepared using lithium evaporation have shown satisfactory close distribution of cell parameters and lithium concentrations.

Some of the evaporated lithium groups had wide spread in all parameters. Systematic tests showed where the evaporation method was technique-dependent, and allowed greater control to be imposed. In analysis of these wide-range groups, the methods developed to test lithium distribution proved to be effective over the whole range.

C. Lithium Diffusion Cycles

This year's work has concentrated on the range of temperatures from 375 down to 325°C, with various times from 2 up to 8 h at these temperatures.

Two-stage diffusion cycles, e.g., those combining a tack-on followed by a redistribution cycle, are now considered to be inherently more difficult to control. First, the lithium concentration must be controlled on application; later the amount of the initial source left after tack-on must also be closely controlled. Also, these two-stage cycles often involve longer times at a given temperature than a single cycle, with more chance of variations occurring. At the lower lithium levels now being used, it is possible for the wide spread in lithium characteristics during the two cycles to be masked by the general improvement in cell characteristics. In other words, the cell performance before irradiation may be relatively insensitive to the differences in lithium distribution. In addition, tests using thin slices (approximately 7 mils) showed that the redistribution cycle could lead to severe cell degradation as a result of excess lithium present in the PN junction depletion region, although the average lithium level was low throughout the N region.

D. Lithium Distribution

More information and insight has been added to the way in which the lithium is distributed and the resultant effects on cell properties.

1. Surface concentration (C_s). The buildup of the lithium concentration at the back surface where the lithium was applied, was measured as a function of time at various temperatures.

Figure 5 shows the measured values. Qualitatively, the results are as expected, with a gradual buildup of C_s for longer times, to a maximum value – the rate of increase and the maximum value being higher for higher temperatures.

Two other features were noted. First, the buildup was slower than expected, often requiring around one hour to reach the maximum C_s value. Second, after the saturation region, C_s decreased for longer diffusion times. The points shown on Fig. 5 for times greater than 2 h are those calculated for the C13 cells, discussed in Section E1 following.

2. Concentration near the PN junction. Theoretically, both the lithium concentration and its gradient at any plane in the cell, including the important region near the PN junction at the front of the cell, are both directly proportional to C_s. However, as Figs. 3 and 4 showed the lithium concentration gradient near the junction must be much increased over the theoretical value in order to give concentrations which agree with those calculated from C-V measurements. Gradients up to seven times the theoretical value have been measured. The cause of this increase and the associated lower concentration at the junction are believed to be the perturbation of the theoretical lithium distribution by the electric field in the junction depletion region, which assists the flow of lithium into the P^+ layer.

The changes in lithium distribution were followed by measurements on samples diffused at a given temperature for several different times. Figure 6 shows the results of such a test. The lithium buildup at the PN junction was followed by capacitance measurements. For the three shorter times, no measurable increase at the junction was observed in keeping with the theoretical curves shown. The two longer times are seen to give increases in lithium near the junction. The changes needed in the theoretical distribution are shown by the dotted lines. Good consistency between measured and theoretical lithium distributions was obtained if the dotted line changes occurred over a distance around 20 μm.

3. Changes in concentration with diffusion time. The trend noted in the foregoing Subsection D(1) for the C_s value at a given temperature to decrease steadily with diffusion time gave

increased spread in C_s values. This, in turn, led to increased spread toward lower values of lithium concentrations and gradient near the junction. Although the cause of these changes was first sought in effects near the junction, the C_s measurements showed that the likely cause was the decrease in C_s resulting from depletion of the lithium source.

This depletion can be reduced by controlling the amount of lithium deposited or by modification of the diffusion procedure to minimize losses. In the following Subsection E2 the cell parameters resulting from wide variation in C_s are compared to the tighter grouping obtained when the lithium source depletion was reduced.

E. JPL Shipment C13

This shipment consisted of ten groups, each with thirty cells. The lithium diffusion schedules used were between those used for C11 and they are shown in Table 1. At each diffusion temperature, the lithium was applied to batches of slices and the diffusion was performed on a split boat, allowing withdrawal of the shorter time group first, leaving the longer time group in the furnace. The differences in cell properties for both short and long time diffusions showed more correlation with the separate batches, showing that the main variable was in the paint-on lithium application. The fabrication sequence applied front contacts and coating before lithium diffusion.

In general, the cells showed good control and good I-V performance. The controlling variable was the diffusion time. Figure 7 shows the average values of P_{max}, V_{oc}, I_{sc}, and capacitance for the thirty cell groups in C13. P_{max} varies over about 4%. V_{oc} and I_{sc} show slightly larger ranges (up to 5.5%) but their out-of-phase variations led to reduced spread in P_{max}. Also V_{oc} and capacitance vary in phase, the spread in capacitance being up to 30%.

Figures 8 and 9 show in more detail some of the parameters for the C13 groups. In these figures, average values and the spread in the groups for P_{max}, V_{oc}, capacitance, and donor concentration gradient near the junction are plotted as a function of increasing diffusion time. The P_{max} values are satisfactorily high and tightly grouped. The other parameters all show a trend toward lower values and larger spreads at the longer time. These two figures show that the I-V characteristics can have small spread, but may be associated with larger spread in the lithium concentration or its gradient.

Figure 10 plots the cumulative percentage of P_{max}, averaged for all 300 cells in C13 with the upper and lower thirty cell groups shown also. For comparison, the distribution for C12 is given. This figure shows that the general level of cell output was good.

Figure 11, for ten cells in C13G and C13H shows good correlation between V_{oc} and the lithium concentration and concentration gradient near the junction, calculated from capacitance measurements. For C13G, the shorter time diffusion, the grouping is tighter and both V_{oc} and the lithium parameters are higher. Even for cells with less lithium, the V_{oc} values are generally high, and this figure shows that greater resolution of the underlying correlations is now feasible.

Figure 12 plotted for 100 cells, ten in each C13 group, shows that V_{oc} is approximately proportional to the logarithm of the lithium concentration. The estimated slope of the curve is approximately 0.026 V^{-1}, a value expected if the PN junction is operating at current levels where it approaches diode diffusion theory operation. The total spread in V_{oc} is around 5%, whereas the total spread in concentration is 400%.

Table 2 lists the values of surface concentration calculated for each of the C13 groups. These C_s values were obtained by combining the lithium concentration and concentration gradient near the PN junction (estimated from C-V methods). Assuming the gradient occurred for a distance of 20 μm from the junction, a value of lithium concentration was obtained at this 20-μm plane. Then the theoretical distribution was extrapolated from this plane to the back surface to give the C_s value. The groups in Table 2 are plotted in increasing order of diffusion time, and show the steady fall-off of C_s.

In summary, C13 provided 300 cells of good output, but with sufficient differences between the groups to show that diffusion time was a more important controlling parameter than had been suspected earlier. To reduce the effects of source depletion at the longer times, a later shipment (C15) was planned to include both paint-on and evaporated sources, to check that the source depletion was reduced for the more concentrated source.

1. JPL shipment C14. The intention in C14 was to compare oxygen-rich (C.G.) silicon and oxygen-lean (Lopex) silicon in two of the lower temperature single time cycles. Also lower resistivity Lopex silicon (15 Ω-cm) was used to check if the five-fold increase in background concentration was of advantage for higher fluence irradiations. The fabrication sequence for C14 applied lithium before any contacts or coatings were present. Table 3 gives details of the silicon and lithium cycles used.

Figure 13 gives the average values and the spread of P_{max}, V_{oc} and capacitance for the C14 groups. The general level of P_{max} (and V_{oc}) was good. For a given lithium cycle, the C.G. silicon cells had higher V_{oc} (and I_{sc}) than the Lopex cells. However, this higher V_{oc} was accompanied by the lower capacitance (and thus lower lithium concentration near the junction) usually found for C.G. silicon. This lower capacitance can explain the higher I_{sc} values obtained for C.G. silicon, but does not explain the V_{oc} differences. In this case, the differences in silicon grown by the two methods have more effect on I-V characteristics than the differences obtained in lithium concentration.

2. JPL shipment C15. The purpose of C15 was to compare three different silicon ingots using either paint-on or evaporated lithium sources for each group and a diffusion schedule similar to those used in C13. A schedule of 350°C for 240 min was chosen; and in addition, a group of C.G. cells was fabricated using the evaporated source and 350°C for 480 min to check if the lithium depletion was reduced for the longer diffusion time.

Table 4 shows details of the C15 groups.

Figure 14 plots the average values and the spread for the various C15 groups. Again, the overall level of P_{max} is good and, as seen in C11 and C14, the P_{max} values for C. G. silicon are slightly higher than those for Lopex cells. There is no significant difference in these preirradiation measurements between the medium and high resistivity Lopex groups. Also, as for C14, the lithium concentration near the PN junction, as measured by capacitance, was higher for the Lopex ingots.

The overall spread is not markedly lower for the lithium evaporation groups, possibly because the diffusion time is not long. However, the spread in P_{max} and especially in capacitance for the 8-h diffusion group C15G was much lower than obtained for the longer time C13 groups. This shows that lithium depletion has been minimized by the more concentrated source.

During fabrication of the evaporated lithium groups, some batches showed signs of severe lithium depletion. These signs included both serious reduction in V_{oc} (with accompanying higher I_{sc}) and low capacitance values often near the level found for cells made with no lithium. Resistance probe measurements showed that the lithium concentration was much reduced for these batches. These tests showed that lithium evaporation was technique dependent. Using improved techniques mainly in reducing the interaction of lithium and silicon before the slices were placed in the diffusion furnace, gave increased lithium concentrations with very closely grouped sets of parameters. Figure 15 compares the spread of three cell parameters, V_{oc}, capacitance and P_{max} for three different conditions of lithium application — namely paint-on, lithium evaporation with varying interaction, and well-controlled lithium evaporation. The silicon used for these three tests was the same (Lopex, 75 Ω-cm) as was the lithium diffusion schedule at 350°C for 240 min. The paint-on source again shows tight grouping of P_{max} and V_{oc} with a wider spread in capacitance. The less controlled evaporation group had lower values for P_{max}, V_{oc}, and capacitance with wide spreads. The well-controlled evaporation group had high values with small spread for all parameters.

F. More Complex Structures

The present design of lithium cell with suitably chosen silicon and lithium diffusion conditions can give cells with good performance for many possible missions. Any further complexity added to the cell design must be justified by the more severe conditions imposed by particular missions.

The study of two of the possible complexities needed to maintain cell stability following high fluence irradiation has been continued this year.

1. Use of additional N^+ layer at the back surface. This layer, using donors other than lithium, has been used particularly with oxygen-lean silicon to reduce the back contact resistance. However, as will be noted in the following Subsection G1, present contact resistances are satisfactorily low. More tests are needed to check the threshold fluence at which carrier removal by lithium depletion (occurring during the recovery phase following irradiation) increases the contact resistance appreciably.

2. Use of additional N^+ layer near the front surface. Past results have shown that this layer can increase the stability of the PN junction when lithium carriers are removed following high fluences. Again tests are needed to find the threshold fluence which makes this N^+ layer necessary. The threshold fluence will be higher as the starting donor concentration is increased. Thus comparison of the C15 Lopex groups will be of interest.

The other possible use of the front surface N^+ layer is to control the final distribution of lithium near the PN junction after the lithium diffusion cycle. Tests in progress will show if any advantageous distributions can be obtained.

3. Front surface introduction of lithium. In the past year, tests continued on the possible merits of introducing lithium through the front surface of both P/N and N/P cells. The cells made to date with this method did not show any advantages over the conventional design cells.

G. Other Topics

1. Contacts. For the levels of lithium used in the past year, Ti-Ag contacts have given curve fill factors (CFF) values between 0.70 and 0.76. The sequence used for shipment C13 (front contacts applied before lithium) generally gave CFF around 0.72. The later shipments C14 and C15, where both contacts were applied after lithium diffusion, had CFF around 0.74 with minimum lithium depletion at the back surface, CFF > 0.75 have been obtained. This lessens the need for an extra N^+ layer at the back surface to reduce contact resistance.

Evaluation of various contact sintering cycles is in progress. The cycles will be compared for adhesion of the contacts, the effects on the I-V characteristics of the lithium cells, and the effects on lithium distribution within the cells.

2. Improved antireflective coatings. Improved coatings, using double layers of dielectrics have given slight increase (2%) in the output of lithium cells. The increase was less than that obtained on N/P cells because present lithium cells already have a form of double-layer coating.

3. Maximum output versus lithium concentration. A search was made for the highest P_{max} values obtained for different lithium concentrations near the PN junction. The curve joining the pairs of corresponding points for all the cells measured is given in Fig. 16. For lithium concentrations around 5×10^{14} cm^{-3}, P_{max} = 33 mW is possible for 2-cm^2 cells. 31 mW was obtained for 10^{15} lithium atoms cm^{-3} for C. G. silicon, and for $>10^{15}$ lithium atoms cm^{-3} for Lopex silicon. This figure shows the current feasibility of reaching an optimum trade off between P_{max} and recovery characteristics.

IV. SUMMARY

This year has shown further improvement in the performance and understanding of lithium cells.

They have proved to be superior to N/P cells for several possible missions, particularly when energetic heavy particles (protons or neutons) are a significant fraction of the bombarding particles. The high output and repeatability are obtainable from both oxygen-rich and oxygen-lean silicon. The precision of analysis of cell behavior has been improved.

The analytical techniques developed will allow even further control of the lithium distribution, aiding in closer grouping of both pre- and post-irradiation performance.

The fabrication sequence alterations have led to higher cell output, better appearance, and increased contact strength.

The present methods of fabrication and analysis are well suited to beginning the evaluation of possible pilot-line scaling up.

There is still a need for a figure of merit to allow assessment of the radiation capability of the cells. Before lithium cells are used in large numbers, they must pass a relatively simple test to prove that all the cells on the array will degrade and recover in a similar fashion. At present, the test suggested by RCA (Ref. 2), wherein the lithium concentration gradient is measured, provides the best figure of merit, but further tests are necessary.

As shown in Fig. 15, there is still some room for improvement in the cell output for a given lithium concentration. It will be of interest to see if other papers on irradiation effects substantiate the optimism that the cell fabricators have regarding lithium cells.

REFERENCES

1. Iles, P. A., "Progress Report on Lithium-Diffused Silicon Solar Cells" in Proceedings of the Third Annual Conference on Effects of Lithium Doping on Silicon Solar Cells, Jet Propulsion Laboratory, Pasadena, Calif., April 1970.

2. Faith, T. J., Corra, J. P., and Holmes-Siedle, A. G., "Room Temperature Stability and Performance of Lithium-Containing Solar Cells – An Evaluation," in the Conference Record of the Eighth IEEE Photovoltaic Specialists Conference, Seattle, Wash., August 1970.

ACKNOWLEDGMENT

We would like to thank NASA and JPL for their support under Contract No. 952546 and Mr. Paul Berman for his technical support.

Table 1. Lithium diffusion schedules for C11 and C13

Cell group	Diffusion temperature, °C	Diffusion time, min
C11A	325	480
C11B	325	480
C11C	325	480
C13A	330	180
C13B	330	420
C13C	340	180
C13D	340	420
C13E	350	300
C13F	350	300
C13G	360	180
C13H	360	420
C13I	370	240
C13J	370	360
C11D	375	180

Table 2. Surface concentration of lithium for C13 groups

Cell group	Temperature, °C	Time, min	Calculated C_s, cm^{-3}
C13A	330	180	1.3×10^{17}
C13C	340	180	1.7×10^{17}
C13G	360	180	1.6×10^{17}
C13I	370	240	0.95×10^{17}
C13E	350	300	1.2×10^{17}
C13F	350	300	1.2×10^{17}
C13J	370	360	0.75×10^{17}
C13B	330	420	0.70×10^{17}
C13D	340	420	0.50×10^{17}
C13H	360	420	0.65×10^{17}

Table 3. Details of JPL shipment C14

Cell group	No. of cells	Silicon used	Lithium diffusion
C14A	30	Lopex – 15 Ω-cm	Paint on at 375 °C for 180 min
C14B	30	C. G. – 30 Ω-cm	Paint on at 375 °C for 180 min
C14C	30	Lopex – 15 Ω-cm	Paint on at 350 °C for 300 min
C14D	30	C. G. – 30 Ω-cm	Paint on at 350 °C for 300 min

Table 4. Details of JPL shipment C15

Cell group	No. of cells	Silicon used	Lithium diffusion
C15A	30	Lopex – 15 Ω-cm	Paint on at 350 °C for 240 min
C15B	30	Lopex – 15 Ω-cm	Evaporated at 350 °C for 240 min
C15C	30	Lopex – 75 Ω-cm	Paint on at 350 °C for 240 min
C15D	30	Lopex – 75 Ω-cm	Evaporated at 350 °C for 240 min
C15E	30	C. G. – 30 Ω-cm	Paint on at 350 °C for 240 min
C15F	30	C. G. – 30 Ω-cm	Evaporated at 350 °C for 240 min
C15G	30	C. G. – 30 Ω-cm	Evaporated at 350 °C for 480 min

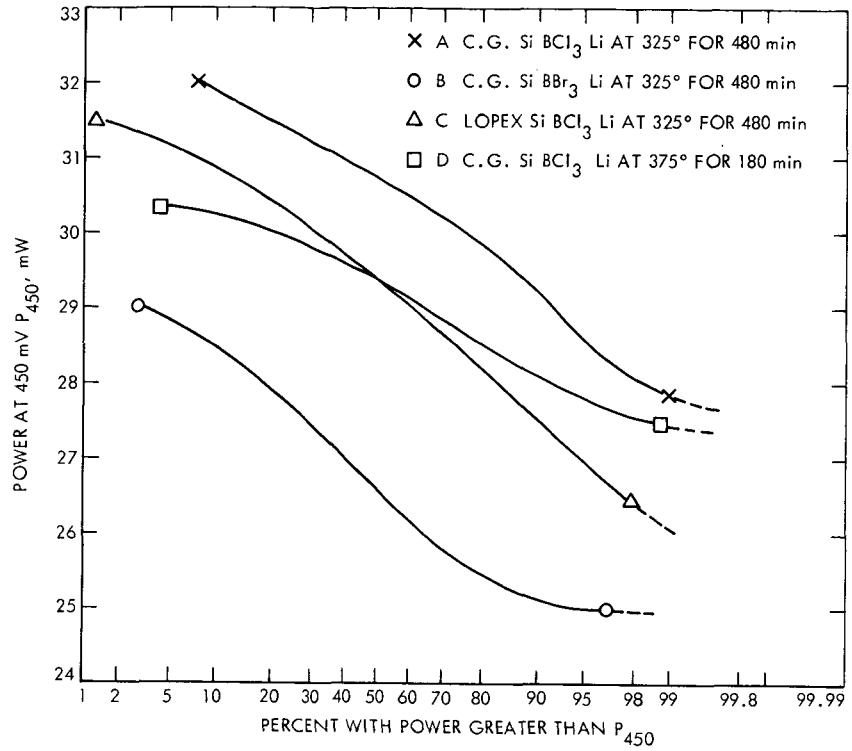

Fig. 1. Cumulative P_{max} distribution for JPL shipment C11

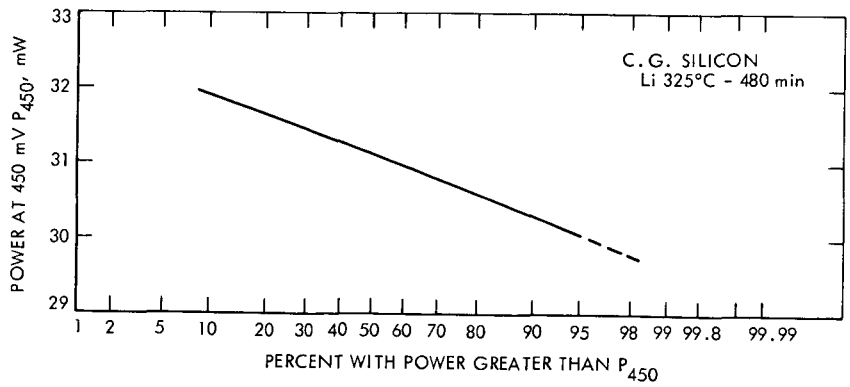

Fig. 2. Cumulative P_{max} distribution for JPL shipment C12

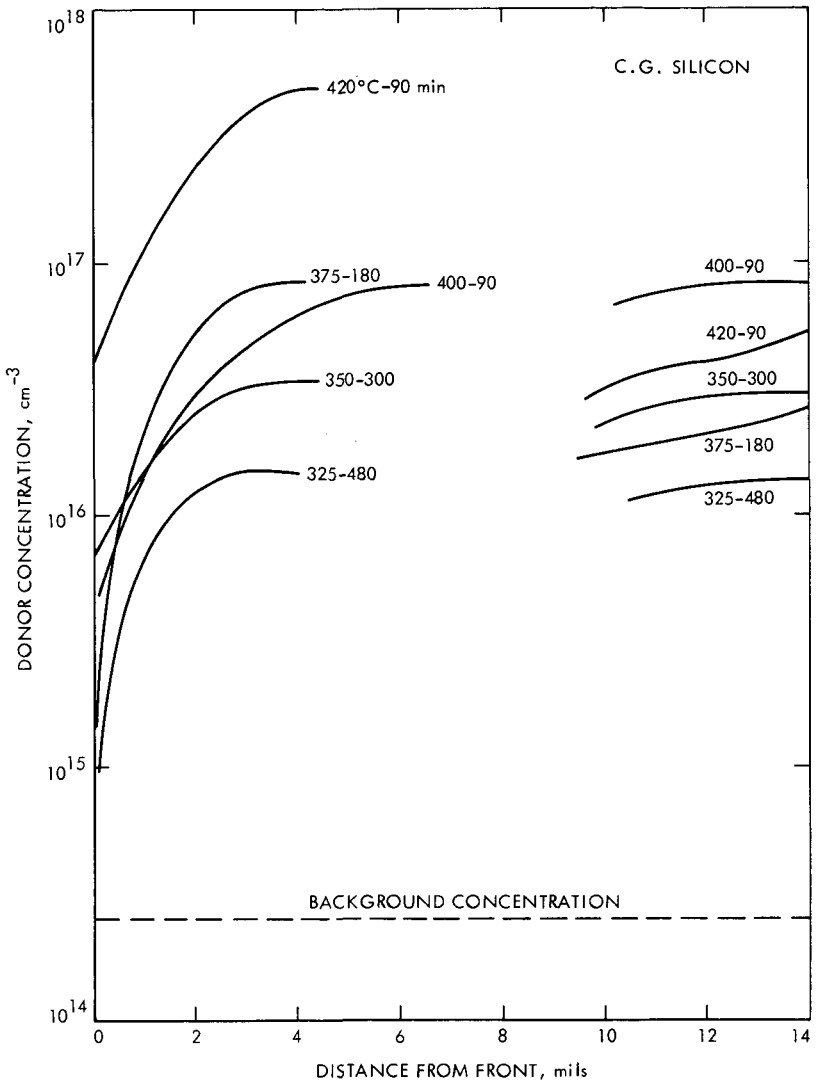

Fig. 3. Donor concentration profiles (in the bulk) for various lithium diffusion schedules

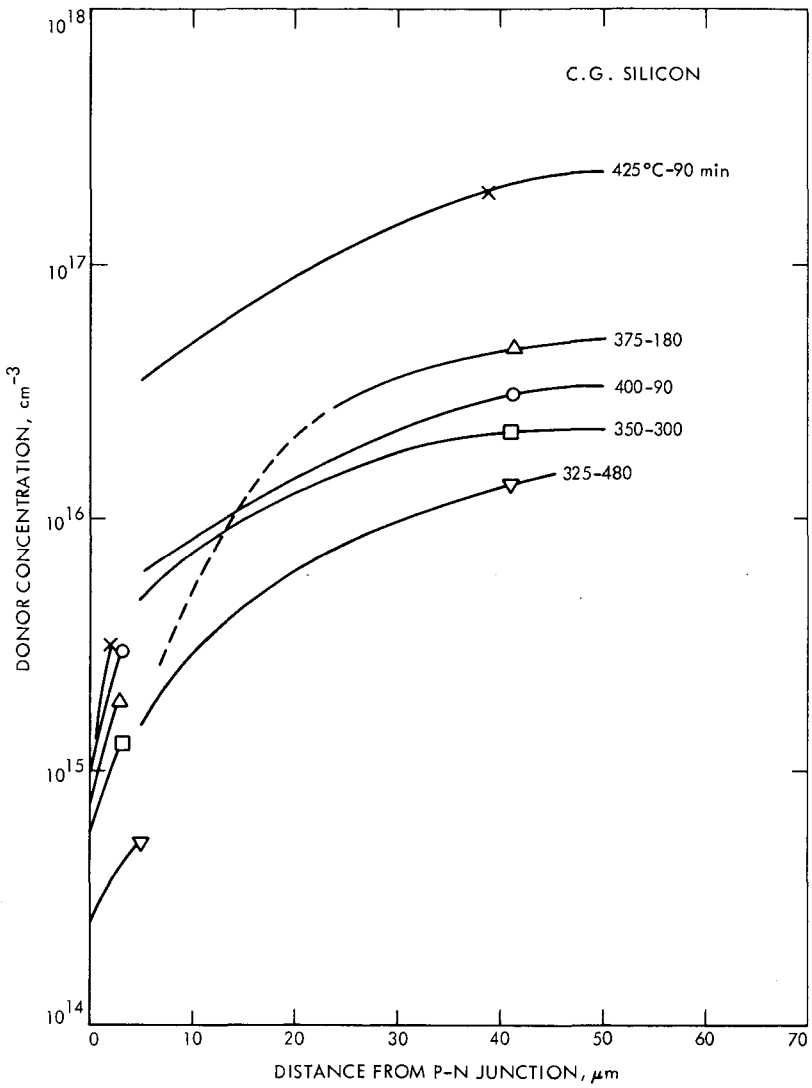

Fig. 4. Donor concentration profiles (near the P/N junction) for various lithium diffusion schedules

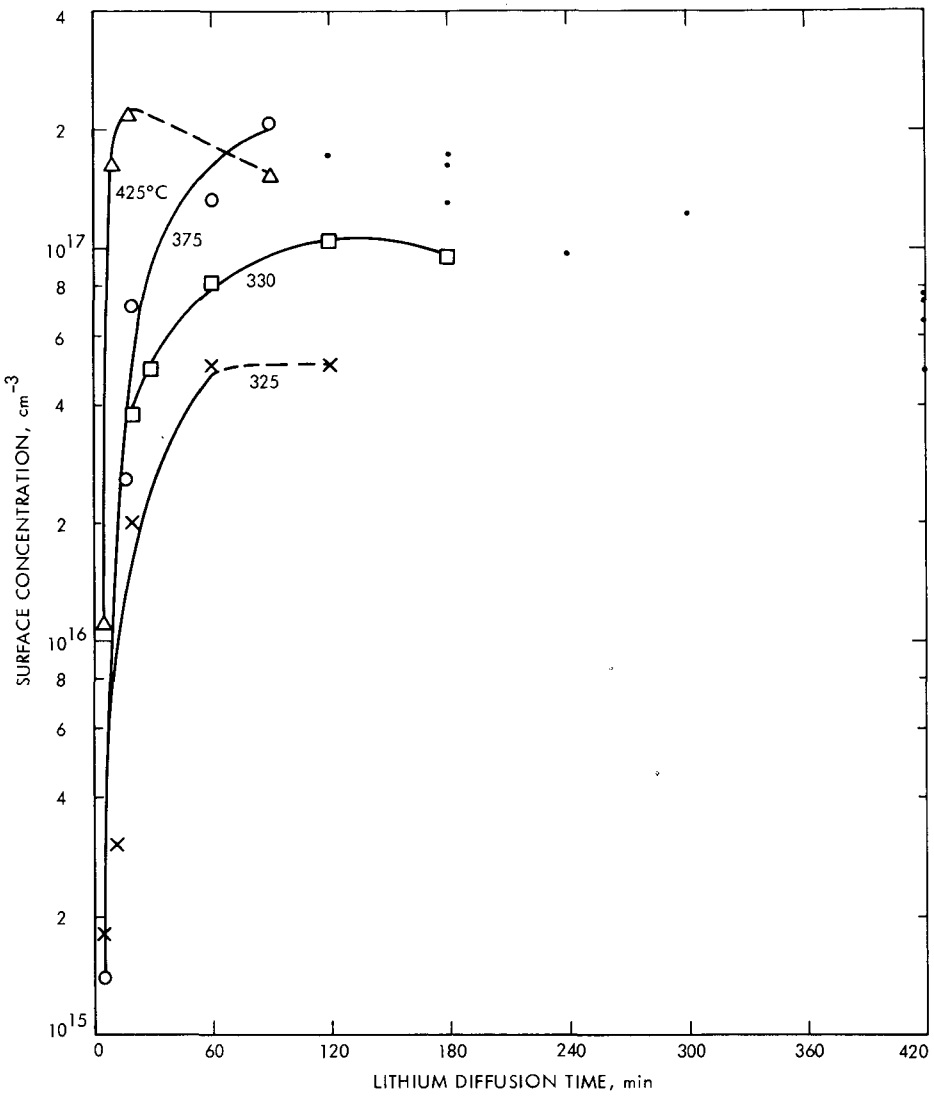

Fig. 5. Build-up of surface concentration of lithium for increasing time at various temperatures

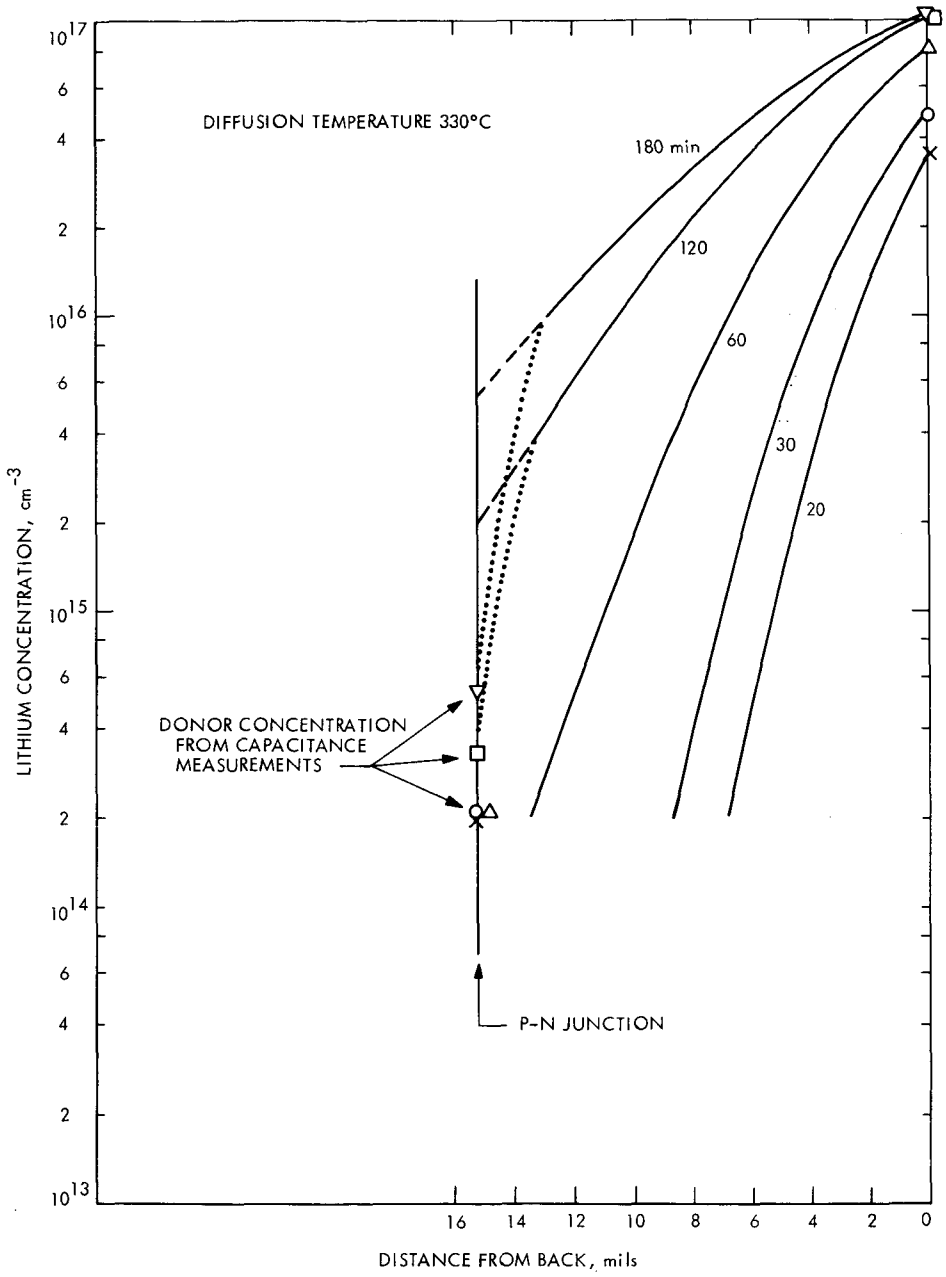

Fig. 6. Changes in lithium concentration profile and the values measured at the P/N junction as the diffusion time at 330°C was increased

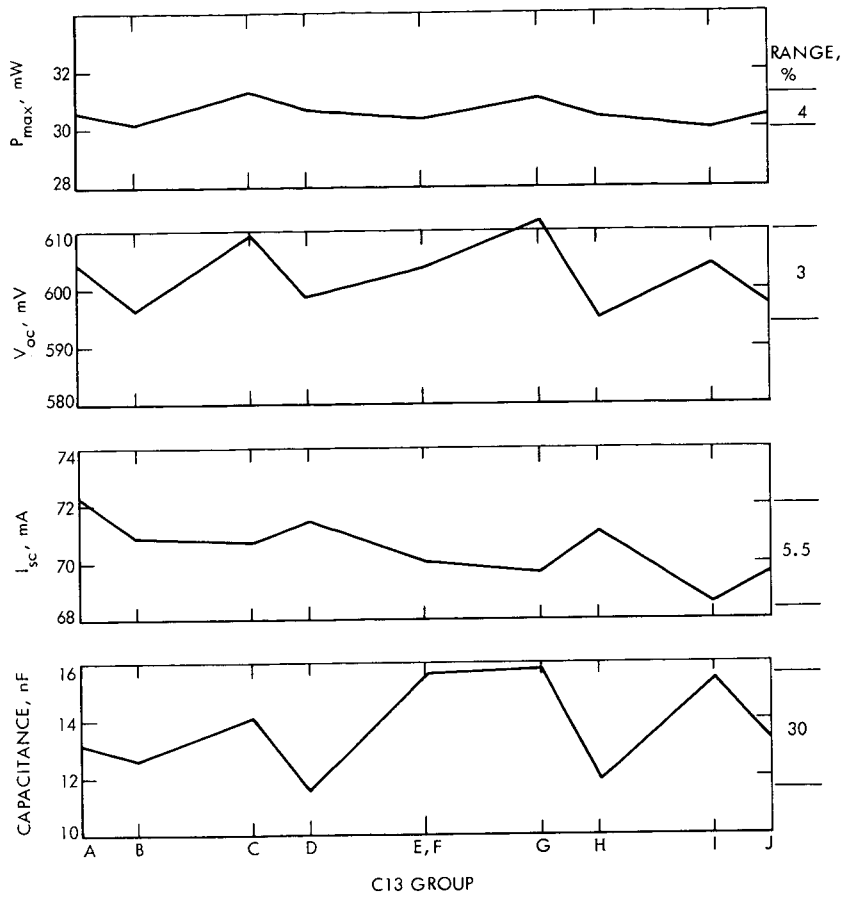

Fig. 7. Average values for P_{max}, V_{oc}, I_{sc}, and capacitance for the ten C13 groups

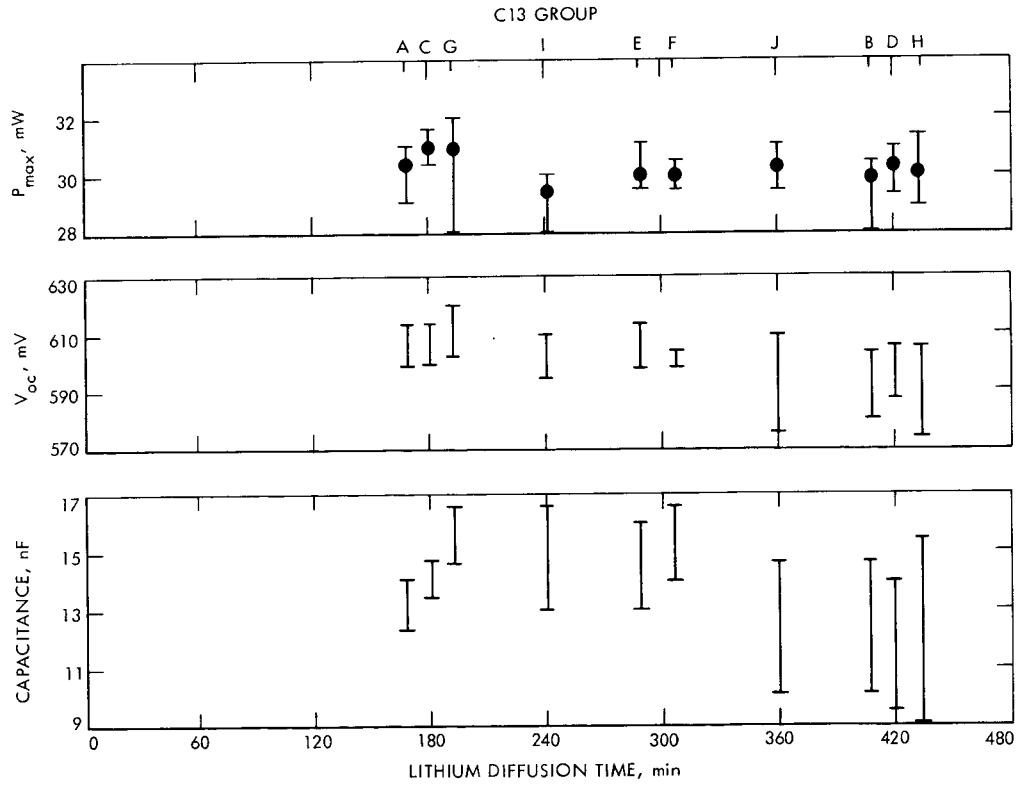

Fig. 8. Average values and spread for P_{max}, V_{oc}, and capacitance for the C13 groups, plotted as a function of diffusion time

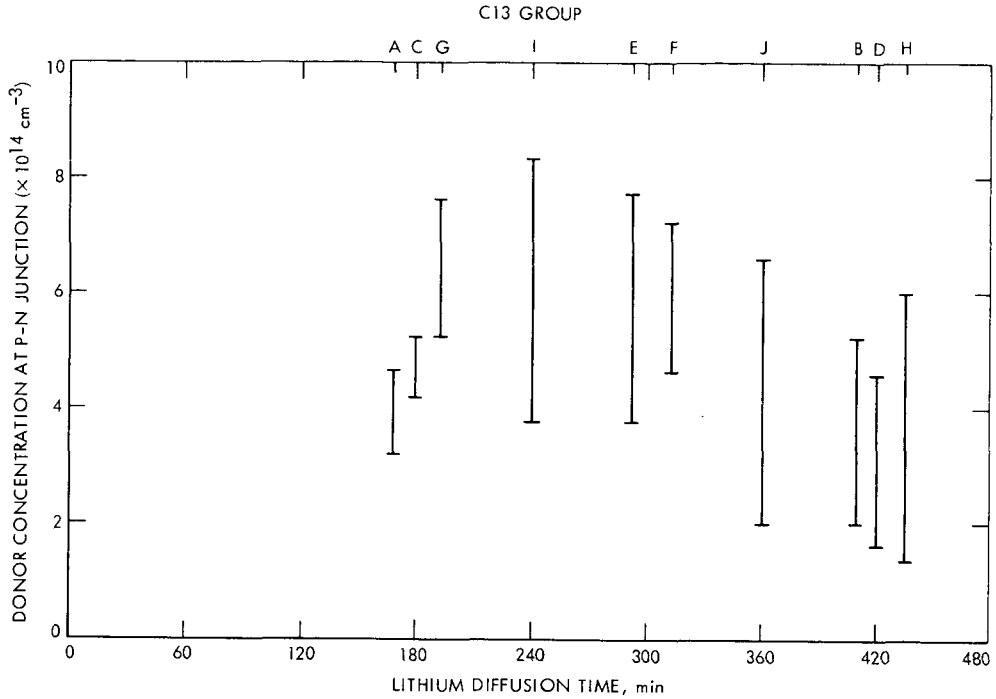

Fig. 9. Average values and spread of donor concentration gradient at the P/N junction, for the ten C13 groups, plotted as a function of diffusion time

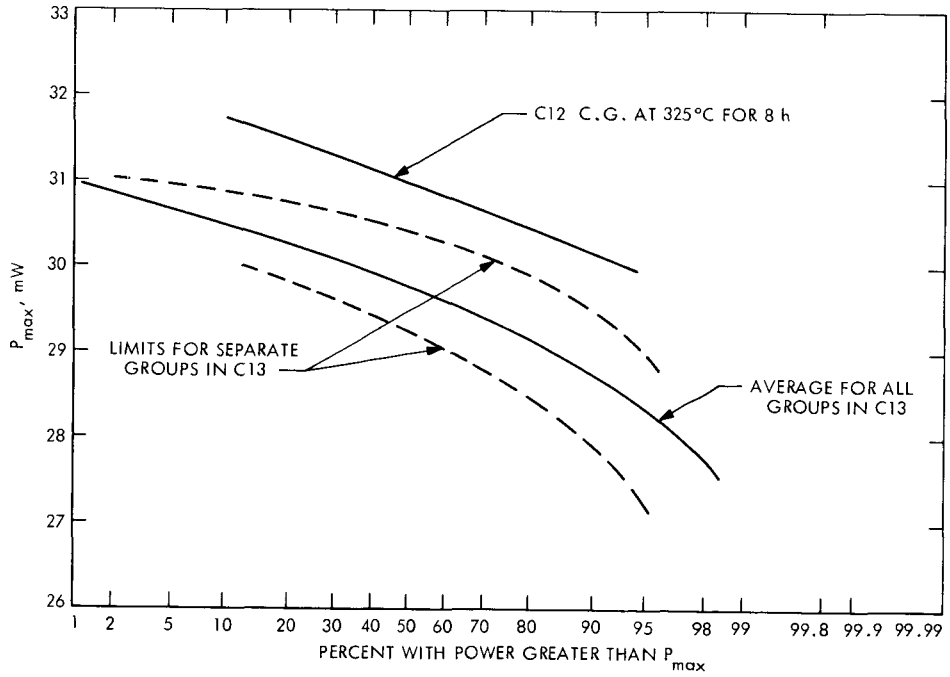

Fig. 10. Cumulative P_{max} distribution for total and extreme groups in C13 (C12 shown for comparison)

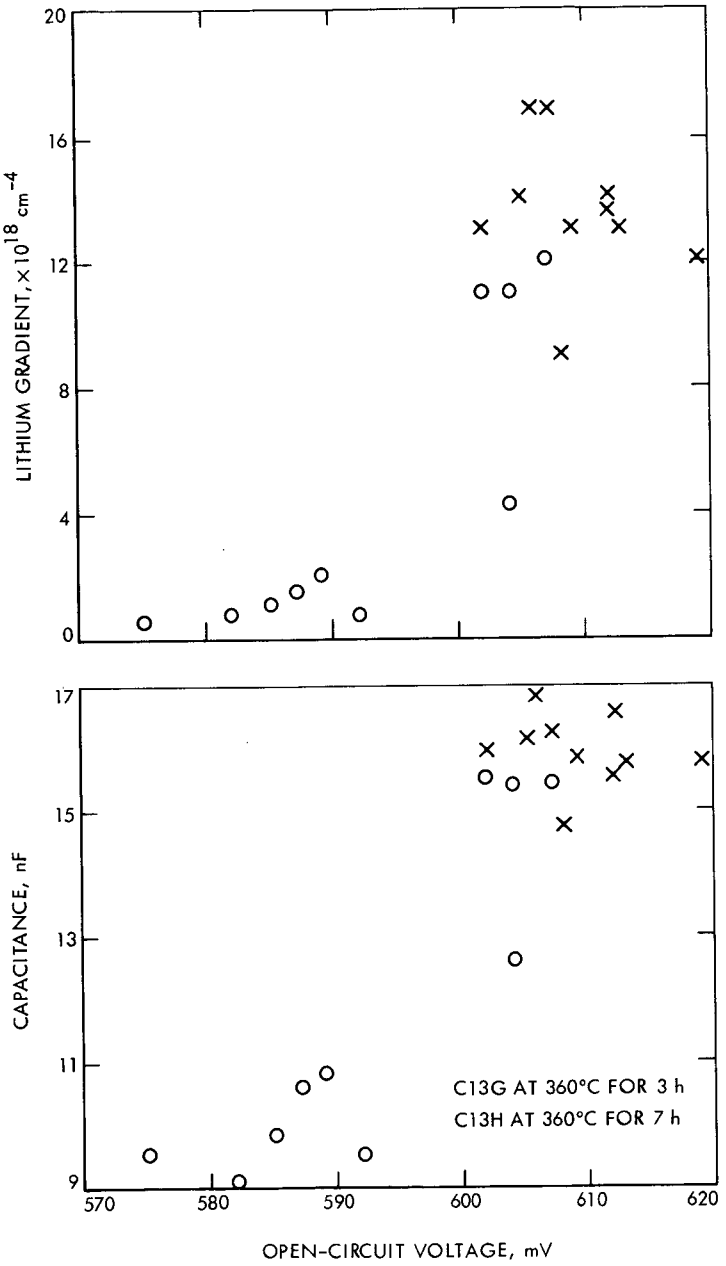

Fig. 11. V_{oc} plotted versus capacitance and lithium concentration gradient near the junction for two 10-cell groups in C13

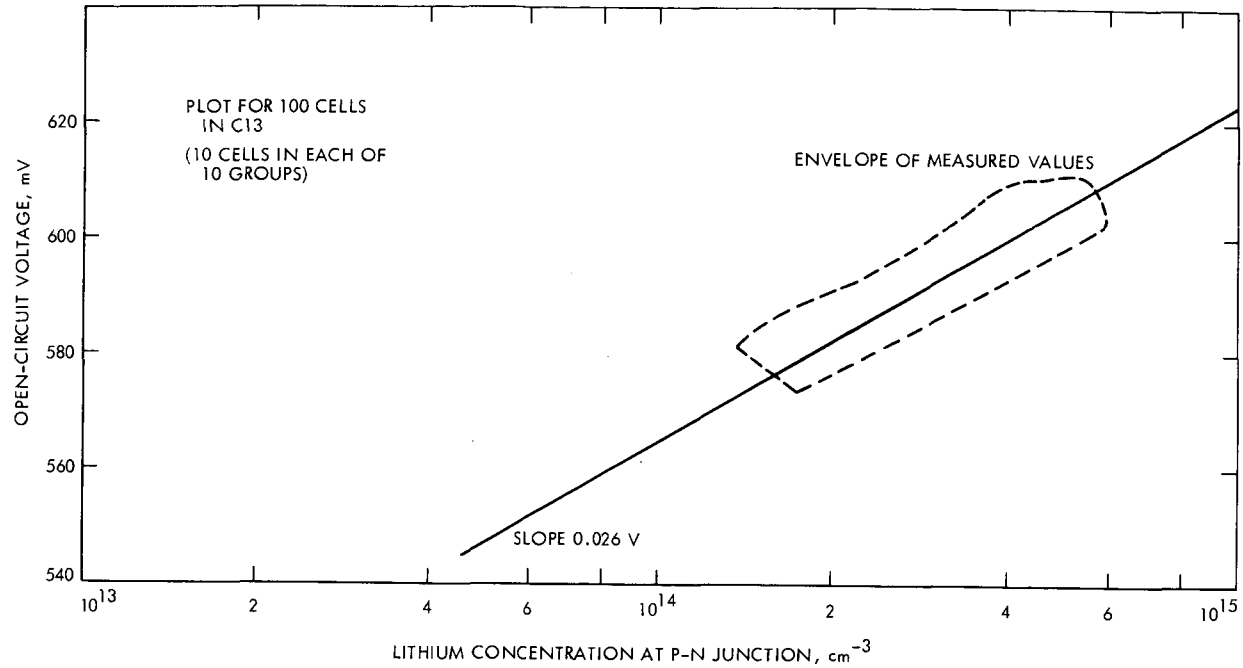

Fig. 12. V_{oc} plotted against logarithm of the donor concentration for 100 cells, 10 in each C13 groups

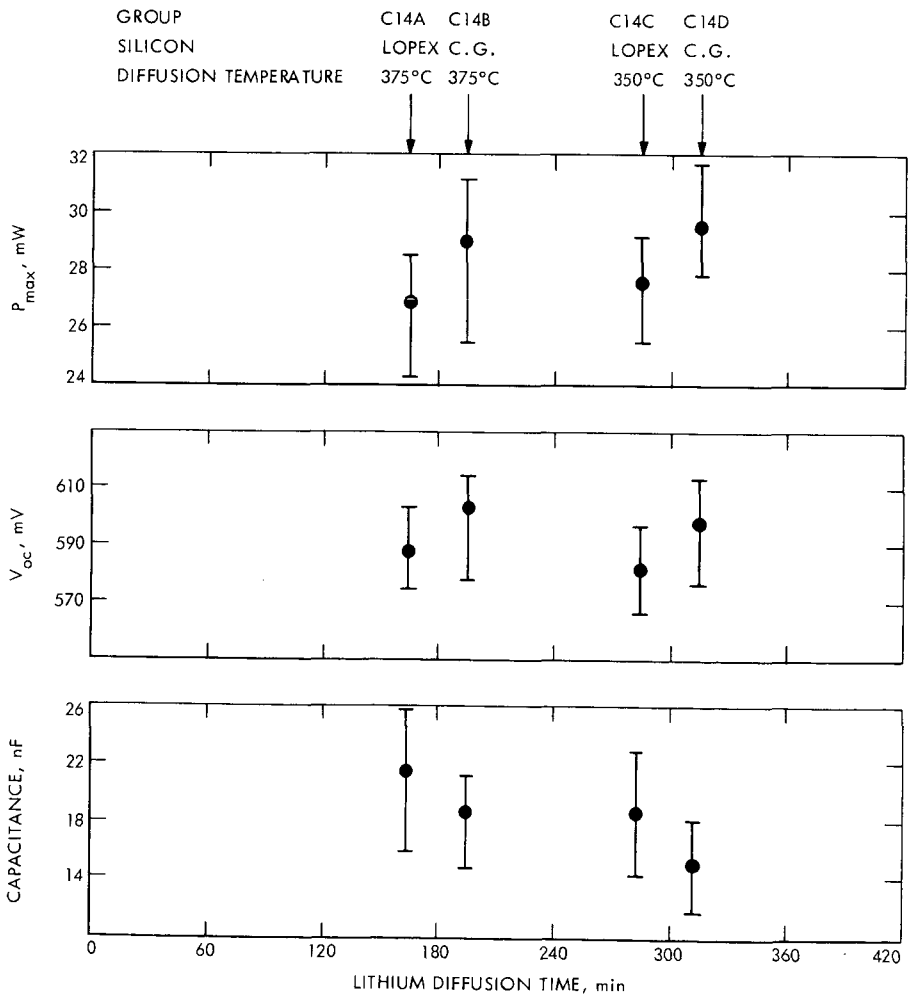

Fig. 13. Average values and spread of P_{max}, V_{oc}, and capacitance for C14 cell groups

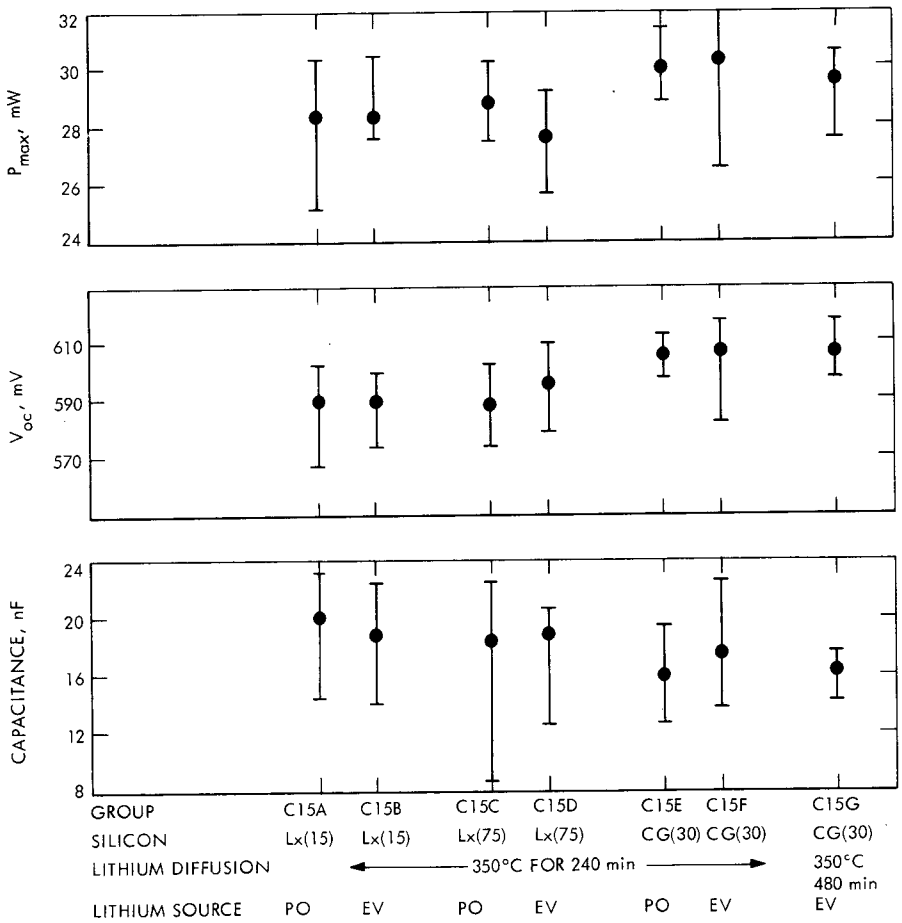

Fig. 14. Average values and spread for P_{max}, V_{oc}, and capacitance for C15 cell groups

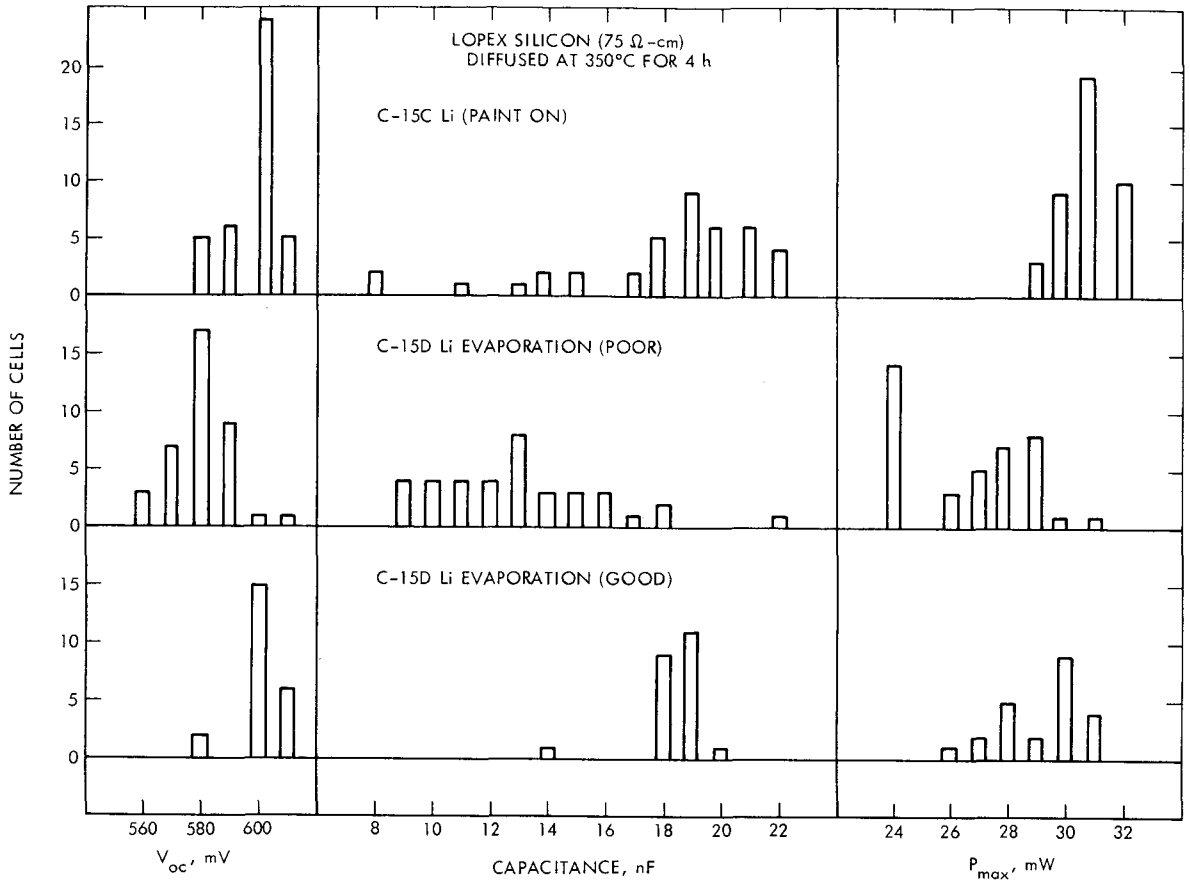

Fig. 15. Histogram plots of V_{oc}, capacitance, and P_{max} for three different conditions of lithium application in two C15 groups

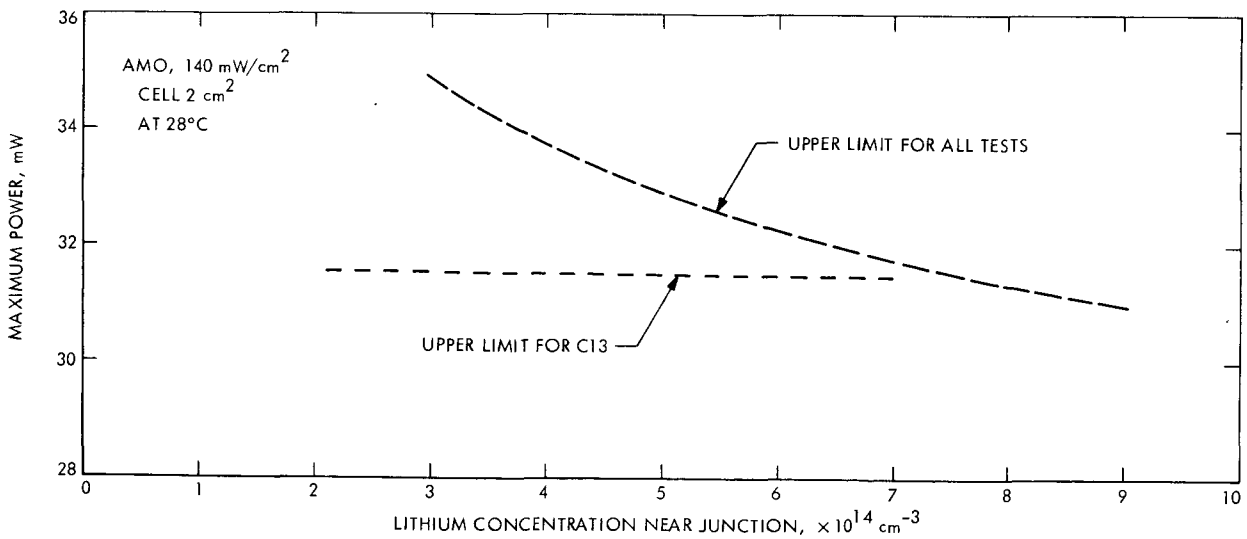

Fig. 16. Highest observed pairs of values for P_{max} and lithium concentration

N72-10056

AIR FORCE/ION PHYSICS HARDENED LITHIUM DOPED SOLAR CELL DEVELOPMENT

A. Kirkpatrick, F. Bartels, C. Carnes,
J. Ho, and D. Smith
Ion Physics Corporation
Burlington, Massachusetts

I. INTRODUCTION

Ion Physics Corporation (IPC) is working under Air Force Contract F33615-70-C-1491 to develop a lithium-doped solar cell hardened against both space radiation and nuclear weapons burst environments. Performance objectives for the hardened cell are sufficiently severe that they are not met by any of the lithium cells which have been reported on to date. IPC is developing a cell structure designed to meet these program goals. The first 12 months of the 24-month program have involved development of elements of the cell structure. The completed structure is now to be assembled and optimized.

II. THE IPC CELL STRUCTURE

Because the performance characteristics of the lithium-doped solar cell are determined by the concentration profile of lithium throughout the cell, IPC is attempting to develop a structure allowing independent control over profile shape in the base, concentration in the base and profile in the vicinity of the junction.

The IPC cell is illustrated in Fig. 1. The cell is 10 mils thick and has 5-μm aluminum contacts. Base material is 20 Ω-cm phosphorus-doped silicon with <100> orientation. The cell is a $P^+ N^+ NN^+$ structure in which the N^+ phosphorus-doped region completely encloses the base N region. Purpose of the N^+ region at the front below the P^+ layer is to reduce diffusion of lithium into the P^+ layer and to prevent widening of the space charge region due to lithium depletion after irradiation. The N^+ layer at the cell back prevents outdiffusion of lithium and insures low resistance ohmic contact.

The cell is fabricated in the following sequence:

(1) The silicon wafer is diffused at 1000°C with PH_3 to produce the back N^+ layer.

(2) The front P^+ layer is produced by diffusion at 950°C with B_2H_6.

(3) The cell is sized using an orientation dependent etch which leaves <111> planes as the cell edges.

(4) Phosphorus is ion implanted from the front to produce the buried N^+ layer which also extends down the cell edge surfaces.

(5) Lithium is introduced through the back surface by ion implantation and is distributed through the cell using conventional elevated temperature distribution cycles.

(6) Aluminum contacts and antireflection coating are applied.

A. Lithium Implantation

Implantation of the lithium is fundamental to the IPC cell design. In the implantation process a high energy beam of the desired ion is formed, analyzed and rastered over the surface to be

implanted. The number of ions introduced is measured directly by integration of total charge collected at the substrate. Typically IPC used 250 keV Li^7 which penetrates approximately 1 μm into the silicon.

Implantation of the lithium offers many important advantages over other lithium introduction techniques:

(1) The amount of lithium introduced is precisely controlled and is uniform and reproducible.

(2) The amount of lithium introduced is independent of the distribution temperature.

(3) No surface treatment is required after implantation as there is no surface residue, surface etching or pitting.

Following implantation, the lithium is distributed using distribution cycles approximately equivalent to those employed with diffused lithium cells. During distribution a large portion of the implanted lithium is lost from the back surface of the cell. The N^+ barrier layer at the back surface into which the implant is made reduces this loss by more than an order of magnitude. Shown in Fig. 2 are experimental lithium profiles after distribution at high temperature of cells with and without the N^+ barrier. Because IPC is able to "count" every lithium ion introduced into the cell, it is possible to determine from each profile a "utilization fraction," f, which is the fraction of initially implanted lithium remaining after distribution. Typically for implants at 250 keV into the N^+ barrier with distribution times of the order of hours at 450°C or below this fraction ranges between 0.02 and 0.03.

Desired cell base lithium concentrations averaging slightly above 10^{16} cm^{-3} are obtained by implanting 1×10^{16} lithium ions cm^{-2}. This level can be produced in about 2 min per cell from the IPC research implantation facility. As seen in Fig. 3, the lithium concentration throughout the base can be varied almost linearly with implant fluence.

The N^+ layer at the back surface into which the lithium implantation is made has an additional important function. Ion implantation into a crystal lattice causes structural damage which for most applications is then annealed at elevated temperatures typically in the range of 700°C and above. When lithium is implanted into silicon, the lattice damage which occurs is not completely annealed at temperatures below 450°C. Short 5-min anneals at 700°C are sufficient but could cause reproducibility problems with the lithium profile. If the implantation is made into 20 Ω-cm silicon without an N^+ surface layer and adequate anneal is not provided, the resulting solar cell has high series resistance of several ohms. However, when the implant is made into the heavily doped N^+ layer, it is found that no anneal is required to insure good ohmic contact and low series resistance.

B. The Implanted Phosphorus Front Barrier

In order to reduce lithium diffusion into the P^+ region and to prevent widening of the junction space-charge region due to lithium depletion after irradiation, IPC will implant a thin N^+ phosphorus layer immediately below the front P^+ layer. Without this N^+ barrier it is possible to control shape and concentration of the lithium profile through the base but desired control over the lithium profile in the junction vicinity is dependent upon use of the barrier. This barrier is the only component of the planned structure on which development has not yet been successfully completed.

Desired concentration profiles near the junction are illustrated in Fig. 4. Phosphorus is implanted at 200 to 300 keV to penetrate approximately 0.15 μm below the junction and to produce a peak concentration of approximately 10^{16} cm^{-3}. The phosphorus N^+ region below the P^+ surface layer is to act as a barrier to reduce loss of lithium into the P^+ layer sink during distribution and consequently to provide control of the lithium level. Peak concentration in the N^+ layer is selected to be approximately equal to the lithium level in the vicinity of the junction and should serve as a barrier to lithium diffusion until concentration reaches this level. If the phosphorus concentration is made much higher than the required lithium level, the N^+ region will retard flow of holes to the junction and will reduce cell performance.

Investigation of the front barrier is proceeding. Results to date have been inconclusive. With a few exceptions, cells having the front barrier have shown losses in V_{oc} of 30 to 100 mV relative to otherwise identical cells without the barrier. Some cells have shown evidence of high junction vicinity lithium concentration and low concentration gradient, but these results have not been consistent or reproducible.

III. PRESENT STATUS

A first lot of 110 crucible-grown silicon cells has been fabricated without the front N^+ barrier. Lithium implant fluence was 1×10^{16} cm^{-2} at 250 keV followed by 450°C 120-min distribution. Layer stripping showed lithium utilization fraction of 0.028 with a profile peak of 1.3×10^{16} cm^{-3}. Median maximum power of these 10-mil thick aluminum contacted cells was 58 mW.

Introduction of lithium by ion implantation eliminates reproducibility and surface problem deficiencies of other introduction techniques. Implantation has been demonstrated to make possible a degree of control over the cell lithium content which has not previously been available. Front barrier development remains to be completed. Successful development of the barrier will make available the freedom to select optimum lithium concentration throughout the cell, including in the vicinity of the junction.

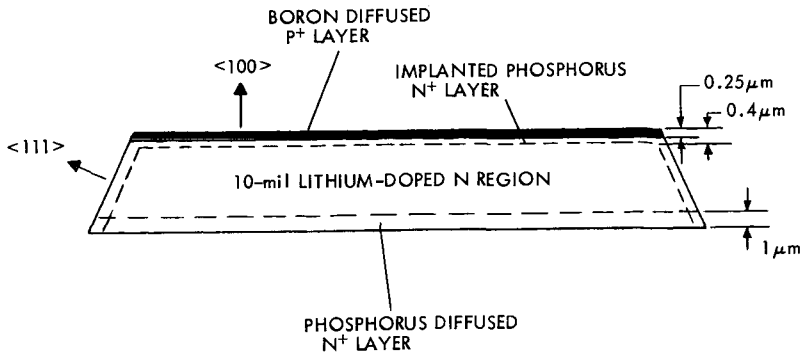

Fig. 1. Ion Physics Corp. lithium-doped cell

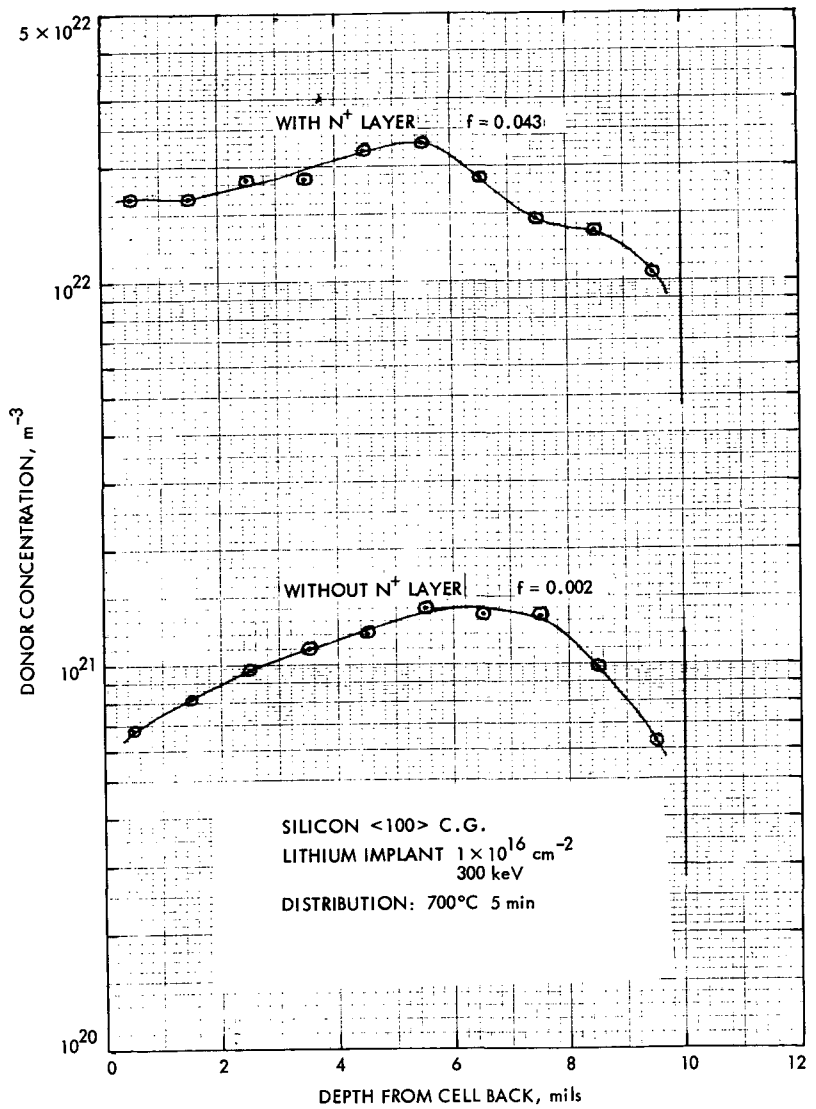

Fig. 2. Effect of back N^+ layer on lithium profile

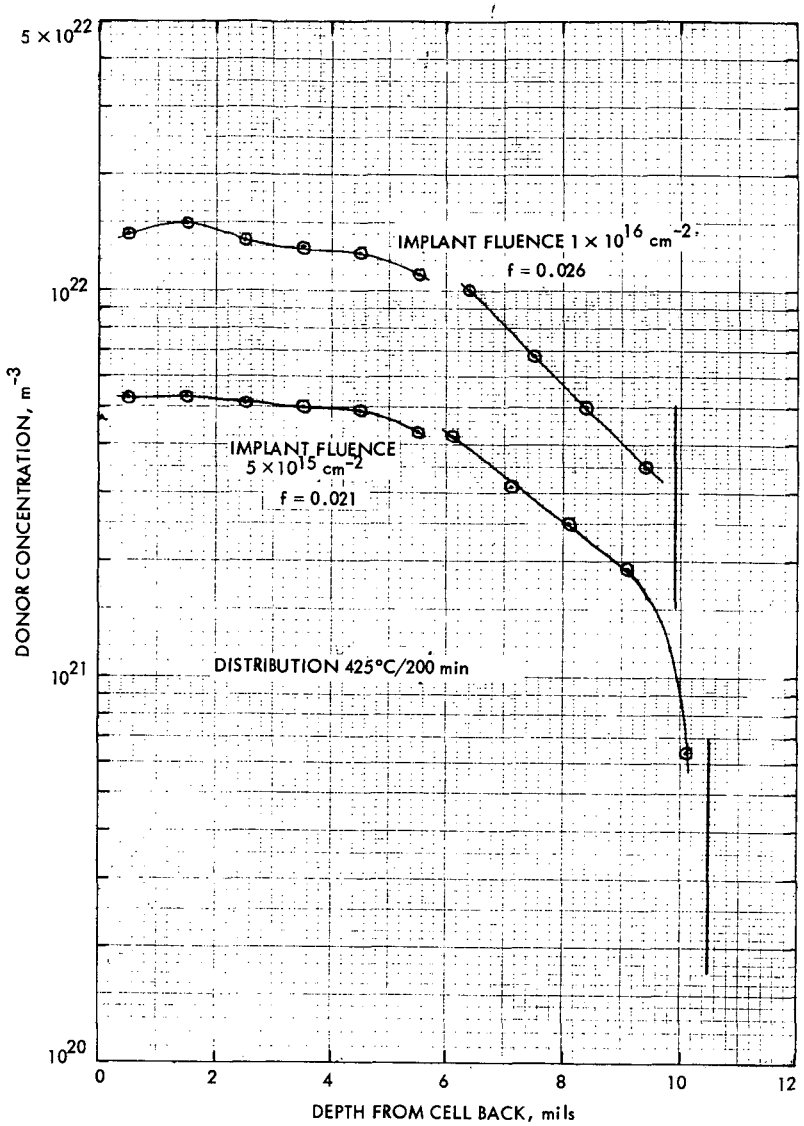

Fig. 3. Effect of implant fluence on profile

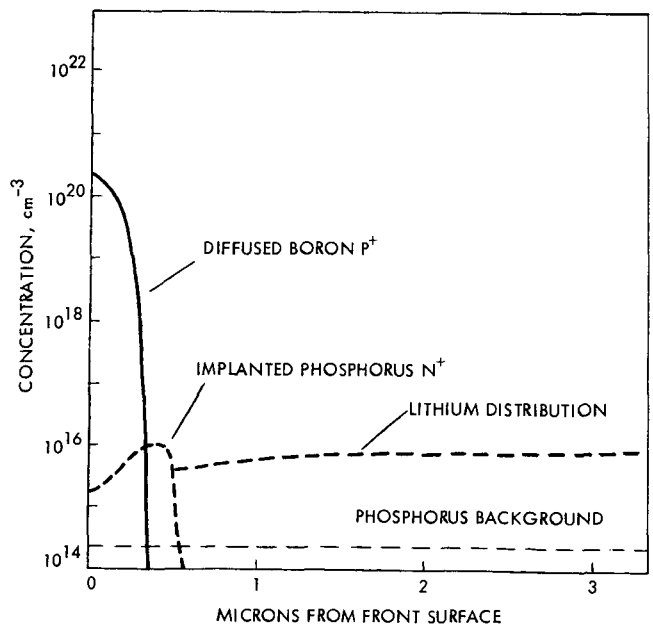

Fig. 4. Planned concentration profiles

N72-10057

DEPENDENCE OF DEFECT INTRODUCTION ON TEMPERATURE AND RESISTIVITY AND SOME LONG-TERM ANNEALING EFFECTS

G. J. Brucker
Astro-Electronics Division of RCA
Princeton, New Jersey

I. INTRODUCTION

The effort reported here represents data which was obtained after the termination (June 1970) of our contractual investigation of lithium properties in bulk-silicon samples before and after irradiation. The objective of this phase of the study was to obtain the analytical information required to characterize the interactions of lithium with radiation-induced defects in silicon, and hopefully to develop a model of the damage and recovery mechanisms in irradiated-lithium-containing solar cells. The approach to the objectives was based on making measurements of the Hall coefficient and resistivity of samples irradiated by 1-MeV electrons. Experiments on bulk samples included Hall coefficient and resistivity measurements taken as a function of: (1) bombardment temperature, (2) resistivity, (3) fluence, (4) oxygen concentration, and (5) annealing time at temperatures from 300 to 373 K.

II. RESULTS

A. Carrier Removal

Previous work of several investigators (Refs. 1, 2) demonstrated that the defect introduction rate in phosphorus-containing silicon decreases as the bombardment temperature is decreased and also as the dopant concentration is increased at a fixed bombardment temperature. One of the objectives of our study was to determine the dependence of carrier-removal rate in irradiated silicon on bombardment temperature and lithium concentration. To achieve this objective, several Hall bars fabricated from 1500 Ω-cm and 5000 Ω-cm float-zone refined silicon and from 30 to 50 Ω-cm quartz-crucible silicon were diffused with lithium to concentrations from 2×10^{20} to 3×10^{23} Li/M^3 and irradiated at bombardment temperatures from 79 to 200 K. The rates of carrier-removal were determined after each bombardment. These rates measured in float zone (FZ) silicon after annealing to a temperature of 200 K versus the reciprocal of the bombardment temperature are shown in Fig. 1. Lithium concentrations of the samples used in the measurements are shown as a parameter. The carrier-removal rates were normalized at a bombardment temperature of 200 K, and the ordinate of the curves is labeled as the probability of defect formation. The curves shift along the temperature axis toward lower temperatures as the lithium density is decreased over three orders of magnitude. These concentrations of lithium correspond to resistivities from 0.03 to 20 Ω-cm. This shift of the temperature dependence portion of the curves is in qualitative agreement with the prediction of the interstitial-vacancy close-pair model (Refs. 1, 2) of radiation damage in silicon at low temperatures. It was previously reported (Ref. 3) that the saturated value of carrier-removal rate measured at a bombardment temperature of 200 K appeared to increase with lithium concentration. This conclusion is in agreement with the results obtained on the samples containing concentrations to 3×10^{23} Li/m^3.

A similar set of curves is shown in Fig. 2 for the samples fabricated from quartz-crucible silicon with lithium concentrations from 2×10^{21} to 3×10^{23} Li/m^3. The saturated value of carrier-removal rate obtained for the samples doped with 3×10^{23} Li/m^3 is equal to 10 m^{-1} which is

the same value obtained for the samples doped with 2×10^{22} Li/m^3.

B. Annealing Properties-High Lithium Concentrations

Following the completion of the bombardments, the float-zone samples doped to 3×10^{23} Li/m^3 were annealed at temperatures ranging from 250 to 300 K. Hall and resistivity measurements were obtained on these samples as a function of time and measurement temperature. The time to half recovery, t_R of the mobility (T_M = 79 K) was determined from these annealing cycles, and the reciprocal of this quantity is shown in Fig. 3. The error in the measurement is large at the higher temperatures since the sample recovered to its original value of mobility in less than a minute at 300 K. Nevertheless, the activation energy determined from the slope of the curve is 0.68 eV which is close to the activation energy (0.66 eV) for lithium diffusion in oxygen-lean silicon measured by Pell (Ref. 4) and also reported (Ref. 5) in measurements made on solar cells.

C. Long-Term Annealing Effects

Results reported (Ref. 6) on the long-term annealing effects in lithium-containing quartz-crucible and float-zone samples with low lithium concentrations showed a disturbing property, namely, the continuous loss of carrier density (measured at low and high temperature) as a function of time in irradiated samples annealing at room temperature. These samples were recently remeasured, and the carrier densities measured as a function of time are shown in Fig. 4 for three samples. Two float-zone samples were doped to a low and a high concentration, respectively, and the quartz-crucible sample contained a high concentration of lithium. It appears that the runaway loss of carriers has finally ceased to occur in the quartz-crucible (>2 yr) and low-lithium-density sample of float-zone silicon. Thus, the precipitation-like process which produces a charge-neutral defect complex and which was previously postulated (Ref. 6) as one of the annealing mechanisms appears to equilibrate. The behavior of the other sample of float-zone silicon is typical of the more heavily doped samples, namely, an initial dissociation of defects with an increase of carrier density, and then they reach equilibrium over the long-term period.

III. DISCUSSION OF RESULTS

The irradiation temperature dependence of the production rate of impurity complexes in silicon has been explained (Refs. 1, 2) by a model based on the formation of close-spaced interstitial-vacancy pairs by electron bombardment. This model yields a probability P_C, of vacancy liberation from the interstitial to form vacancy-impurity defects described by

$$P_C = \left\{1 + g \exp\left[\frac{E_F(n_0, T) - E_M}{KT}\right]\right\}^{-1} \cdots \quad (1)$$

where g is the ratio of the number of ways the state can be occupied to the number of ways the state can be unoccupied, $E_F(n_0, T)$ is the Fermi level for electrons which is a function of initial carrier concentration n_0 and temperature T, and E_M is the energy level of the metastable interstitial-vacancy pair. Equation (1) was used in an attempt to fit the data of Figs. 1 and 2. The preliminary results indicate that there is not a unique pair of values for the parameters g and E_M which will satisfactorily fit the data obtained on the float-zone samples over the three orders of magnitude range in lithium concentration. The best value of E_M appears to be $\approx$0.09 eV, but several values of g are required to fit the entire range of concentrations. In addition, the values of g are small (as low as 10^{-3}) and thus not physically reasonable. This model does not appear to be the complete description of defect production mechanisms in lithium-doped float-zone silicon over this range of concentrations.

The attempts at curve fitting were more successful with the quartz crucible samples. In this case, E_M = 0.07 eV and g = 0.1 gave a reasonable fit over the two orders of magnitude in lithium concentration of these samples. This higher value of g is more physically reasonable, and the lower value of E_M is in agreement with the value used by previous investigators (Ref. 1) in fitting their data on phosphorus-doped silicon. Our investigations have shown (Ref. 4) that the oxygen-vacancy defect is the dominating carrier-removal center in the lithium-containing silicon. Thus, it is reasonable to expect that these samples would behave similarly to the phosphorous-doped (5×10^{20} P/M^3, ρ = 10 Ω-cm) quartz-crucible silicon as our data indicates.

The mobility recovery shown in Fig. 3 demonstrated again in agreement with the detailed measurements obtained on solar cells (Ref. 5) that the diffusion of free lithium is definitely related to the recovery process. This conclusion applies to the short-term recovery period that is within the first few minutes or hours following bombardment.

The long-term annealing effects shown in Fig. 4 are important, since they indicated that the carrier density changes will finally equilibrate in lightly doped float-zone silicon or in the more heavily doped quartz-crucible silicon after a sufficiently long annealing time. This behavior is observed only under the conditions of these irradiations, namely the damage level was not large compared to the lithium concentrations. The author and other investigators (Ref. 7) have observed that after large fluences, the loss of carriers does not equilibrate, and the samples will return to the starting resistivity of the silicon before diffusion with lithium. This applies to both float-zone and quartz-crucible silicon.

IV. CONCLUSIONS

The simple close-pair vacancy-interstitial model does not completely describe the dependence of defect introduction on temperature and resistivity in lithium containing float-zone silicon. Better agreement of the model with experimental results is obtained in samples of lithium-containing quartz-crucible silicon. Further evidence of the relationship between diffusion of free lithium and recovery of damage was obtained. This was deduced from the activation energy for recovery of 0.68 eV measured in lithium-containing float-zone silicon.

Equilibrium and stability of the carrier density is possible after long-term annealing at 300 K in irradiated quartz-crucible ($\gtrsim$2 yr) or lightly doped (2 to 5 $\times$ 10^{20} Li/m^3) float-zone silicon ($\lesssim$1 yr).

REFERENCES

1. Stein, H. J., and Vook, F. L., Phys. Rev., Vol. 163, p. 790, 1967; also in Radiation Effects in Semiconductors, pp. 99 and 115. Edited by F. L. Vook. Plenum Publishing Corp., New York, 1968.

2. Gregory, B. L., and Barnes, E. E., in Radiation Effects in Semiconductors, p. 124. Edited by F. L. Vook. Plenum Publishing Corp., New York, 1968.

3. Brucker, G. J., et al., Third Quarterly Report, RCA, under JPL Contract No. 952555 April 10, 1970.

4. Pell, E. M., Phys. Rev., Vol. 119, p. 1222, 1960; see also J. Appl. Phys. Vol. 32, p. 6 1961.

5. Brucker, G. J., et al., Fourth Quarterly Report, RCA, under JPL Contract No. 952555 July 10, 1970.

6. Brucker, G. J., IEEE Trans. Nucl. Div., Vol. NS-17, p. 144, 1970.

7. Goldstein, B., Final Contract Report, RCA under Contract No. F19628-68-C-0133, July 1968.

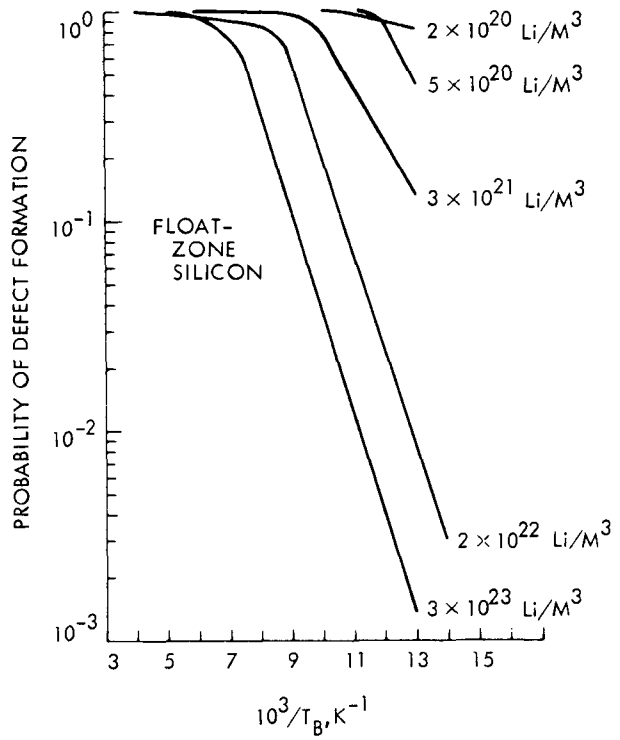

Fig. 1. Probability of defect formation versus reciprocal bombardment temperature for electron irradiated float-zone silicon measured at 79 K after annealing to 200 K. Initial lithium concentration is the curve parameter

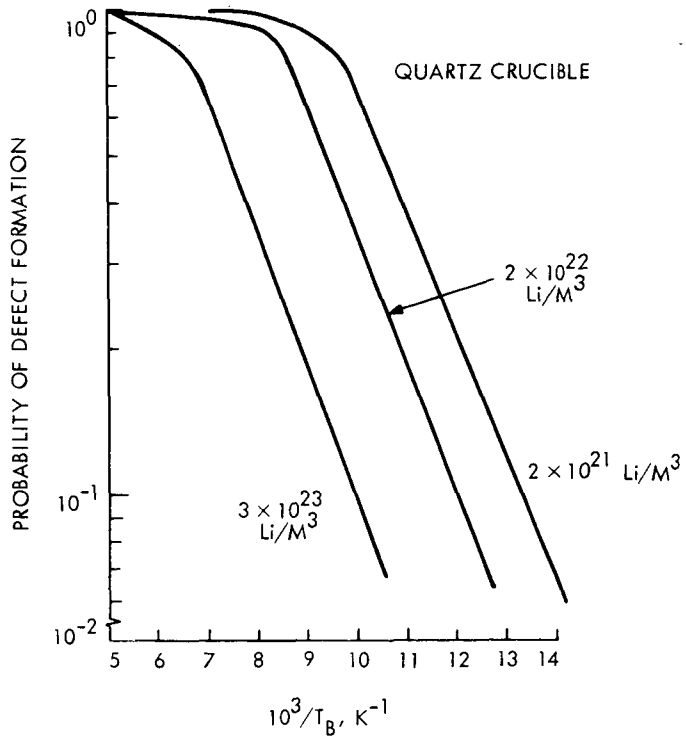

Fig. 2. Probability of defect formation versus reciprocal bombardment temperature for electron irradiated quartz-crucible silicon, measured at 79 K after annealing at 200 K. Initial lithium concentration is the curve parameter

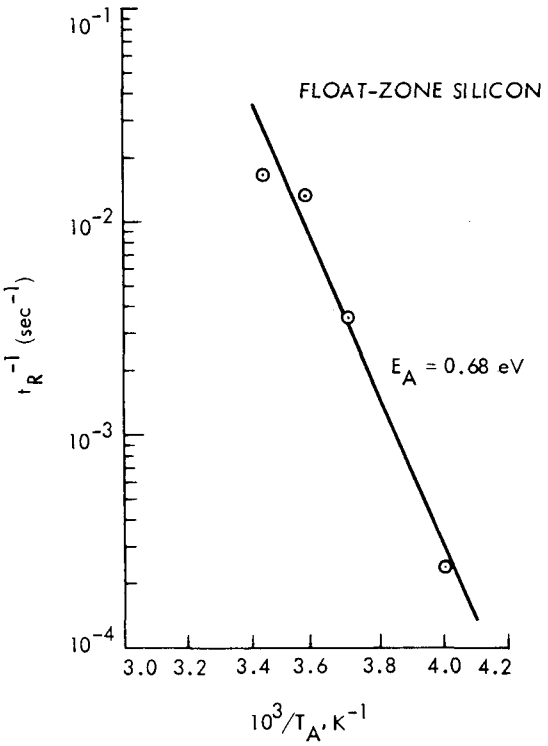

Fig. 3. Reciprocal half recovery time of the mobility in electron irradiated float-zone silicon versus the reciprocal annealing temperature. Measurements of mobility at 79 K. Activation energy for the recovery process is indicated. Initial lithium concentration 3×10^{23} Li/M^3

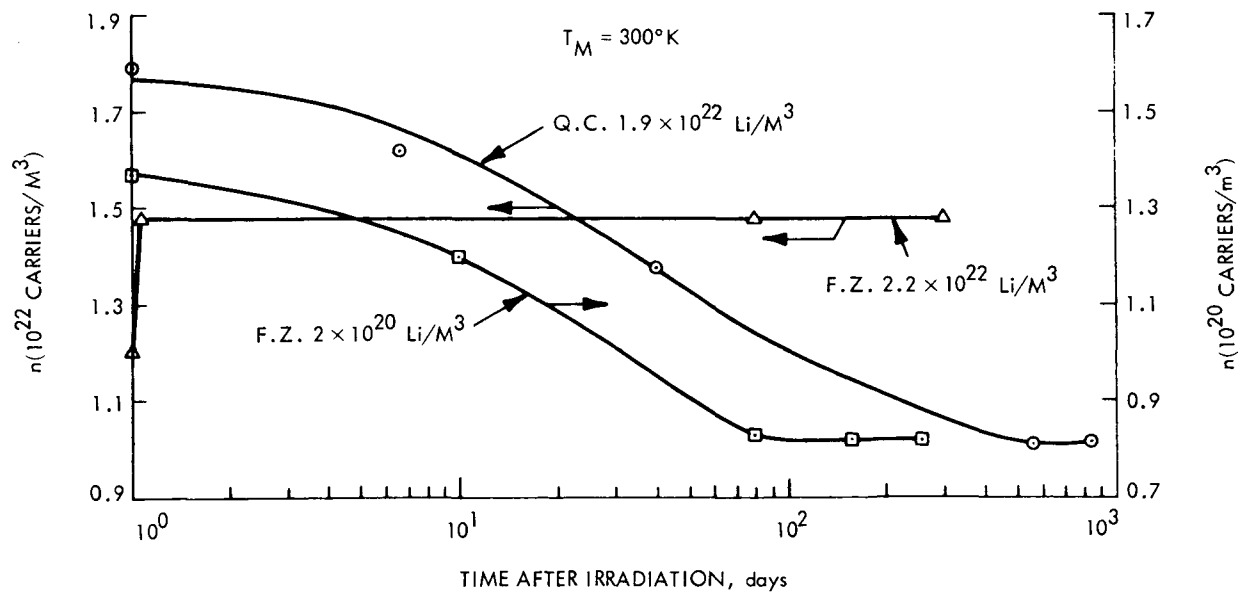

Fig. 4. Carrier density versus time after electron irradiation for samples of float-zone and quartz-crucible silicon, measured at 300 K. Initial lithium concentration is indicated for each sample

Page intentionally left blank

N72-10058

Density and Fluence Dependence of Lithium Cell Damage and Recovery Characteristics

T. J. Faith, Jr.
RCA Astro Electronics Division
Princeton, N. J.

ABSTRACT

Experimental results on lithium-containing solar cells point toward the lithium donor density gradient dN_L/dw as being the crucial parameter in the prediction of cell behavior after irradiation by electrons. Recovery measurements on a large number (180) of oxygen-rich and oxygen-lean lithium cells fabricated by all three manufacturers have confirmed that cell recovery speed is directly proportional to the value of the lithium gradient for electron fluences ranging from 3×10^{13} e/cm^2 to 3×10^{15} e/cm^2. An approximate relationship between the time to half recovery, θ, (at room temperature) the lithium gradient, dN_L/dw, and the 1-MeV electron fluence Φ was derived for oxygen-rich cells:

$$\theta \, dN_L/dw \approx 2.7 \times 10^{12} \Phi^{0.57} \text{ days/cm}^4$$

which holds for the entire range of fluences tested. For oxygen-lean (Centralab and Heliotek) cells the relation

$$\theta \, dN_L/dw \approx 8.5 \times 10^{8} \Phi^{0.61} \text{ days/cm}^4$$

holds up to 1×10^{15} e/cm^2, above which a more rapid increase with fluence occurs, probably due to the greater significance of lithium depletion during irradiation. A similar relationship holds for oxygen-lean Texas Instruments cells, but with a proportionality constant approximately ten times that of the cells from the other manufacturers.

Seventy oxygen-rich (C13) cells with initial performance significantly above a group of commercial 10 Ω-cm n/p cells were recently irradiated to fluences ranging from 3×10^{13} to 3×10^{15} e/cm^2. Through pre-irradiation capacitance measurements (giving dN_L/dw) and pre- and post-irradiation short-circuit current and diffusion length measurements, a relationship was derived between the diffusion length damage constant before recovery, $K_L(O)$, and dN_L/dw and Φ.

$$K_L(O) = 5.3 \times 10^{-18} (dN_L/dw)^{1/2} (1 - 0.063 \log_{10} \Phi)$$

Gradient measurements have also been correlated with lithium diffusion schedules. Results have shown that long diffusion times (≥5 h) with a paint-on source result in large cell-to-cell variations in gradient, probably due to a loss of the lithium source with time. They also indicate that this problem can be overcome either by short diffusion times or by use of an evaporated lithium source.

I. INTRODUCTION

The principal performance parameters characterizing lithium cell behavior in a radiation environment are: (1) the initial (pre-irradiation) performance levels, (2) the rate of cell degradation or damage constant, (3) cell recovery rate versus cell temperature, and (4) final photovoltaic performance after recovery from a given fluence. Under the present contract, experiments on solar cells irradiated by 1-MeV electrons have been designed with the aim of eventually relating the

above performance parameters and the manufacturers' fabrication parameters to a set of physical parameters obtainable through non-destructive measurements on unirradiated cells. This would provide the cell manufacturers with: (1) the optimum set of fabrication parameters for a given cell application, and (2) a set of quality-control tests that can be integrated into the production line.

In earlier work on this contract the dependence of recovery rate on cell temperature was obtained for both oxygen-rich and oxygen-lean lithium cells through measurements of activation energy for diffusion-length recovery (Ref. 1). For a given cell temperature, the recovery rate of short-circuit current in the 10^{14} e/cm^2 fluence range was shown to vary linearly with the lithium density gradient (Ref. 2) for both oxygen-rich and oxygen-lean cells. In recent work: (1) recovery rate versus lithium gradient measurements were extended to cover the fluence range from 3×10^{13} to 3×10^{15} e/cm^2; (2) a relationship between diffusion-length damage constant K_L, lithium gradient dN_L/dw, and 1-MeV electron fluence Φ were obtained through measurements on seventy irradiated cells of lot C13, and (3) pre-irradiation capacitance measurements on one hundred C13 cells established relationship between fabrication parameters (temperature and time of lithium diffusion) and the degree of control of the lithium density gradient, dN_L/dw, near the junction.

II. INITIAL CELL PERFORMANCE

A shipment of one hundred high performance lithium cells fabricated from quartz-crucible silicon (lot C13) were recently received from JPL. They consisted of ten groups (C13A to C13J), ten cells per group, with varying lithium diffusion temperatures and diffusion times. Lithium density gradients were obtained from reverse-bias capacitance measurements (Ref. 3) on all of the C13 cells. Some of the individual groups showed large cell-to-cell variations in gradient. This finding and its relationship to the individual cell groups will be discussed later in the paper; in this section the cells are divided into three batches according to lithium gradient, without distinctions between groups. The three photovoltaic parameters, maximum power, P_{max}; short-circuit current, I_{sc}; and open-circuit voltage, V_{oc}, are plotted in Figs. 1, 2, and 3, respectively. For these figures the cells were divided into batch 1, consisting of 20 cells with gradient ranging from 0.65×10^{18} to 3.3×10^{18} cm^{-4}; batch 2, with 40 cells ranging from 3.3×10^{18} to 9.0×10^{18} cm^{-4}; and batch 3, with 40 cells ranging from 9.0×10^{18} to 1.6×10^{19} cm^{-4}.[1]

The data points appear along the abscissa at the average value of dN_L/dw for the batch and the five ordinates represent (from top to bottom) the highest value, the values exceeded by 20, 50, and 80% of the cells, and the lowest value for the batch. Equivalent values for a batch of 20 commercial 10 Ω-cm N/P cells are shown on the left in each figure. The general trends show the power and short-circuit current to remain approximately constant over the first two batches, then drop with batch 3, while the open-circuit voltage increases monotonically with gradient. The maximum power of all lithium batches exceeds that of the n/p batch, most of this advantage being due to the higher V_{oc} which is due, in turn, to the heavier base doping in the lithium cells.

III. DAMAGE CONSTANT

Seventy of the C13 cells were irradiated with 1 MeV electrons; seventeen cells to a fluence of 3×10^{13} e/cm^2, nine to 1×10^{14} e/cm^2, twenty to 3×10^{14} e/cm^2, eight to 1×10^{15} e/cm^2, and sixteen to 3×10^{15} e/cm^2. The cells were chosen so that seven cells from each group were irradiated, and so that the cells irradiated to 3×10^{13} e/cm^2, 3×10^{14} e/cm^2 and 3×10^{15} e/cm^2 covered the widest possible range of lithium gradients. Room-temperature photovoltaic characteristics under 140 mW/cm^2 tungsten illumination were taken on all cells immediately after irradiation. The cells were then stored at 80°C to recover.

A number of interesting results were obtained from the short-circuit current readings made immediately after irradiation (before recovery). This current is plotted in Fig. 4 versus lithium donor density gradient, dN_L/dw, for the seventy irradiated cells. Within the scatter of the data, the points at each fluence fit well along a straight line, all five lines having approximately the same slope. A best least-squares fit to the equation

$$I_{sc} = I_A - B \log_{10} (10^{-18}\, dN_L/dw) \qquad (1)$$

was calculated for each fluence.

The values of B were found to be 8.4, 8.7, 8.4, 8.5 and 8.9 for $\phi = 3 \times 10^{13}$, 1×10^{14}, 3×10^{14}, 1×10^{15}, and 3×10^{15} e/cm^2, respectively. These equations give a specific relation between the amount of initial damage (before recovery) and the lithium gradient in crucible-grown cells. It is advantageous to describe this damage in terms of a more standard quantity, namely the diffusion-length damage constant before recovery, $K_L(O)$, given by

$$K_L(O)\Phi = \frac{1}{L(O)^2} - \frac{1}{L_0^2} \qquad (2)$$

where L_0 and $L(O)$ are the diffusion lengths in the base region of the cell before irradiation and immediately after irradiation, respectively. To obtain $K_L(O)$, the relationship between I_{sc} and L must be known; Fig. 5 gives such a plot for C13 cells. The data for this figure was generated from simultaneous short-circuit-current and diffusion length[2] measurements (Ref. 4) made on the C13 cells, 30 of which were unirradiated, the other

[1] Batch 1 has the smaller number of cells because of the comparatively small fraction of cells in the low gradient range.

[2] Obtained from measurements using band-gap light that was calibrated with the electron-voltaic method using 15 different lithium and N/P solar cells.

70 being at various stages of recovery after irradiation. The best fit to this data is

$$I_{sc} = 34.4 \log_{10} L \qquad (3)$$

For fluences above 3×10^{13} e/cm^2, $1/L(O)^2 \gg 1/L_0^2$ in Eq. (2) and the latter term can be dropped with less than 10 percent error. This approximation, combining Eqs. (1), (2) and (3), and using B = 8.6 in Eq. (1), gives

$$K_L(O) = \frac{10^{-(1+I_A/17.2)}}{\Phi} \sqrt{\frac{dN_L}{dw}} \qquad (4)$$

which is valid for all of the fluences employed except $\Phi = 3 \times 10^{13}$ e/cm^2. For this lowest fluence $K_L(O)$ was calculated taking L_0 into account. The result, which is shown in Fig. 6, was

$$K_L(O) = 8.5 \times 10^{-19} \sqrt{dN_L/dw} \qquad (5)$$

Equations (4) and (5), together with the appropriate values of I_A listed in Fig. 4, give the fluence dependence of $K_L(O)$, which is plotted in Fig. 7 for $dN_L/dw = 10^{18}$ cm^{-4}. Figure 7 shows a logarithmic dependence on fluence described (for $dN_L/dw = 10^{18}$ cm^{-4}) by

$$K_L(O) = 5.3 \times 10^{-9}(1 - 0.063 \log_{10} \Phi) \qquad (6)$$

Inserting the lithium gradient dependence, the expression for K_L as a function of Φ and dN_L/dw is given by

$$K_L(O) =$$

$$5.3 \times 10^{-18} (dN_L/dw)^{1/2} (1 - 0.063 \log_{10} \Phi) \qquad (7)$$

The applicability of this relationship to other crucible cells was tested using the post-irradiation data on thirteen previously irradiated cells from lot H3A. These H3A cells covered a wide range of gradients: $3 \times 10^{17} \leq dN_L/dw \leq 1.3 \times 10^{19}$ cm^{-4}; they were irradiated to a fluence of 3×10^{14} e/cm^2. Figure 8 shows $K_L(O)$ plotted against dN_L/dw for these cells. The square-root dependence on gradient is evident, the best least-squares fit being obtained with the relationship

$$K_L(O) = 4.4 \times 10^{-19} (dN_L/dw)^{1/2} \qquad (8)$$

This is within 10% of the value of 4.8×10^{-19} $(dN_L/dw)^{1/2}$ obtained for the C13 cells, as can be seen in Fig. 7, where the H3A data point is shown together with the C13 data.

The C13 cells are now recovering at 80°C. At completion of short-circuit current recovery, the effective damage constant, $K_L(R)$, after cell recovery can be computed from

$$K_L(R)\Phi = \frac{1}{L(R)^2} - \frac{1}{L_0^2} \qquad (9)$$

where L(R) is the diffusion length after recovery. There is a large uncertainty in $K_L(R)$ for low fluences since $I(R) \sim I_0$. Results at 3×10^{13} e/cm^2 show a very large scatter, $K_L(R)$ ranging from 0.5×10^{-10} to 2.0×10^{-10} e^{-1}. The results at 1×10^{-14} e/cm^2 are more coherent and show a slight increase with lithium gradient, $K_L(R)$ ranging from 1.0×10^{-10} to 1.6×10^{-10} e^{-1} for gradients ranging from 4×10^{18} to 1.6×10^{19} cm^{-4}.

IV. RECOVERY CHARACTERISTICS

Prior to the tests on the C13 cells, a large number of previously unirradiated oxygen-lean cells from past shipments were gathered and irradiated to fluences ranging from 3×10^{13} e/cm^2 to 3×10^{15} e/cm^2. Cells from Texas Instruments, Heliotek and Centralab[3] of both Lopex[4] and float-zone silicon were represented. They included a wide range of diffusion schedules and initial performance levels. After irradiation, short-circuit current was measured as a function of time on all of the cells. The purpose of the experiment was to test the validity of the previously observed (Ref. 2) linear relationship between recovery speed and lithium density gradient for a large batch of cells covering the widest possible range of lithium gradients and a wide range of fluences.

A typical short-circuit current versus time curve during recovery is shown in Fig. 9. The time to half recovery, θ, defined by

$$\frac{I(R) - I(\theta)}{I(R) - I(O)} = 0.5 \qquad (10)$$

where I(R) is the short-circuit current at peak recovery, provides the most well-defined index of (inverse) recovery rate. For the cell in Fig. 9, θ = 55 min (or 0.038 days). The values of θ for the Centralab and Heliotek cells are plotted against lithium density gradient in Fig. 10 for four fluences ranging from 3×10^{13} to 3×10^{15} e/cm^2. Included are all the cells tested from these manufacturers except those of lots C4 and C5 and those with lithium gradients greater than 10^{20} cm^{-4}. The points on these logarithmic plots

[3]Lots T3, T4, T5, T6, T7, T9, T10, H5, H7, H1A, H5A, H7A, H (NASA-furnished in 1967), C4, C5, C8F, C10C, C10F, and C11C were represented.

[4]Trademark of Texas Instruments Corp.

fit remarkably well along straight lines with minus one slope, confirming the linear relationship between recovery speed and lithium gradient. The $\theta\ dN_L/dw$ products (averaged over the cells at each fluence) are: 1.7×10^{17} days/cm^4 for 3×10^{13} e/cm^2; 3.4×10^{17} days/cm^4 for 1×10^{14} e/cm^2; 7.2×10^{17} days/cm^4 for 3×10^{14} e/cm^2, and 6.8×10^{18} days/cm^4 for 3×10^{15} e/cm^2. There are two cell lots that do not follow these curves, lots C4 and C5, which recover at a faster rate than the curves predict. However, these two lots had already been identified as mavericks in previous work (Ref. 2), having been shown to suffer open-circuit voltage instability due to a decrease in lithium gradient with time. In addition, cells with gradients greater than 10^{20} cm^{-4} (C10C and C10F cells) recovered more slowly at low fluence than predicted by the curves. A feasible explanation for this is that the gradient in these cells is not a good index of the average lithium density near the junction. The capacitance measurements on these high gradient cells give evidence of this in the form of a leveling off of the lithium density; i.e., a decrease in gradient, at distances of less than 1 μm from the junction.

Curves of θ versus dN_L/dw for oxygen-rich crucible cells are shown in the upper portion of Fig. 10. The data are drawn from previous results on cells that recovered at room temperature, 60°C, or 80°C. (In the latter two cases equivalent recovery time at room temperature was calculated using the activation energy previously obtained (Ref. 1) for crucible cell recovery.) At 1×10^{14} e/cm^2 and 3×10^{14} e/cm^2 the separation between the oxygen-lean (FZ and L) curve and the crucible curve is ≈700, which is approximately the ratio of the room-temperature lithium diffusion constant in oxygen-lean silicon to that in oxygen-rich silicon (Ref. 5). At the highest fluence, 3×10^{15} e/cm^2, the separation is only ≈250. This suggests that lithium is lost more rapidly in defect formation in oxygen-lean cells than in oxygen-rich cells, supporting previous carrier removal observations (Ref. 1) in bulk-sample measurements.

A puzzling anomaly was observed in the case of the oxygen-lean T cells. While the constancy of the $\theta\ dN_L/dw$ product was satisfied by these cells at each fluence as shown in Fig. 11, the products were approximately an order of magnitude higher than the equivalent products for the Centralab and Heliotek cells. This can be seen by comparing the products in Fig. 11 with those of Fig. 10. This discrepancy is not understood at present. One of the main differences between the manufacturers is that the TI cells have used an evaporated lithium source whereas all of the oxygen-lean C and H cells tested to date have used a paint-on source. It would seem likely that a difference in silicon type would cause differences in recovery rate. This would be particularly feasible for Lopex versus float-zone recovery since the oxygen-content is generally higher in Lopex silicon. However, as was shown in Fig. 10, the same recovery rate applies for both Lopex and float-zone C and H cells. Dislocation counts are now being made on some of the cells in an effort to confirm the silicon types employed.

The approximate linear dependence of recovery speed on lithium gradient at all the fluences tested enables prediction of the recovery speed of any lithium cell with lithium gradient between 10^{17} and 10^{20} cm^{-4} in this fluence range. This is illustrated in Fig. 12, which gives plots of the $\theta\ dN_L/dw$ products of all the cells tested versus 1-MeV electron fluence.

Below 10^{15} e/cm^2 this product increases gradually with fluence in all types of cells. In oxygen-lean cells there is a more pronounced dependence on fluence above 10^{15} e/cm^2. In the oxygen-rich cells the relation

$$\theta\ dN_L/dw = 2.7 \times 10^{12} \Phi^{0.57}\ \text{days/cm}^4 \qquad (11)$$

provides a good approximation of cell recovery speed over the entire range of fluences.

V. LITHIUM DIFFUSION SCHEDULE AND DENSITY CONTROL

From the above and previous results, it is evident that many of the characteristics of lithium cells under electron irradiation can be predicted through knowledge of the lithium density gradient, dN_L/dw. Consequently, it is desirable to find relationships between this parameter and the fabrication parameters of the cell manufacturers. This has been accomplished for cell lots C13 (100 cells) and H3A (15 cells). Lot C13 consists of 10 groups of 10 cells, comprising nine different lithium diffusion schedules with diffusion temperatures ranging from 330°C to 370°C and diffusion times from 3 to 7 h. The lithium source was a lithium-in-oil suspension painted on the back surface of the cell. Figure 13 gives the distribution of lithium gradients measured for the cells in each of the 10 cell groups. There are five separate ordinates, each running from 1 to 10. The value of the ordinate at a given lithium gradient indicates the number of cells of that particular group with a lithium gradient greater than the value of the abscissa. A pair of cell groups shares each ordinate, since two groups were diffused at each lithium diffusion temperature. Each group is identified by a letter followed by a number in parentheses which gives the lithium diffusion time in hours.

Several important factors are brought out in Fig. 13: (1) for a given diffusion temperature, the shorter diffusion time gives a narrower gradient distribution; i.e., better gradient control; (2) the gradient distribution for the shorter diffusion time is always situated near the upper limit of that for the longer diffusion time; (3) at the highest diffusion temperature, even the short time diffusion shows a rather broad distribution; and (4) the average gradient (for short diffusion times) increases with diffusion temperature. Items (1), (2), and (3) indicate that as the diffusion time increases the lithium reservoir is somehow lost to the cell, either through lithium depletion or through interruption of the lithium-silicon interface. Therefore, for lithium introduction by the paint-on technique, the shortest practical diffusion time should be used.

A previously received cell lot, H3A, consisted of 15 quartz-crucible cells diffused with lithium for 8 h at 325°C. Ten of the cells used a paint-on source; the other five, an evaporated lithium

source. The cell distribution versus lithium gradient is shown in Fig. 14. The cells using the paint-on source have a very broad distribution similar to those of the C13 cells using long diffusion times. The cells using an evaporated source, however, have a narrow distribution at the high end of the gradient scale. This supports the hypothesis of loss of the lithium source in the paint-on cells and also indicates that an evaporated source may provide the solution to this problem.

VI. CONCLUSIONS

Previous work has shown the lithium density gradient, dN_L/dw, obtained from non-destructive capacitance measurements, to be a convenient and useful way to characterize the lithium density in a lithium cell by a single parameter. The present work has investigated the relationship between this physical parameter and the performance and recovery parameters of the lithium cell. Results show that knowledge of the lithium gradient enables the prediction of recovery speed for both oxygen-rich and oxygen-lean cells within a factor of approximately 2 for 1 MeV-electron fluences from 3×10^{13} to 3×10^{15} e/cm^2.

A relationship between the diffusion-length damage constant immediately after irradiation (before recovery) $K_L(O)$, the lithium gradient, dN_L/dw, and the electron fluence, Φ, has been obtained for C13 crucible cells:

$$K_L(O) = 5.3 \times 10^{-18} (dN_L/dw)^{1/2} (1 - 0.063 \log_{10} \Phi)$$

A check on previous post-irradiation data shows that this relationship also holds for H3A cells irradiated to 3×10^{14} e/cm^2. One additional relationship, that between the damage constant after recovery $K_L(R)$, dN_L/dw, and ϕ, is required to complete the description of cell dynamics under electron irradiation. The C13 cells are now recovering, and this will be investigated upon completion of recovery.

These relations make it possible, in principle, to predict cell behavior in an electron environment using a simple non-destructive capacitance measurement. It is evident that a similar approach to predicting cell behavior under heavy particle irradiation should also be examined.

Gradient measurements have also been correlated with lithium diffusion schedules. Results have shown that long diffusion time ($\gtrsim$5 h) with a paint-on source result in large cell-to-cell variations in gradient, probably due to a loss of the lithium source with time. The results also indicate that this problem can be overcome either by short diffusion times or by use of an evaporated lithium source.

REFERENCES

1. Brucker, G., et al., Fourth Quarterly Report, RCA under JPL Contract No. 952555, July 10, 1970.

2. Faith, T., Brucker, G., and Holmes-Siedle, A., Sixth Quarterly Report, JPL Contract No. 952555. Prepared by RCA and issued Jan. 10, 1971; see also Faith, T., Corra, J. P., and Holmes-Siedle, A., Conference Record of the Eighth Photovoltaic Spec. Conf., IEEE Catalog No. 70C 32 ED, p. 247, 1970.

3. Hilibrand, J., and Gold, R. D., RCA Rev. Vol. 21, p. 245, 1960.

4. Rosenzweig, W., Bell Sys. Tech. J., Vol. 41, p. 1573, 1960.

5. Pell, E. M., J. Appl. Phys. Vol. 31, p. 291, 1960; Vol. 32, p. 6, 1961; and Phys. Rev. Vol. 119, p. 1222, 1960.

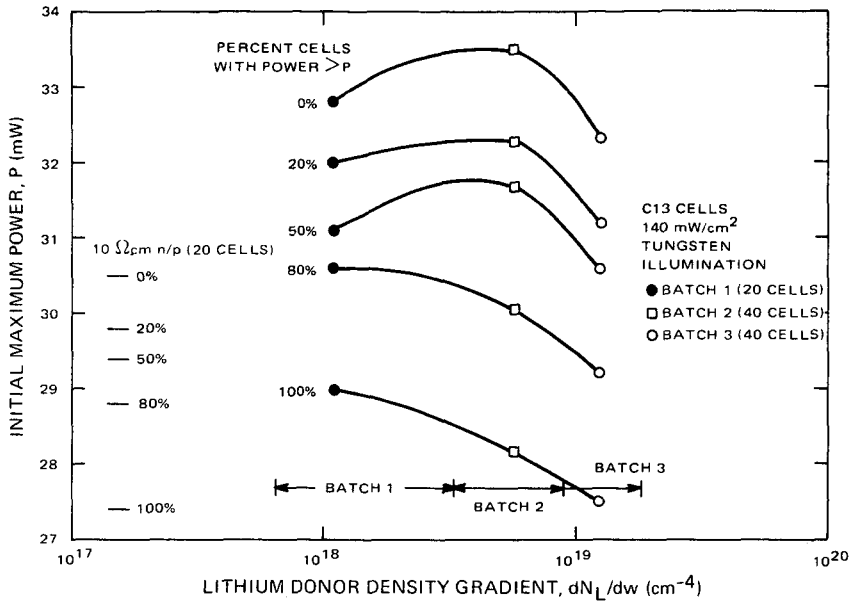

Fig. 1. Initial maximum power distributions for C13 quartz-crucible lithium cells versus lithium donor density gradients with comparisons of 10 Ω-cm commercial N/P cells

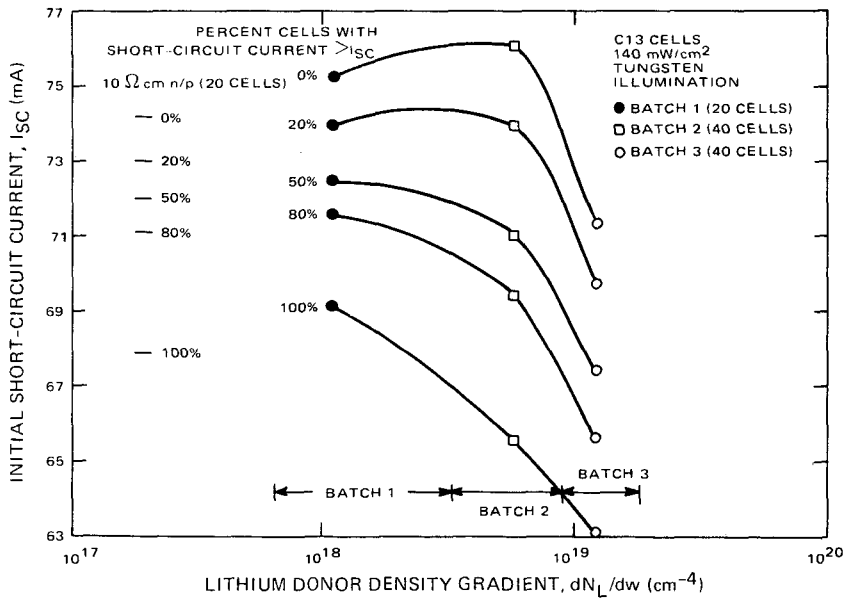

Fig. 2. Initial short-circuit current distributions for C13 quartz-crucible lithium cells versus lithium donor density gradients with comparisons of 10 Ω-cm commercial N/P cells

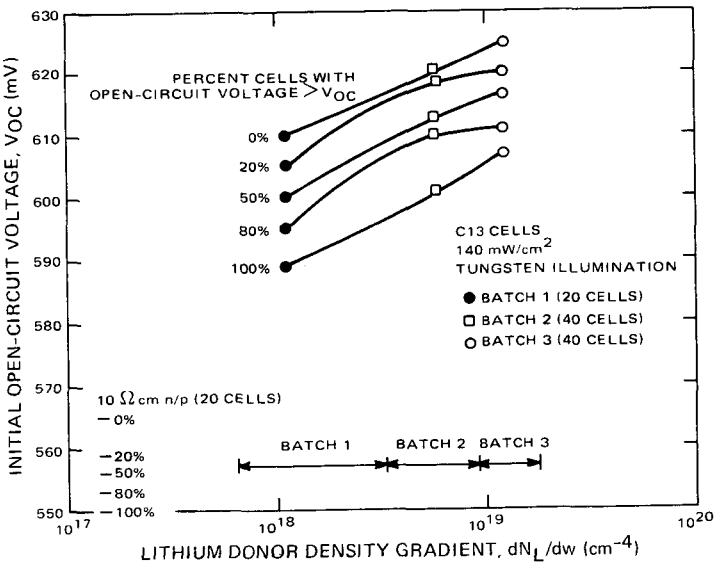

Fig. 3. Initial open-circuit voltage distribution for C13 quartz-crucible lithium cells versus lithium donor density gradients with comparisons of 10 Ω-cm commercial N/P cells

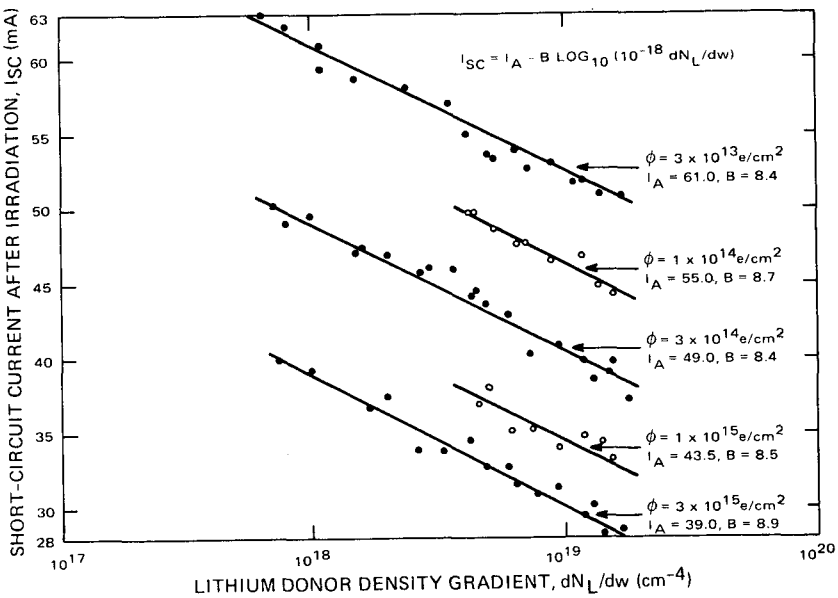

Fig. 4. Short-circuit current immediately after irradiation versus lithium density gradient for seventy C13 cells irradiated by 1-MeV electrons to fluences ranging from 3×10^{13} e/cm^2 to 3×10^{15} e/cm^2

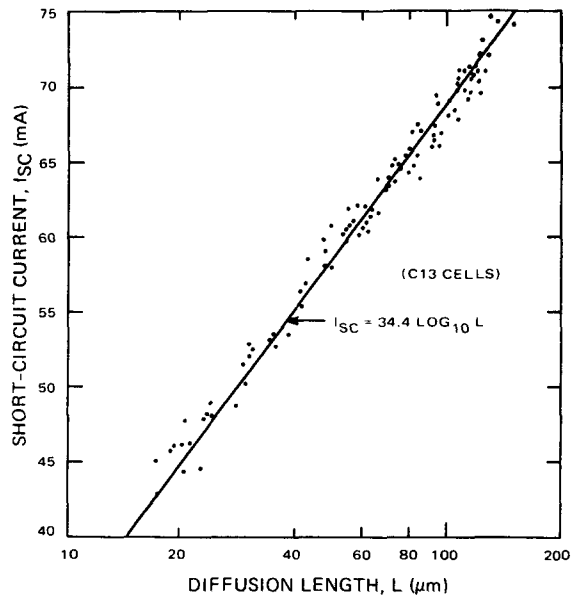

Fig. 5. Short-circuit current versus diffusion length for 100 crucible C13 cells (30 cells unirradiated, 70 cells at various stages of recovery after irradiation)

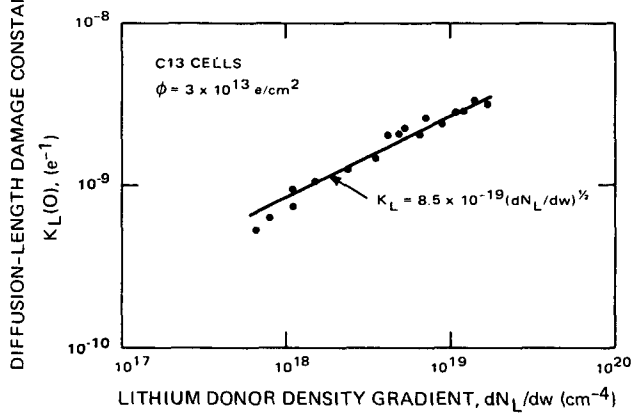

Fig. 6. Diffusion-length damage constant immediately after irradiation (before recovery) versus lithium gradient for seventeen C13 cells irradiated to a fluence of 3×10^{13} e/cm^2

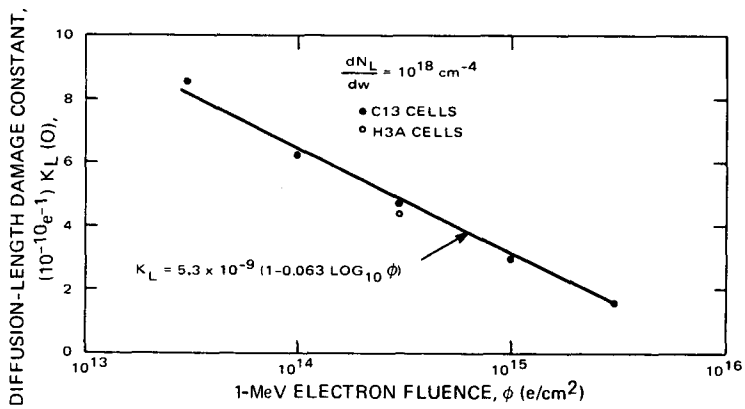

Fig. 7. Diffusion-length damage constant immediately after irradiation (at $dN_L/dw = 10^{18}$ cm^{-4}) versus 1-MeV electron fluence for C13 and H3A cells

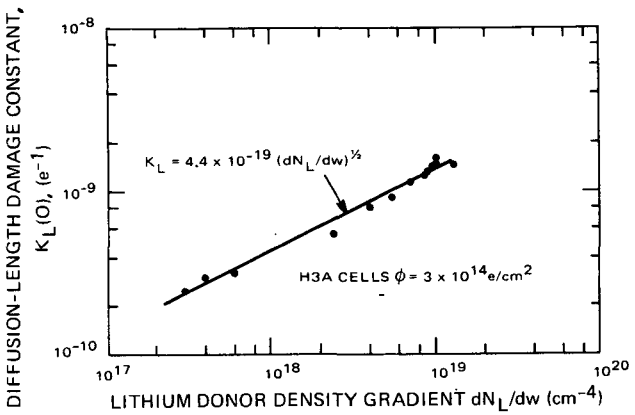

Fig. 8. Diffusion-length damage constant immediately after irradiation versus lithium gradient for H3A cells irradiated to a fluence of 3×10^{14} e/cm^2

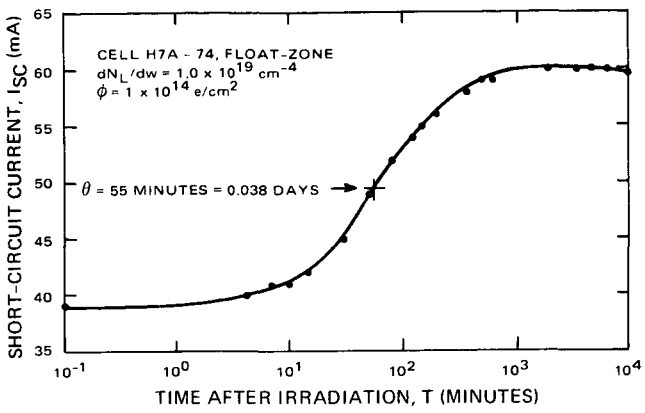

Fig. 9. Typical short-circuit current recovery curve illustrating the index of cell recovery rate θ used in subsequent illustrations

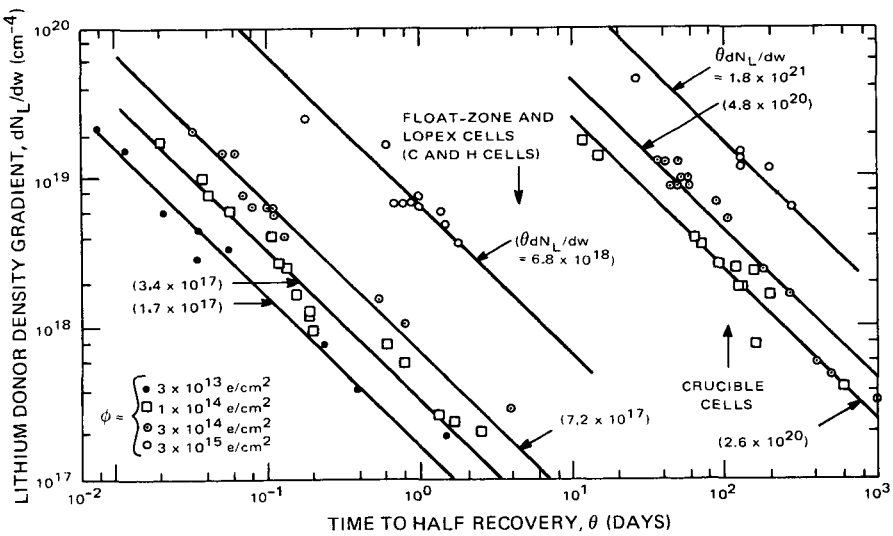

Fig. 10. Time to half recovery at room temperature versus lithium gradient for oxygen-rich cells and for Centralab and Heliotek oxygen-lean cells irradiated to fluences ranging from 3×10^{13} to 3×10^{15} e/cm^2

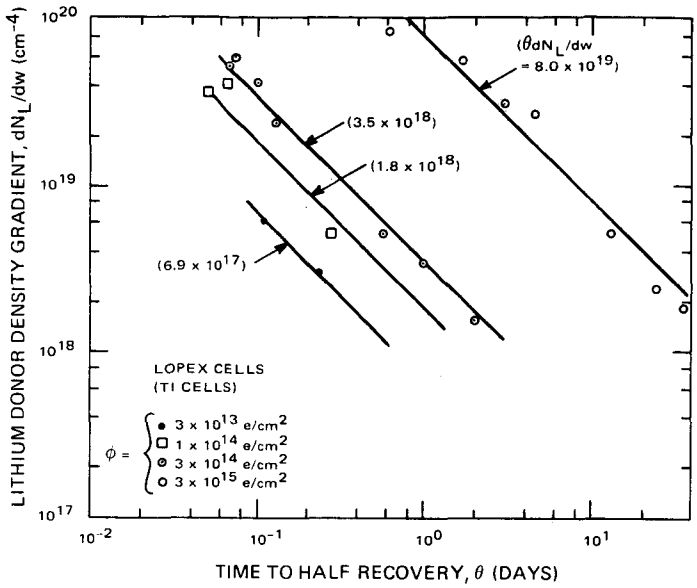

Fig. 11. Time to half recovery at room temperature versus lithium gradient for oxygen-lean Texas Instruments cells irradiated to fluences ranging from 3×10^{13} to 3×10^{15} e/cm^2

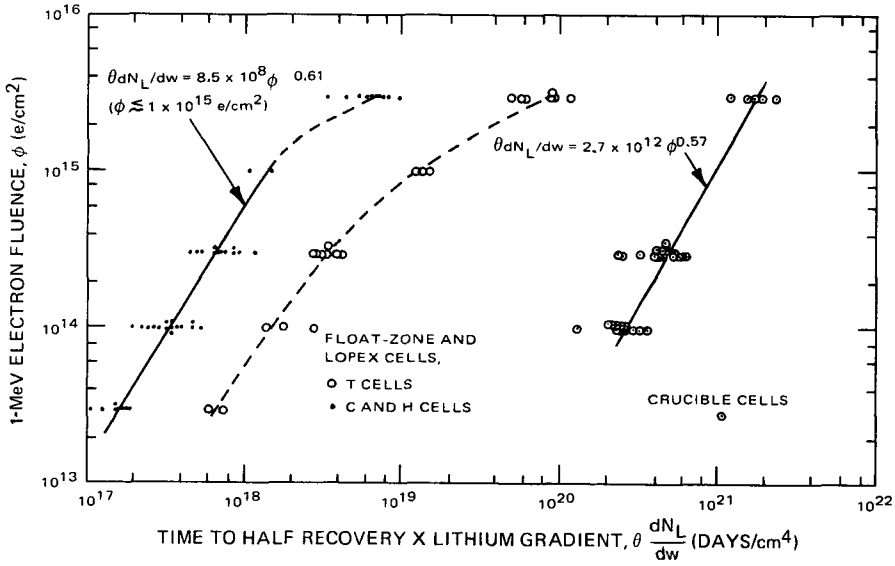

Fig. 12. Product of time to half recovery and lithium gradient, θ dN_L/dw plotted versus 1-MeV electron fluence for oxygen-rich and oxygen-lean lithium cells

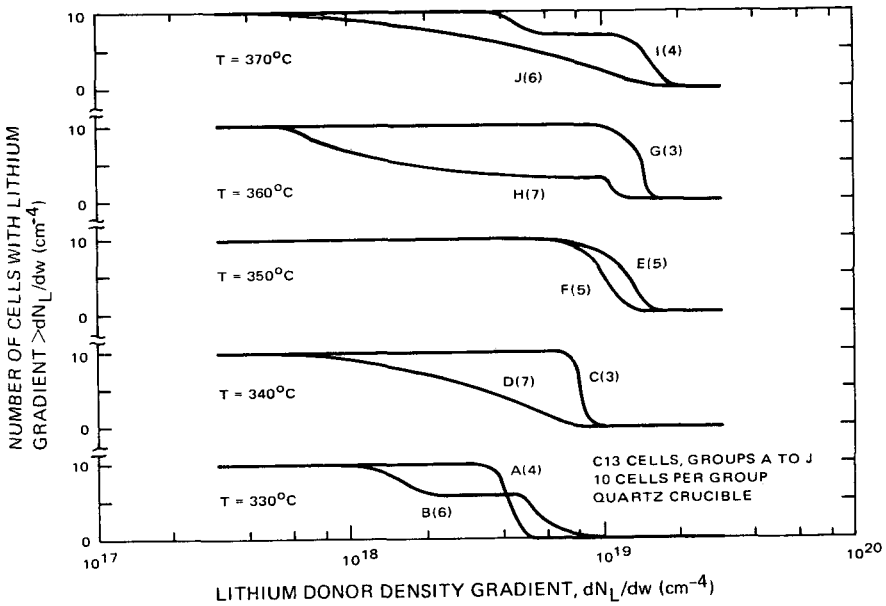

Fig. 13. Distribution of cells versus lithium gradient for the ten different cell groups within Lot C13. Numbers in parentheses indicate duration of lithium diffusion in hours; T = diffusion temperature

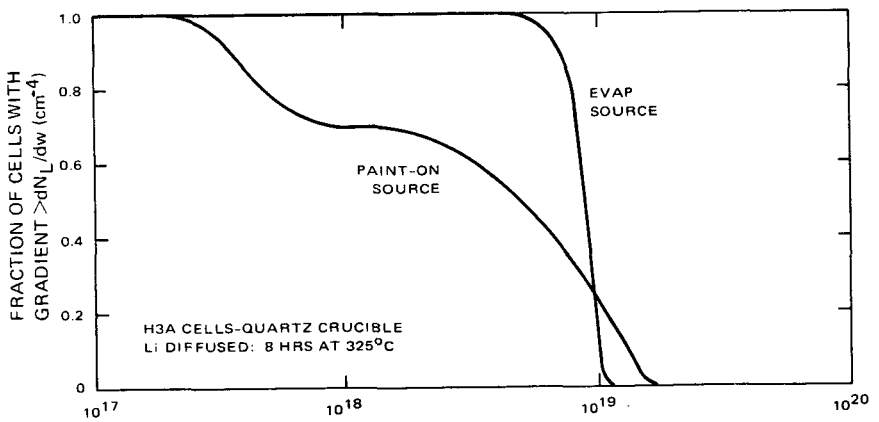

Fig. 14. Distribution of cells versus lithium gradient for H3A cells using two different lithium sources, paint-on and evaporated

Page intentionally left blank

DEGRADATION AND RECOVERY MECHANISMS IN LITHIUM-DOPED SOLAR CELLS*

R. G. Downing and J. R. Carter, Jr.
TRW Systems Group
Redondo Beach, California

I. INTRODUCTION

Several large groups of lithium-doped solar cells were received from JPL for radiation hardness evaluation. These cells included some of the most advanced devices produced to date. The evaluations consisted of the determination of the lithium concentrations in the devices and the effect of irradiations with 3×10^{14} and 3×10^{15} e/cm^2 with 1-MeV electrons. In addition some studies were performed using 28-MeV electrons. Capacitance measurements were used to systematically study the changes in lithium concentration which occur during irradiation and recovery.

II. LITHIUM-DOPED SOLAR CELL EVALUATION

During the past year, lithium-doped solar cells from Centralab and Heliotek have been irradiated with 1-MeV electrons and their recovery characteristics have been studied. Several different processing techniques were represented in these cells, including different diffusion gases and varying percentage of lithium coverage of the rear surface. Data for cell groups C11A through C11D, H1A, H2A, H4A, H5A1, H5A2 and H5A3, are listed in Table 1. All of the cells received radiation exposure to 1-MeV electrons. Tungsten I-V characteristics and capacitance versus voltage measurements were then obtained as a function of time at either room temperature or 60°C. The general radiation damage and recovery characteristics of each cell group are summarized in Tables 1 and 2. The recovered levels given in the tables are the peak of the recovery curve and do not take into account any redegradation that may have occurred. In general, it can be observed that the higher lithium concentrations result in lower initial characteristics, higher recovered levels, and more rapid annealing rates, whereas with lower lithium concentrations, higher initial and slower recovery rates exist. It should be noted that most cell groups tested were superior to the contemporary N/P cells in recovered level. The initial short-circuit current of many of the cells studied was inferior to the contemporary N/P cells.

A. Centralab Cells

The Centralab cells submitted for evaluation were all fabricated from quartz-crucible-grown silicon, with the exception of group C11C. The variable of boron dopant gas was investigated by diffusing the P-type front surface with boron trichloride in the case of group C11A and boron tribromide in the case of group C11B. The short-circuit current values of cells received in group C11B were rather low (53 mA) compared to that group C11A. This difference is not believed to be related to the use of boron tribromide. It is known that when Texas Instruments manufactured solar cells, their P-type diffusions were made with boron tribromide. A second important difference between the cells of these two groups is concentration of lithium found at the junction. Although the cells of both C11A and C11B groups were lithium diffused in the same manner (480 min at 325°C), the data in Table 2 indicates that group

*This work was performed for the Jet Propulsion Laboratory, California Institute of Technology, sponsored by the National Aeronautics and Space Administration under Contract No. NAS 7-100.

C11A contains twice the lithium concentration of group C11B. This difference is not considered to be related to use of boron tribromide. The effect of this lower lithium concentration can be seen in the 60°C recovery data in Table 2. The cells of group C11A are nearly fully recovered 200 h after irradiation; however, those of C11B appear to be only half recovered at a comparable recovery time. This slower recovery is probably due to the lower lithium concentration. The recovered I_{sc} values of the C11A group cells are 38 mA after irradiation of 3×10^{15} e/cm^2. The value is significantly better than the comparable data for conventional N/P cells. Recovery in the C11B group has not progressed sufficiently to determine final recovered I_{sc} value.

The cells of group C11D were lithium diffused at the slightly higher temperature of 375°C for 180 min. This diffusion schedule resulted in a higher concentration of lithium at the junction. These cells have about 5×10^{14} lithium atoms/cm^3. The C11A cells diffused at 325°C for 480 min had only 3×10^{14} Li/cm^3. It is also noted that slope of the log capacitance versus log voltage is -0.26. This is the lowest value found in the current group of cell under evaluation. The high lithium concentrations in group C11D are reflected in a slightly more rapid recovery after irradiation. The initial I_{sc} values of the cells in groups C11A and C11D are comparable with those of conventional N/P solar cells. The cells of groups C11A, C11B, and C11D are interesting in that they have the lowest lithium concentrations of any quartz-crucible-silicon cell evaluated by TRW. The relatively poor performance of cells in group C11B indicate that for this type of cell, the concentration of lithium at the junction should be kept above 2×10^{14}/cm^3.

The remaining Centralab group, C11C, was fabricated from Lopex (low oxygen, low dislocation) silicon. In general, the performance of the group was very good. The cells were lithium diffused at 325°C for 480 min. The resulting lithium concentration in this group was 1.5×10^{14}/cm^3. The results of the 3×10^{14}e/cm^2 and 3×10^{15}e/cm^2 radiations are shown in Table 1. In both cases, the I_{sc} recovered to values greater than those of comparably irradiated N/P solar cells, as shown by the dashed lines on these graphs. Although the recovery kinetics are relatively slow in these cells, due to the lower lithium concentration, the irradiated cell performance is among the best received to date.

The cells from the C13 series, manufactured by Centralab, represent a matrix of lithium diffusion temperatures and times. The matrix is designed to investigate the optimum lithium diffusion and the reproducibility of the process. All the cells were fabricated from quartz crucible grown silicon with resistivities between 25 and 40 Ω-cm. The diffusion matrix is shown in Table 2. Also shown in the table are the mean donor concentrations at the junction of the cells of each group in the matrix. The voltage-capacitance relationship or range of relationships is also shown for each group. The donor concentrations were determined by means of capacitance. Since the phosphorus concentration is approximately 1.5×10^{14} atoms/cm^3, the lithium concentrations were estimated by subtracting the phosphorus concentration from the donor concentrations. Since the phosphorus concentration may go as high as 2×10^{14} atoms/cm^3 (i.e., 25 Ω-cm), some groups may contain cells with very low lithium concentrations. Specifically these are the cells which received diffusions of 6 or 7 h. It can also be observed that both higher temperatures and longer diffusion times result in greater variations in lithium concentration.

It can be seen from the data in Table 2 that, in the time span studied, the lithium concentrations at the junction are decreasing with time. Such a decreasing lithium concentration is inconsistent with diffusion from an infinite source. Since the donor concentration originally was equal to the phosphorus concentration, it was necessary for the donor concentration to rise from the original to a maximum before declining. This decrease in lithium concentration with diffusion time is characteristic of diffusion from a starved source. As the lithium source is exhausted, the surface concentration of the cells will decrease and concentrations at the junction will decrease. In the past, manufacturers of lithium solar cells have interrupted the lithium diffusion and removed the lithium source to produce starved source diffusion. This second diffusion has been referred to as a redistribution. The data in Table 2 indicate that redistribution is not necessary. It is not clear what causes the exhaustion of the lithium source.

Three cells of each C13 series group were irradiated with 3×10^{15}e/cm^2 (1 MeV) and were allowed to recover at 60°C. The most pronounced changes during recovery occur in the short-circuit current. The open-circuit voltages of nearly all cells in the C13 series were about 0.6 V. After a 3×10^{15}e/cm^2 irradiation, the V_{oc} was reduced to about 0.45 V in all cases. Very little recovery is subsequently observed in this parameter. The changes in I_{sc} for cells of the C13 series are shown in Table 2. Several general observations can be made about these cells. With a few exceptions, the 3×10^{15}e/cm^2 irradiation reduced the I_{sc} to 20 to 25 mA. In most cases, the time necessary for the I_{sc} to reach the half recovery point was 100 to 200 h at 60°C. This time is somewhat longer than what was previously found in similar cells. Except for cells with low lithium concentration, most cells ultimately recover to I_{sc} values of 35 to 40 mA. The most important factor in the extent of the recovery is the lithium concentration at the junction rather than the diffusion schedule. As previously noted, the shorter low-temperature diffusions produce the more consistent results. The donor concentration of each cell irradiated is noted in Table 2.

B. Heliotek Cells

All Heliotek cells received for evaluation during the past quarter were fabricated from either floating zone or Lopex silicon and, therefore, had lower oxygen concentrations. There are two different experimental variables represented in these Heliotek cells. Two groups (H1A and H4A) were diffused at lower temperatures: 325°C lithium diffusion for 480 min. Group H2A was lithium diffused at 425°C for 90 min with a 120-min redistribution cycle. This latter diffusion schedule has been used extensively in the past and can be regarded as control. The capacitance measurements results from the H1A group, shown in Table 1, indicate that very little or no lithium

reached the junction. For this reason the irradiation recovery results shown in Table 1 are very poor. Although some recovery is observed after 3×10^{14}e/cm^2, the higher fluence of 3×10^{15} e/cm^2 exhausts the lithium and no recovery is observed. These results are in direct conflict with those for group H4A which had an identical history. The H4A cells had approximately 5×10^{14} lithium atoms/cm^3 at the junction, and exhibited satisfactory recovery as shown in Table 1. The recovered I_{sc} values of the H4A cell would probably have been higher if the before-irradiation I_{sc} values had been higher than 46 mA. This condition is not necessarily a result of the lithium diffusion, as other cells with similar lithium concentrations have initial I_{sc} values in excess of 60 mA. Despite this difficulty, the data indicated that cells of group H4A recover to I_{sc} values of 40 mA after a fluence of 3×10^{15}e/cm^2. This is considerably higher than a comparable irradiated N/P solar cell.

The irradiation recovery results for the cells of group H2A are shown in Table 1. As mentioned previously, this lithium diffusion schedule has previously been used many times to produce superior lithium cells. The results in Table 1 confirm that such cells exhibit excellent I_{sc} values when recovered from an irradiation. The results in the case of the 3×10^{15}e/cm^2 fluence are particularly interesting in that the recovered I_{sc} reached a value of 44 mA. The fact that these cells were fabricated from Lopex silicon as opposed to float-zone silicon is not considered significant.

The remaining groups of Heliotek cells represent a series of experiments to determine the effectiveness of area coverage during the application of lithium diffusion source material to the back of the cell. Groups H5A1, H5A2, and H5A3, respectively, received 100, 80, and 50% back surface area coverage. The results of this experiment are very interesting for comparative analysis. The first point of interest is the measured lithium concentrations at the junctions of the various groups as seen in Table 1. The cells with 100% coverage (H5A1) have approximately 6×10^{14} lithium atoms/cm^2 at the junction. The groups which received less coverage (H5A2, H5A3) had roughly half the above lithium concentration. The results indicate quite clearly that decreased area coverage reduces the concentration of lithium at the junction. The relationship does not appear to be linear, since the cells with 80% coverage (H5A2) have lithium concentrations nearly as low as those with 50% (H5A3). It can be concluded that incomplete area coverage with the lithium source material significantly reduces the lithium concentration at the junction. It is also of interest to compare the cells of these groups to cells of other groups. The cells of group H2A were made with the same material and diffusion schedule, but presumably no control on area coverage. The data in Table 1 indicate the H2A cells had much lower lithium concentrations than any of the cells in H5 groups. It must be concluded that there are other unknown factors which extend strong influences on the concentration of lithium reaching the junction. One possible factor could be the chemical activity of the lithium in the source material.

The effects of various lithium source area coverages on radiation response can be seen in Table 1. The initial I_{sc} values of these cells are all relatively low. The values average approximately 51 mA. This parameter influences radiation recovery behavior, because the maximum recovered parameters can only approach and not exceed their initial values. Despite this problem, the cells of group H5A1 (100% coverage) recovered to a maximum I_{sc} of 50 mA after an irradiation of 3×10^{14}e/cm and 39 mA after 3×10^{15}e/cm^2. In both cases these values are above those of similarly irradiated conventional N/P solar cells. The H5A1 cells, irradiated with 3×10^{14}e/cm^2, show some redegradation of I_{sc} after the maximum was reached. The radiation recovery of cells of group H5A2 (80% coverage) was not drastically altered by the reduced coverage. The cells of group H5A2 which were irradiated with 3×10^{14} e/cm^3 recovered to I_{sc} values of 45 mA. The recovery probably would have exceeded the above value if the initial I_{sc} value had been greater than 46 mA. The 3×10^{15}e/cm^2 irradiation of H5A2 cell allowed the I_{sc} recovery to 39 mA after irradiation. This value is equal to that achieved in the group having 100% coverage (H5A1). This result is difficult to explain, considering the lower lithium concentration and the studies of D. L. Kendall at Texas Instruments which indicated very little lateral spreading of lithium during diffusion. The results for cells of H5A3 (50% coverage) show comparable performance after 3×10^{14}e/cm^2 (Table 1). In the case of the higher electron fluence on the H5A3 cell, the recovered I_{sc} values were significantly reduced. It appears that incomplete coverage with diffusion source material does not reduce recovery behavior, except in extreme cases.

III. ELECTRON ENERGY DEPENDENCE OF LITHIUM-DOPED CELL RECOVERY

Most of the studies of radiation behavior of lithium-doped cells have been done with a 1-MeV electron environment. With the exception of a few studies with reactor neutrons and one early study with protons, there is a complete lack of much of the data needed to accurately predict behavior in space. One area in which more data are desirable is response of these cells to electrons with energies greater than 1-MeV. Through the courtesy of Dr. J. A. Naber of Gulf Radiation Technology, several lithium-doped cells were irradiated with 28-MeV electrons.

Because of the necessary delays between the irradiation at the Gulf facilities and analysis at TRW, cells made from quartz-crucible-grown silicon were selected because of their slow recovery rate at room temperature. This allowed the cells to be mailed to TRW before any post-irradiation recovery occurred. The cells used in this experiment were from the C11D series, manufactured by Centralab. These cells are considered to be typical of good lithium-doped cells and adequate 1-MeV electron data had previously been obtained. Cells were irradiated with 3×10^{14} and 3×10^{15}e/cm^2. The I_{sc} recovered at 60°C to 46 and 31 mA, respectively, for the two fluences. The degraded and recovered I_{sc} values as a function electron fluence are shown in Fig. 1. The previously accumulated 1-MeV data are also shown and typical 1- and 28-MeV data for a 10 Ω-cm N/P solar cell are also shown as dashed lines. The dotted line indicates the I_{sc} value (38 mA) at which the critical fluence has been arbitrarily defined. It has been observed that all solar cells are

2A

degraded by penetrating radiation at a rate of about 6.5 mA/cm^2 under tungsten illumination for each decade of fluence added. It is apparent that the initially degraded I_{sc} values of the lithium-doped cells decrease at a much smaller rate. In this case, the lower rate is probably due to annealing of defects which occurs during the irradiation. After the 60°C recovery, the I_{sc} of the lithium-doped cells decline 13 mA per decade of fluence. The important point in Fig. 1 is that, while at 1-MeV the lithium cells are slightly superior to the conventional N/P cell, at 28-MeV the lithium cell will withstand over ten times the fluence before being degraded to the same I_{sc} value of a similarly irradiated conventional cell.

IV. LITHIUM-DOPED SOLAR CELL REMOVAL RATE STUDIES

During the past quarter, extensive capacitance studies were made on Heliotek and Centralab cells previously evaluated under 1-MeV electron irradiation. By using techniques previously discussed in reports of this series, the donor concentration in the N-type base can be determined as a function of distance into the base. These studies can be made before irradiation, after irradiation, and after recovery. In this manner the changes in carrier concentration occurring during irradiation and recovery can be determined. These data can be of use in the construction of physical models of the damage and recovery processes and to provide information for the design of improved solar cells. The basic equation used in the analyses is

$$N_d = \frac{SVC^2}{q\epsilon}$$

where

N_d = donor concentration
V = voltage
C = capacitance
q = electronic charge
ϵ = dielectric constant

The factor S is related to the exponent of the $k = VC^n$ relationship for the cell.

A capacitance study was done on Centralab cells from the C11C group. These cells were fabricated from Lopex silicon and showed excellent initial and recovery characteristics. The phosphorus concentration of the silicon was approximately 6×10^{13}/cm^3. The before-irradiation data indicate a very much lower donor concentration compared to other cells which have exhibited good recovery. Cell C11C-7 and C11C-3 were irradiated with 3×10^{14} and 3×10^{15}e/cm^2 electrons, respectively. After recovery from an irradiation of 3×10^{15}e/cm^2, the donor concentration is approaching the phosphorus concentration. This indicates near exhaustion of lithium donors. The removal rates were calculated for these cells and are plotted in Fig. 2 as a function of barrier width. The removal rates are of interest in this case because of the two different electron fluences used. Although there was some difference in lithium concentration between the two cells, the differences in removal can be considered to be largely due to differences in fluence. One might expect that the removal rates would be relatively independent of electron fluence, if the behavior is based upon discrete solid-state reactions in which one atomistic species reacts stoichiometrically with another. The fact that during satisfactory recoveries the removal rate has been observed to vary between 1.5 to 4 times that observed during irradiation, indicates that no discrete quantity of lithium appears to react with the radiation products. The data in Fig. 2 indicate that in C11C cells, the removal rates during irradiation and recovery from a 3×10^{14}e/cm^2 fluence are significantly greater than those resulting from a 3×10^{15}e/cm^2 fluence. Not only are the removal rates lower with the higher fluence, but the ratio of the rates during recovery and irradiation decrease from 4 to 2 when the fluence is increased from 3×10^{14} to 3×10^{15}e/cm^2. It is obvious that the models which we have proposed in the past must be modified to account for the widely varying removal rates which we have observed in cells made from low-oxygen silicon.

Our analysis of lithium distributions also included two cells made from silicon grown from quartz crucibles. Our previous studies have shown that the very small removal rate observed during irradiation of this type cell can be explained by the production Si-A centers (oxygen-vacancy pairs) with an introduction rate of about 0.2 cm^{-1}. The two cells (C11A-13, C11D-3) had previously exhibited excellent recovery when irradiated with 3×10^{15}e/cm^2. The result indicated a very low removal rate during irradiation of both cells. This is because the concentrations of Si-A centers produced are barely detectable in these donor concentrations. Much larger changes in donor concentration occur during the recovery phase. To further study possible relationships, the removal rate data are replotted in Fig. 3 as a function of lithium concentration present at the particular barrier width position after irradiation. In addition similar data from a cell (H14-4921) analyzed during our previous years work are added to Fig. 3.

It can be seen from the data of the three cells shown in Fig. 3 that the removal rate during recovery is directly proportional to the concentration of lithium present at that point in the cell. Since our previous work has shown that Si-A centers are introduced uniformly throughout the active N-type area of the cell, it must be concluded that the amount of lithium which reacts with the radiation produced defects is independent of the concentration of Si-A centers. The earlier proposed models involved the reaction of one or possibly two lithium donor atoms with a Si-A center. It is clear that this model will require considerable modification. It is possible that precipitation rather than ion pairing may be the basis of the recovery reaction. It has already been proposed that the O-V vacancy pair is the nucleation site for the precipitation of lithium in silicon and germanium. In such a process the quantity of lithium donors reacting during recovery would be independent of the number of radiation defects, and the ratio of lithium donors reacting during recovery to the number of radiation defects could vary considerably.

Using previously described capacitance versus voltage methods, the donor concentrations at various distances into the N-type base were determined

before and after irradiation and during the recovery process. The results of such a study of cell C13D-1 are shown in Fig. 4. After 720 h the recovery process, as indicated by the I_{sc} is nearly complete and the changes in donor concentration have diminished. To allow a more systematic study of the lithium donor changes, the data for specific barrier widths were reduced to lithium donor concentration and normalized to that present immediately after an irradiation with 3×10^{15} e/cm^2. These data are shown as a function of time after irradiation, at three different points in the cell, in Fig. 5.

The mathematical form of the change in lithium concentration with time could indicate information regarding the nature of the recovery process. The data in Fig. 5 are plotted in semilog form to detect any relationship between the logarithum of the lithium concentration and the time elapsed. Such relationships may indicate first-order chemical kinetics or some aspects of the precipitation of a second phase. The data in Fig. 5 indicate that the lithium concentration decreases in a nearly straight line form until half of the lithium donors have reacted. The rate of reaction appears to slow to zero as the lithium concentration approaches about 25% of its original value.

It was established earlier that an irradiation of $3 \times 10^{15} e/cm^2$ produced a uniform concentration of defects (probably Si-A centers) of 6×10^{14} cm^{-3} in a lithium-doped cell made from quartz-crucible silicon. Our work has indicated that such an irradiation will cause at least 70% of lithium present to react with the defects. Using cell C13D-1 as an example, this means that near the zero bias position of the N-type side of the space charge region (2 μm) about $6 \times 10^{14} cm^{-3}$ lithium donors react during the recovery. This amounts to a one-to-one relation between defects and reacting lithium donors. At a distance of 3 μm deeper in the N-type region, about $3 \times 10^{15} cm^{-3}$ lithium donors react during recovery. At this point, the concentration of lithium donors reacting during the recovery period is five times that of the radiation defects detected. It would be highly desirable to extend these measurements to deeper areas of the N-type base. After the $3 \times 10^{15} e/cm^2$ irradiation of cell C13D-1, the measured diffusion length of the cell was 4.3 μm. The data in Fig. 4 indicate that immediately after the irradiation, the capacitance-voltage measurement investigates the lithium concentration of the entire active portion of the N-type base. During the recovery phase, the measured diffusion length increased to 17.5 μm. The distance is currently beyond the limits of the capacitance technique. If the original concentration of donors found before irradiation is extrapolated to 17.5 μm, about $2 \times 10^{16} cm^{-3}$ lithium donors are present. If 75% of these react during recovery phase, 50 lithium donor ion cores react for each radiation defect detected. Such behavior is clearly beyond explanation by models previously proposed. A model involving the nucleation of lithium precipitation by the radiation defects appears to be the only one consistent with observed results.

V. CONCLUSIONS

Several groups of lithium-doped solar cells have been evaluated under 1-MeV electron irradiation. Many of these groups indicated superior electrical output after irradiation and recovery as compared to similarly irradiated N/P solar cells. The superior cells are those with lithium concentrations of 2 to 5×10^{14} atoms/cm^3 at the junction. An irradiation of lithium-doped cells with 28-MeV electrons indicated a tenfold advantage of lithium-doped cell over N/P cells. Studies of the changes in the lithium concentration during recovery have shown the amounts of lithium reacting is highly nonlinear in regard to the electron fluence and varies greatly with distance from the junction. The results indicate that precipitation of lithium on radiation defects may be the cause of recovery rather than ion pairing.

Table 1. Float-zone silicon cell recovery characteristics

Cell group	Diffusion schedule (°C/min/min)	N_{Li}, cm^{-3}	Average C versus V slope	1-MeV electron fluence, e/cm^2	Initial level I_{sc}, mA	Damaged level I_{sc}, mA	Recovered level I_{sc}, mA
C11C	325/480/0	1.1×10^{14}	-0.37	3×10^{14}	60.3	34	54
H1A	325/480/0	0	-0.47	3×10^{14}	58	33	45
H2A	425/90/120	0.4×10^{14}	-0.32	3×10^{14}	51	31	48
H4A	325/480/0	4.9×10^{14}	-0.35	3×10^{14}	47	27	46
H5A1	425/90/120	4.2×10^{14}	-0.34	3×10^{14}	52.5	27	50
H5A2	425/90/120	2.8×10^{14}	-0.34	3×10^{14}	46.5	27	45.5
H5A3	425/90/120	2.3×10^{14}	-0.36	3×10^{14}	52.0	27	47
C11C	325/480/0	1.9×10^{14}	-0.34	3×10^{15}	58.5	24.3	39
H1A	325/480/0	0	-0.47	3×10^{15}	56	24	25
H2A	425/90/120	2.7×10^{14}	-0.30	3×10^{15}	56	22	44
H4A	325/480/0	5.6×10^{14}	-0.33	3×10^{15}	46	19.5	40
H5A1	425/90/120	8.5×10^{14}	-0.32	3×10^{15}	47.5	17.2	39
H5A2	425/90/120	4.4×10^{14}	-0.35	3×10^{15}	51	19	39
H5A3	425/90/120	3.8×10^{14}	-0.36	3×10^{15}	53	18	33

Table 2. Crucible lithium solar cell recovery characteristics, 60°C recovery

Cell group	Diffusion schedule, °C/h	N_{Li}, cm^{-3}	Average C versus V slope	1-MeV Electron fluence, e/cm^2	Initial level I_{sc}, mA	Damaged level I_{sc}, mA	Recovered level I_{sc}, mA
C11A	325/8	3.1×10^{14}	-0.28	3×10^{15}	64.2	22.0	>37
C11B	325/8	1.5×10^{14}	-0.32	3×10^{15}	53.3	24.9	>27
C11D	375/3	5.1×10^{14}	-0.26	3×10^{15}	61.5	20.7	>36
C13A	330/4	2.5×10^{14}	-0.29	3×10^{15}	64.5	22.5	39.0
				3×10^{14}	64.0	33.8	53.0
C13B	330/6	1.6×10^{14}	-0.29	3×10^{15}	61.8	22.7	37.0
				3×10^{14}	61.8	35.7	51.8
C13C	340/3	2.3×10^{14}	-0.28	3×10^{15}	64.0	21.4	39.4
				3×10^{14}	62.5	30.0	50.2
C13D	340/7	2.1×10^{14}	-0.29	3×10^{15}	63.8	22.5	37.8
				3×10^{14}	65.0	35.8	50.5
C13E	350/5	3.1×10^{14}	-0.28	3×10^{15}	64.2	24.5	35.0
				3×10^{14}	59.0	30.1	47.2
C13F	350/5	4.8×10^{14}	-0.28	3×10^{15}	61.5	22.0	36.0
				3×10^{14}	59.8	29.8	49.0
C13G	360/3	6.5×10^{14}	-0.26	3×10^{15}	57.0	19.5	36.5
				3×10^{14}	61.5	29.5	48.0
C13H	360/7	3.7×10^{14}	-0.31	3×10^{15}	63.5	26.0	35.0
				3×10^{14}	61.5	30.0	49.0
C13I	370/4	5.8×10^{14}	-0.29	3×10^{15}	61.0	23.0	35.0
				3×10^{14}	58.0	30.5	47.8
C13J	370/6	3.0×10^{14}	-0.31	3×10^{15}	60.5	24.0	34.0
				3×10^{14}	62.8	37.8	47.0

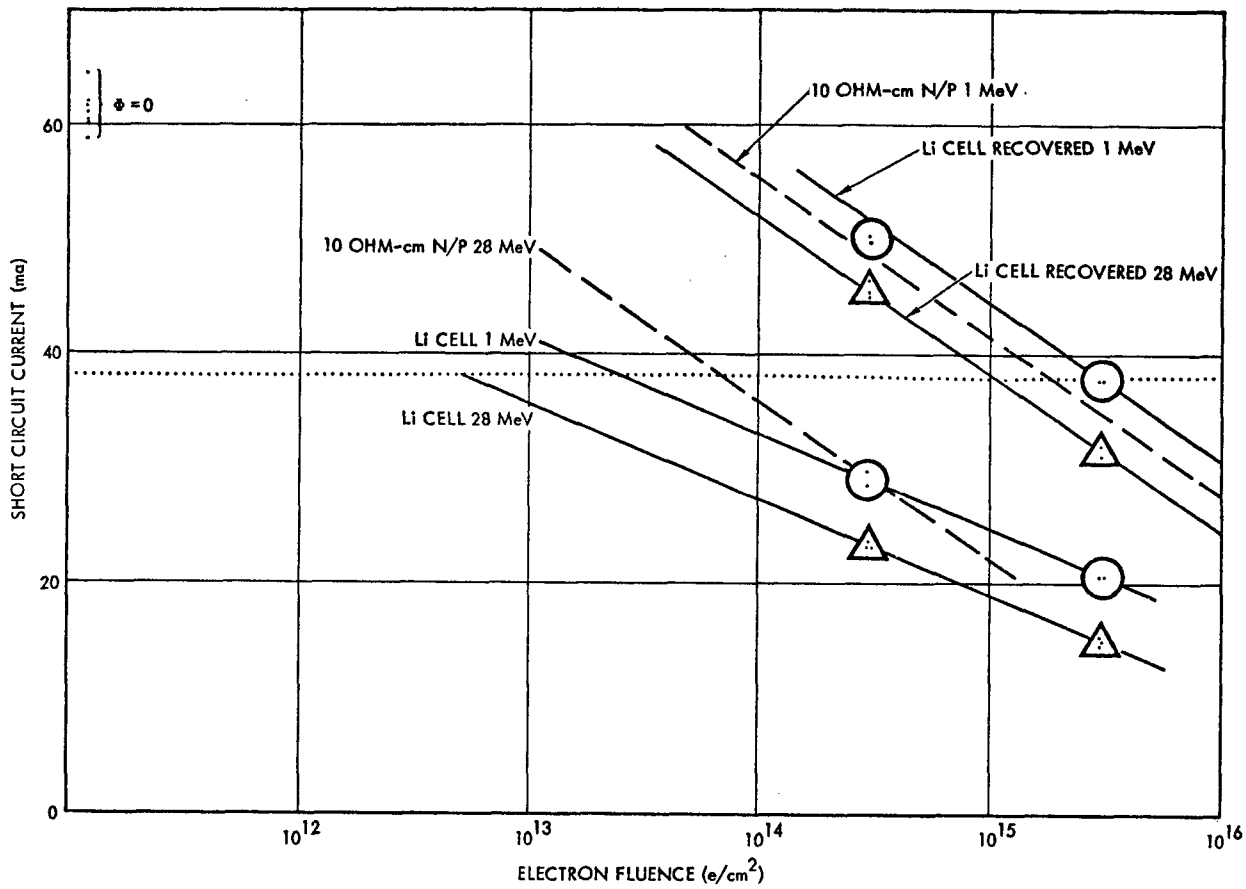

Fig. 1. Short-circuit current versus electron fluence

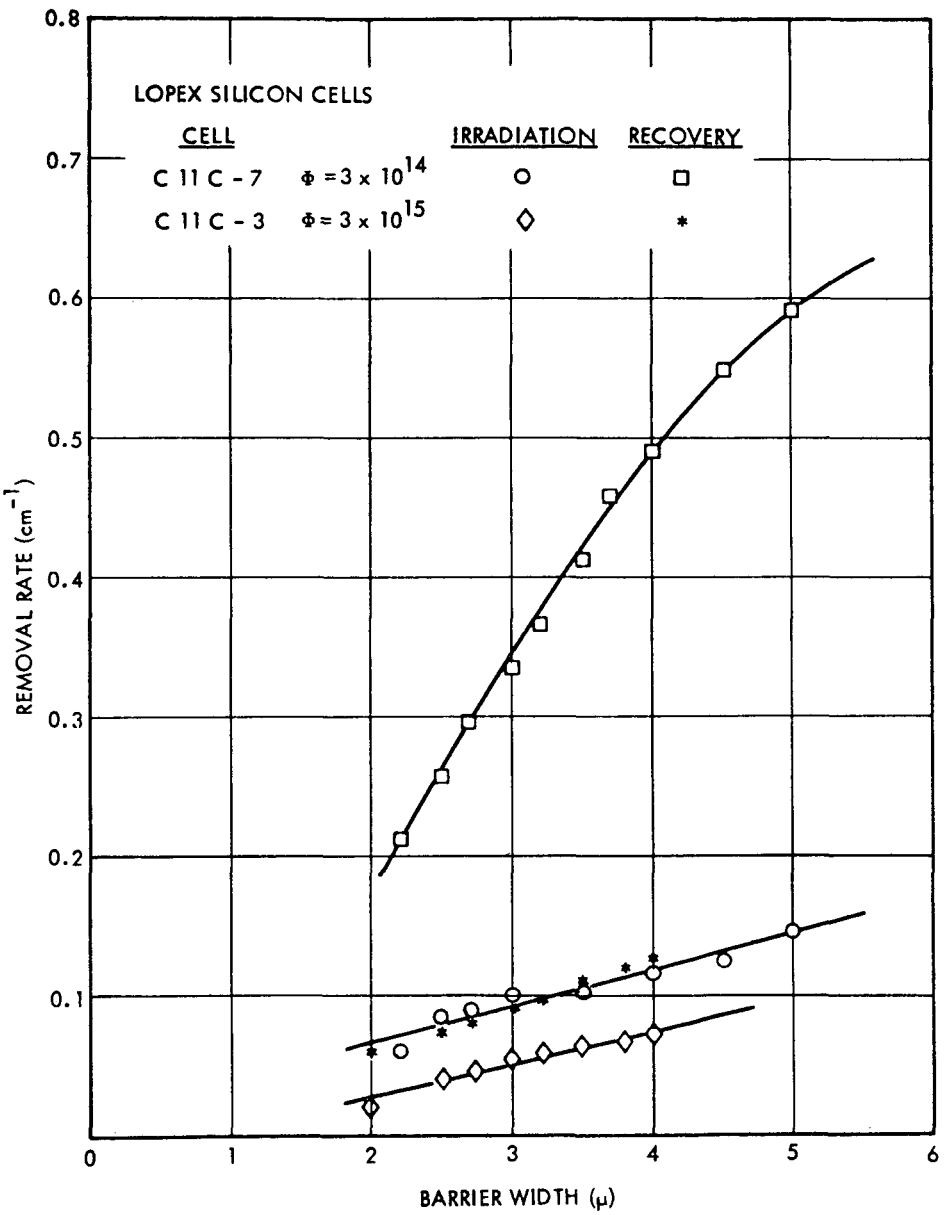

Fig. 2. Removal rates of cells of C11C group

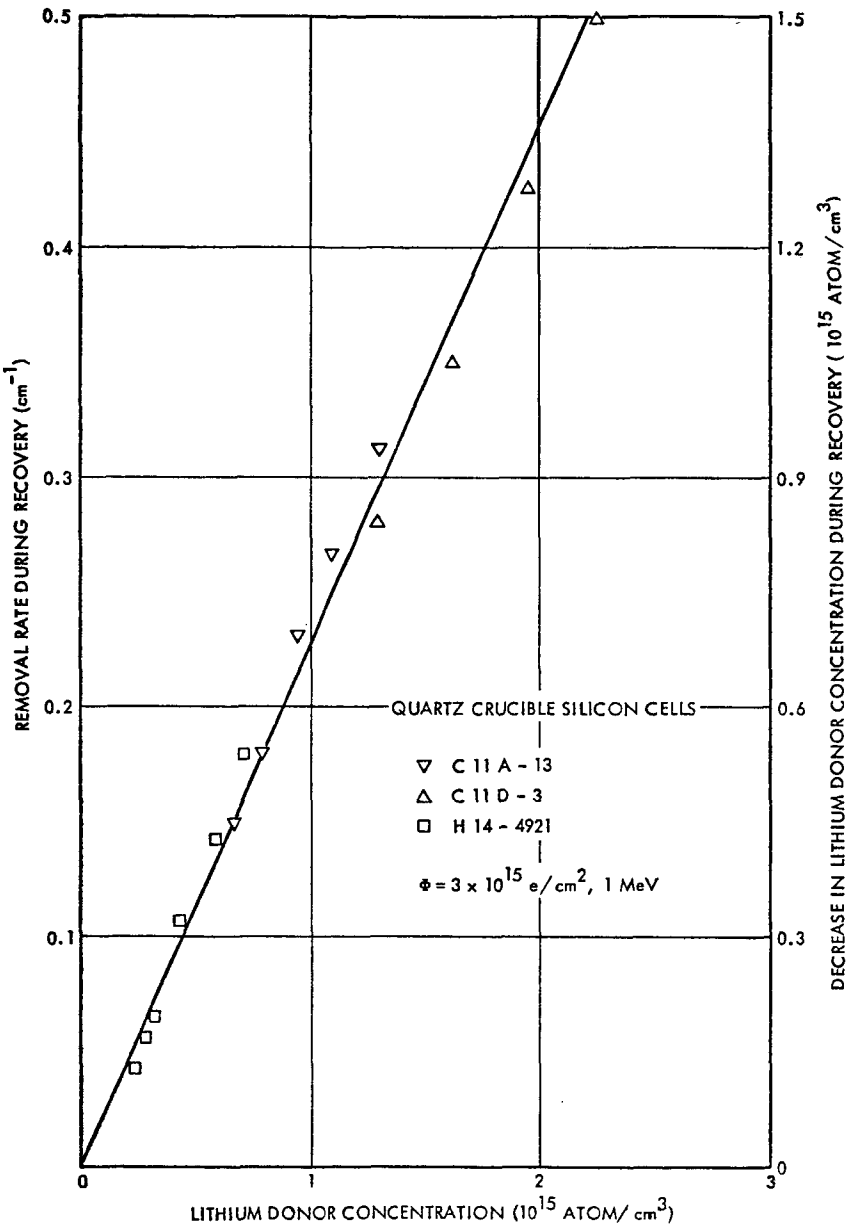

Fig. 3. Removal rate versus lithium donor concentration

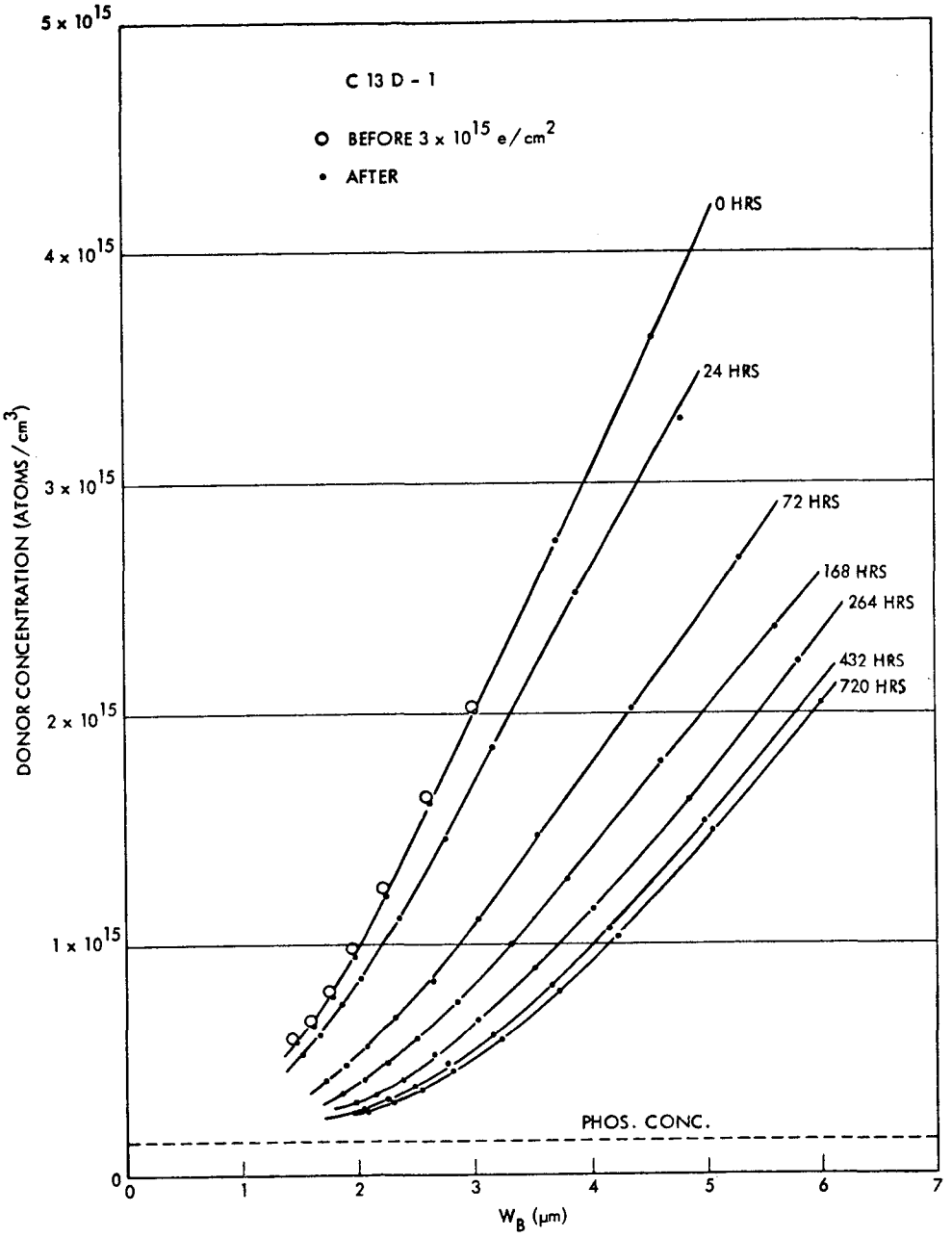

Fig. 4. Donor concentration during recovery, C13D-1 cell

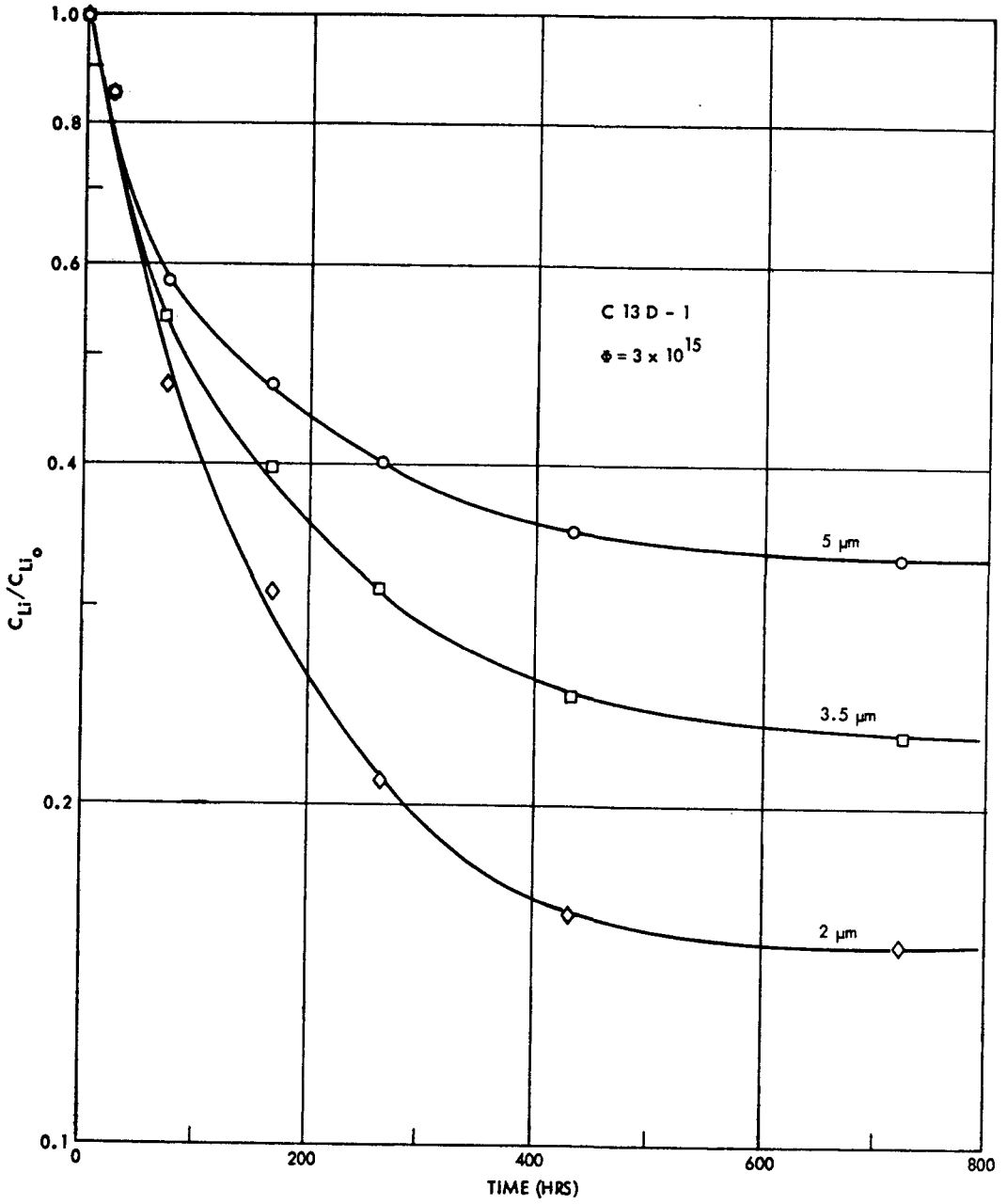

Fig. 5. Change in lithium donor concentration during recovery, C13D-1 cell

RADIATION TOLERANCE OF ALUMINUM-DOPED SILICON*

O. L. Curtis, Jr., and J. R. Srour
Northrop Corporate Laboratories
Hawthorne, California

ABSTRACT

Data are presented that indicate that heat-treated Czochralski-grown aluminum-doped silicon that undergoes an appreciable resistivity increase ($\gtrsim$ a factor of two) during heating at ~450°C is significantly more resistant to both neutron and gamma irradiation than boron-doped material (or aluminum-doped material that either has not been heat-treated or does not experience an appreciable resistivity change during such a treatment). Data interpretation is, however, quite difficult due to the occurrence of severe trapping effects in heat-treated material. Studies of radiation effects on aluminum-doped silicon solar cells are planned for the near future to resolve these uncertainties in the bulk material results.

I. INTRODUCTION

The development of methods for increasing the radiation tolerance of silicon could result in significant additions to the technology employed in fabricating semiconductor devices that are to be used in a radiation environment. Lithium-doped silicon, for example, exhibits radiation resistance (Refs. 1, 2) and is currently being studied in detail for possible solar-cell applications by various workers. The quite interesting properties exhibited by lithium-doped material lead one to speculate as to whether there might be other dopants which would create desirable radiation-tolerance characteristics. (As a recent example, it has been reported (Ref. 3) that copper-doped N/P silicon solar cells appear to be more radiation tolerant than conventional cells.)

During recent years, there have been occasional reports by different researchers within the technical community that aluminum-doped silicon is more resistant to radiation than is material doped with other acceptors. For example, Mandelkorn, et al., (Ref. 4) reported that aluminum-doped silicon solar cells were more radiation-tolerant than boron-doped units (1-MeV electron and 10-MeV proton bombardment). Additionally, we have reported (Ref. 5) that neutron-irradiated aluminum-doped bulk silicon exhibits a lifetime damage constant[1] significantly larger (i.e., more radiation-resistant) than that for boron- and gallium-doped material. Attempts by other workers to reproduce results obtained on aluminum-doped material apparently were not successful. Our previous finding for neutron-irradiated bulk material (Ref. 5) was reproduced (Ref. 6), but it was not entirely clear at that time what conditions were necessary in order to prepare radiation-tolerant aluminum-doped silicon. In this paper, we present results of a study of the radiation resistance of aluminum-doped silicon in which it

*Work supported in part by the National Aeronautics and Space Administration through the Jet Propulsion Laboratory, California Institute of Technology, and in part by the Defense Atomic Support Agency through Harry Diamond Laboratories.

[1] Defined as the amount of radiation required to reduce the lifetime of initially perfect material to 1 μs. That is, damage constant = $K = \phi[(1/\tau) - (1/\tau_o)]^{-1}$, where ϕ is the fluence, and τ_o and τ are the pre- and post-irradiation lifetimes, respectively.

is shown that heat-treated aluminum-doped Czochralski-grown material can be prepared that appears to exhibit significantly improved tolerance to both neutron and gamma irradiation when compared to boron-doped silicon.

II. BACKGROUND

A chronological review of the results of our previous studies on aluminum-doped silicon is presented first for the purpose of placing our most recent results in the proper perspective. Figure 1 shows the results of a systematic study (Ref. 5) of damage constants for neutron-irradiated P-type silicon of various resistivities. The increase in damage constant with increasing resistivity is readily explained in terms of the Hall-Shockley-Read model, but the particular parameters shown should not be considered significant. The sample designation system used in Fig. 1 is as follows: first letter corresponds to manufacturer (K = Knapic, D = Dow, M = Merck, T = Texas Instruments); second letter corresponds to growth process (C = Czochralski, V = vacuum float zone, L = Lopex); third letter(s) corresponds to dopant (gallium, boron, and aluminum). Only one aluminum-doped specimen was examined, but it was found that the damage constant was significantly higher than for boron- and gallium-doped material of the same resistivity. However, since the pre-irradiation lifetime for this sample was very low, and since a significant amount of trapping was observed in the photoconductivity decay, this result was considered tentative at best.

Following our initial finding, a more detailed investigation of aluminum-doped material was conducted (Ref. 7). Samples prepared from a Czochralski-grown silicon ingot exhibited an extremely short pre-irradiation lifetime, so it was decided to anneal the specimens in an attempt to increase the lifetime. Anneals at 350 and 400°C apparently increased the lifetime but also changed the resistivity. The samples were neutron-irradiated along with boron-doped control samples, and damage constant results of this earlier study are shown in Fig. 2 (circles only). It was found that the aluminum-doped material was considerably more radiation-resistant that the boron-doped specimens. However, trapping was still present to such an extent that the data was not considered to be highly accurate.

In an attempt to remedy the trapping problem, which was presumably associated with the presence of a large oxygen concentration, we repeated the above experiment with aluminum-doped float-zone material. These samples had long lifetimes and trapping effects were small. However, the float zone specimens were found to be just as radiation-sensitive as boron-doped silicon. Subsequent experiments with better Czochralski-grown material were likewise unsuccessful. This led us to postulate that the radiation resistance observed earlier was associated with the heat-treatment given to the specimens. Additional work indicated that heat-treated samples were not radiation resistant unless the annealing resulted in appreciable carrier concentration changes, which is the topic of the present paper. Before presenting out most recent findings, a brief review of pertinent literature on the effects of heat-treating on silicon is presented.

Resistivity changes in undoped heat-treated pulled-crystal silicon were first reported 16 years ago (Ref. 7). Such changes were explained qualitatively on the basis of the formation of silicon-oxygen compounds, one of which (SiO_4) acts as a donor below ~500°C (Ref. 8). A detailed study of the effects of acceptors and oxygen on heat-treated silicon was performed by Fuller, Doleiden, and Wolfstirn (Ref. 9). In this study, results for gallium-doped material were found to be quite similar to those obtained for boron doping, but aluminum-doped material exhibited a somewhat different behavior. Before discussing the differences, some general features of the results of Fuller, Doleiden, and Wolfstirn are summarized. Heating oxygen-containing acceptor-doped silicon for long periods at the proper temperature (typically in the range of 400 to 500°C) results in the formation of donor sites with accompanying carrier concentration changes. The amount of change depends primarily on four parameters: (1) acceptor concentration; (2) oxygen concentration; (3) heat-treatment temperature; (4) amount of time the specimen is heat-treated at a particular temperature. The reactions that produce the observed carrier concentration changes were not definitely determined by Fuller, Doleiden, and Wolfstirn, but the data supported the postulation of the formation of primarily three distinct compounds: (1) SiO_4 donor sites; (2) neutral oxygen-acceptor sites; (3) acceptor-oxygen sites that act as donors. Considerably larger carrier concentration changes could be obtained in aluminum-doped material than in comparable boron-doped specimens. In fact, particular aluminum-doped samples were actually converted to N-type; this was not possible in the boron case. It is postulated that the reason for this difference may be that acceptor-oxygen donor sites are formed more readily in the aluminum case than for boron doping.

III. EXPERIMENTAL RESULTS

A considerable amount of research on aluminum-doped silicon was performed, the primary conclusion of which was the following: heat-treated Czochralski-grown aluminum-doped material that undergoes an appreciable resistivity increase ($\gtrsim$a factor of two) is apparently much more radiation tolerant than boron-doped material or aluminum-doped material that either has not been heat-treated or does not experience an appreciable resistivity change during such a treatment. It should be noted that float-zone aluminum-doped silicon is excluded as a radiation-tolerant material by this conclusion because the resistivity does not change appreciably during heat-treatment.

Much of the work leading up to the conclusion stated above involved studying the variation of resistivity during heat-treatments of ~450°C, employing the results of Fuller, Doleiden, and Wolfstirn as a guide. Resistivity was monitored at various times during anneals using four-point probe techniques. Figure 3 shows the resistivity variation with time at 450°C for a low-resistivity specimen. After 315 h, the resistivity had increased by a factor of ~1.7. In a number of ~1 Ω-cm specimens examined, the resistivity typically doubled after 24 h at 450°C.

Following heat treatment, pre-irradiation lifetime measurements were performed and then specimens were gamma-irradiated at a Co^{60} source (dose rate ~1.2×10^5 R/h). Other specimens were subjected to neutron irradiation in a TRIGA reactor. Following irradiation, damage constants were determined. Figure 4 shows typical results for gamma-irradiated specimens. It is seen that aluminum-doped material that experienced a 50 to 100% resistivity change upon heat treatment was significantly more radiation tolerant than both the boron-doped control samples and the aluminum-doped samples which did not undergo an appreciable resistivity change. Figure 2 shows results for neutron-irradiated aluminum- and boron-doped specimens (triangles only). It is seen that the earlier results (circles) were qualitatively reproduced, once again indicating tolerance to neutron irradiation.

A carrier removal experiment was performed on neutron-irradiated heat-treated aluminum-doped silicon. The study involved examination of both pre- and post-irradiation resistivity profiles for both boron- and aluminum-doped samples. The neutron dose employed was 1.65×10^{14} nvt (>10 keV). No significant differences between the two types of samples were observed; i.e., the percent resistivity increase in aluminum-doped material due to carrier removal was similar to that observed in boron-doped material. This result suggests that heat-treated aluminum-doped silicon may be advantageous from the standpoint of lifetime degradation but may offer no improvement of the carrier removal problem.

IV. DISCUSSION

The interesting question is raised as to whether heat-treated boron-doped material, which experiences an appreciable resistivity change, would also be more radiation tolerant. Fuller, et al., (Ref. 9) indicate that significant resistivity changes are possible for oxygen-rich boron-doped specimens. However, they also found that donors produced in heat-treated boron-doped material disappear above ~800°C, as compared to ~1100°C in aluminum-doped material. Hence, heat-treated boron-doped material would seem to be less suitable for applications requiring high-temperature diffusions (>800°C).

It is difficult to specify at present what mechanism is responsible for the observed decrease in radiation sensitivity for aluminum-doped material. The effect of the radiation-induced defects on carrier lifetime is presumably diminished by an interaction between these defects and one or more of the three types of compounds (mentioned above) thought to be formed during heat treatment. The SiO_4 donors can most likely be ruled out because they are presumably present in considerable quantity in heat-treated material which has not experienced a significant resistivity change. Because of the indicated correlation between resistivity change and decreased radiation sensitivity, it is tempting to speculate that the stable aluminum-oxygen donor sites are involved in reducing the effectiveness of the radiation-induced defects.

There is a problem regarding the interpretation of our data which should be emphasized. Damage constant measurements for bulk material have all been based on minority carrier lifetimes determined using photoconductivity decay techniques (Ref. 10). Because of severe trapping that occurs in the heat-treated aluminum-doped material, analysis of transient decays has been quite difficult at best. Our feeling is that the radiation-tolerance results are still qualitatively accurate. However, final proof will not come until diffusion length measurements are made on heat-treated aluminum-doped material before and after irradiation. We are currently working toward this goal. Solar cells are presently being fabricated from aluminum-doped material, and radiation testing will follow. If the cells are radiation hard, as our bulk studies have predicted, a considerable effort would undoubtedly have to be expended to optimize the fabrication technique in terms of maximizing both the pre-irradiation conversion efficiency and the radiation tolerance of aluminum-doped solar cells.

REFERENCES

1. Vavilov, V. S., in Radiation Damage in Semiconductors, p. 45. Academic Press, New York, 1964.

2. Wysocki, J. J., IEEE Trans. Nucl. Sci. Vol. 13, p. 168, December 1966.

3. Usami, A., Solid-State Elect., Vol. 13, p. 1202, 1970.

4. Mandelkorn, J., et al., J. Appl. Phys., Vol. 35, p. 2258, 1964.

5. Curtis, O. L. Jr., IEEE Trans. Nucl. Sci., Vol. 13, p. 33, December 1966.

6. Curtis, O. L., Jr., Paper 7G.1 in Record of the 1969 IEEE International Convention, New York, March 24-27, 1969.

7. Fuller, C. S., et al., Acta Met. Vol. 3, 97, 1955.

8. Kaiser, W., Frisch, H. L., and Reiss, H., Phys. Rev. Vol. 112, p. 1546, 1958.

9. Fuller, C. S., Doleiden, F. H., and Wolfstirn, K., J. Phys. Chem. Solids, Vol. 13, p. 187, 1960.

10. Curtis, O. L., Jr., and Wickenhiser, R. C., Proc. IEEE, Vol. 53, p. 1224, 1965.

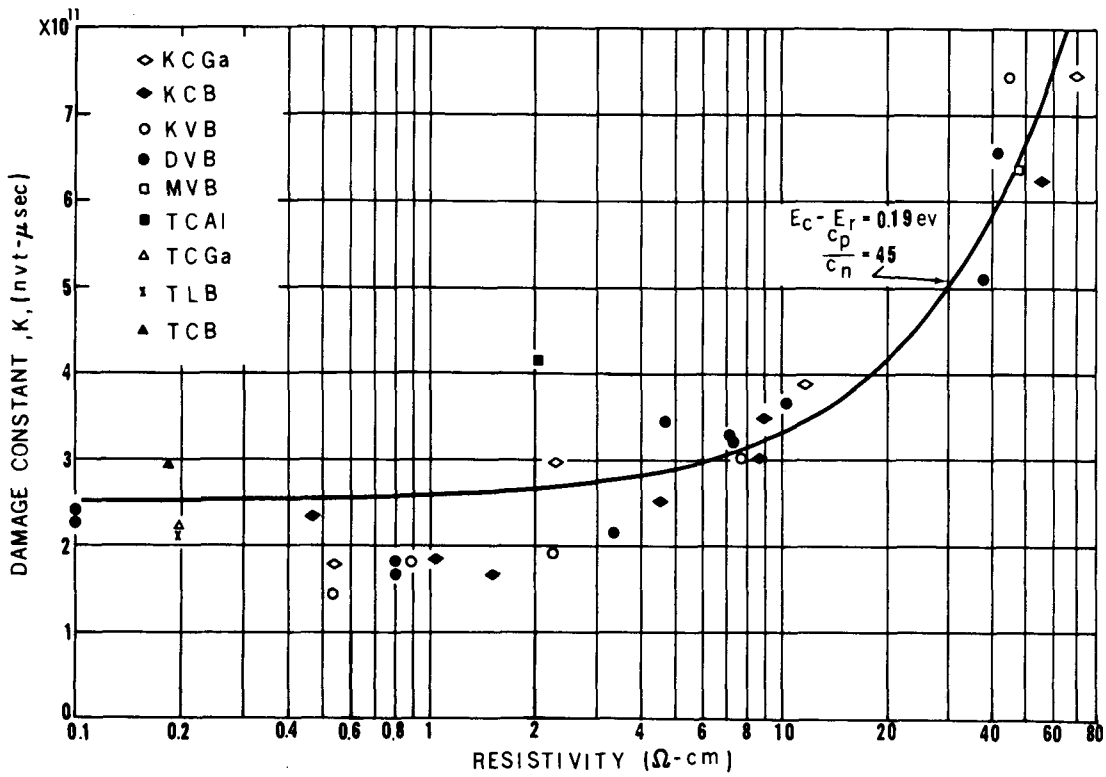

Fig. 1. Damage constant versus resistivity for neutron-irradiated P-type silicon. Damage constant is expressed in nvt (>10 keV) required to reduce the lifetime of an initially perfect sample to 1 μs. The theoretical curve corresponds to energy level parameters determined from temperature dependence measurements.

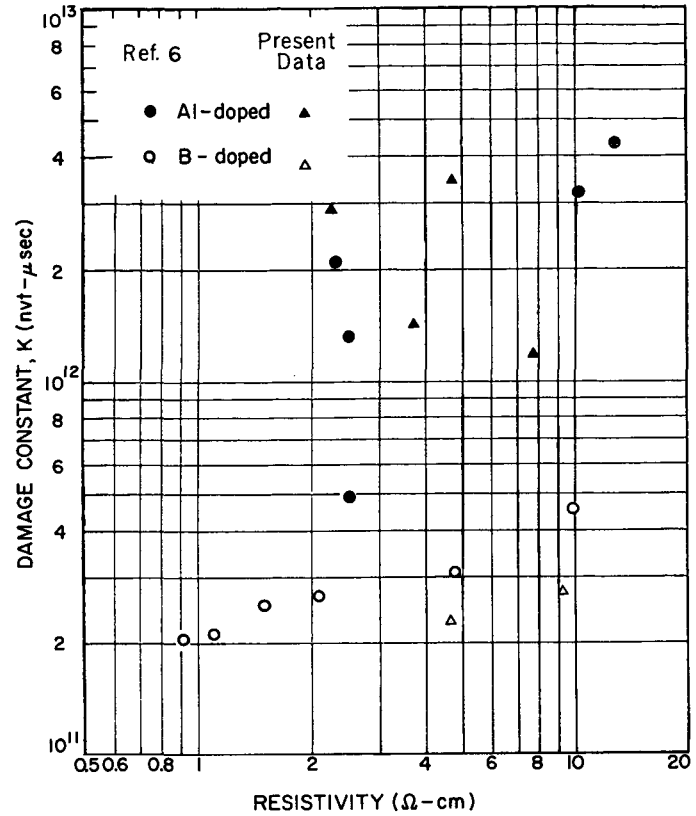

Fig. 2. Comparison of damage constants for neutron-irradiated Czochralski-grown aluminum- and boron-doped silicon. The aluminum-doped specimens were heat-treated.

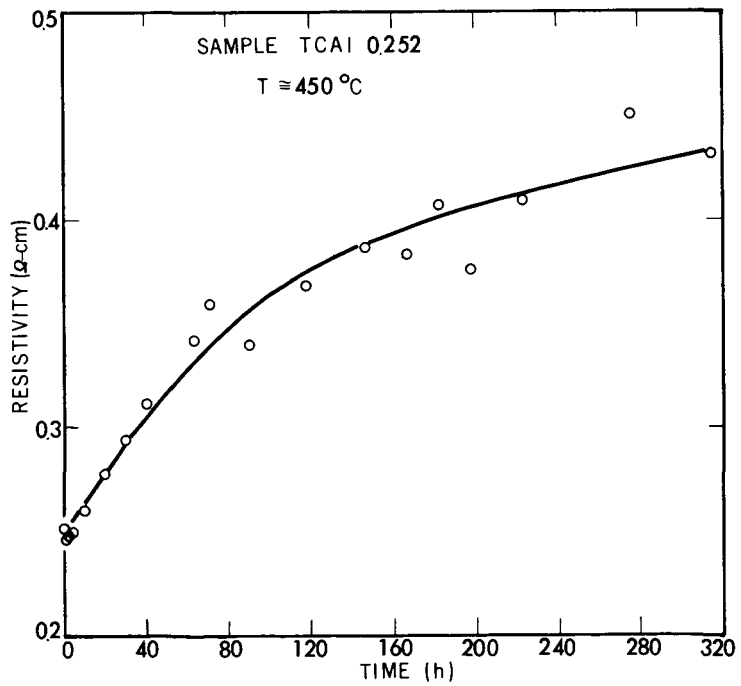

Fig. 3. Variation of resistivity with time at ~450 °C for a low-resistivity aluminum-doped silicon sample

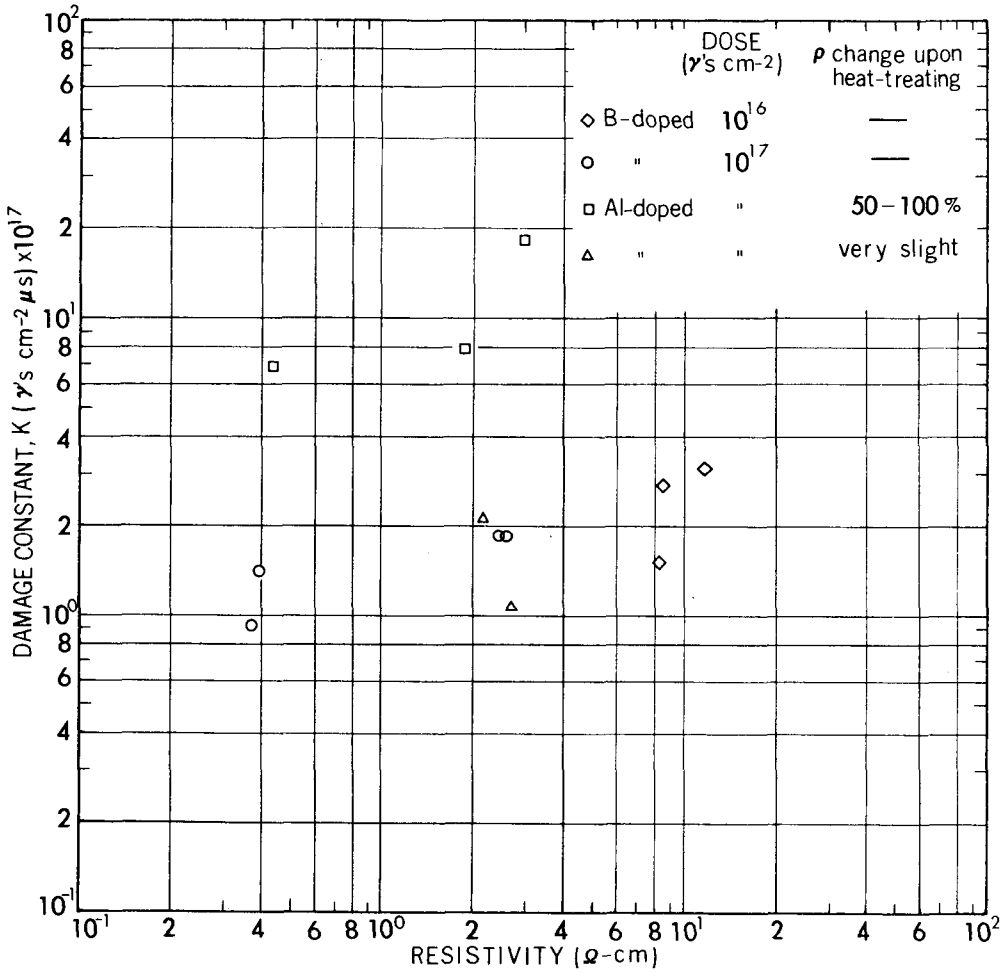

Fig. 4. Comparison of damage constants for gamma-irradiated Czochralski-grown aluminum- and boron-doped silicon. The aluminum-doped specimens were heat-treated.

EXPERIMENTAL AND COMPUTER STUDIES OF THE RADIATION EFFECTS IN SILICON SOLAR CELLS*

R. E. Leadon, J. A. Naber, and B. C. Passenheim
Gulf Radiation Technology
San Diego, Calif.

I. INTRODUCTION

This paper is presented in two parts. The first section will be a summary of selected experimental results obtained on lithium-diffused bulk silicon. Particular emphasis was placed on the radiation-induced degradation and thermal anneal of minority-carrier in bulk silicon because solar cell output is related to the minority-carrier lifetime. The temperature dependence of the minority-carrier lifetime indicates the density and energy levels of the recombination centers, providing clues to their identity. Electron spin resonance and infrared absorption techniques were used to investigate the introduction and anneal of three specific radiation-induced defects, which are thought to contribute to the recombination process.

The results reported herein are a continuation and summary of work previously reported (Refs. 1-8).

The second part of the paper will discuss the merits of a computer code developed by Gulf Radiation Technology which calculates the current-voltage (I-V) output of a computer simulated P-N junction. With this code, the user stipulates the initial properties and environment of a cell. The cell's properties and environment may then be varied in a manner which might reflect the anticipated radiation exposure and mission environment, and the current-voltage output is recalculated. Thus, a variety of cell types and experimental conditions can be rapidly evaluated. This code can also be utilized by cell manufacturers to evaluate the merit of different cell types, doping profiles, and cell parameters. It can be utilized by those engaged in solar cell testing programs to evaluate a greater variety of cell types, radiation histories, and ambient conditions than is feasible by experimental techniques alone. Systems engineers can use the code to predict the radiation vulnerability of solar cells in varied environments.

II. EXPERIMENTAL PROGRAM

A. Samples and Radiation

The experimental program has been devoted to an investigation of bulk lithium-diffused silicon. Electron spin resonance and infrared absorption were used to study certain specific defects, and minority-carrier lifetime measurements were used to study radiation-induced recombination centers. Samples were lithium-diffused by either a lithium-oil paint-on technique or by a lithium-tin bath technique. Samples with lithium donor densities from as low as 2×10^{20} Li/m^3 (2×10^{14} Li/cm^3) to as high as 4×10^{23} Li/m^3 (4×10^{17} Li/cm^3) were investigated. Resistivity profiles were used to monitor samples for diffusion uniformity. Donor density was occasionally verified

*Work performed for the Jet Propulsion Laboratory, sponsored by the National Aeronautics and Space Administration under Contract NAS 7-100.

by Hall effect measurements. Samples were diffused from vacuum float-zone (FZ) and quartz-crucible (QC) phosphorus-doped silicon, ranging in initial room-temperature resistivity from 10^2 Ω-m (10^4 Ω-cm) to 0.005 Ω-m (0.5 Ω-cm). While QC silicon has approximately a hundred times the oxygen concentration of FZ silicon, its dislocation density is much less.

Samples were damaged with 30-MeV electrons at temperatures ranging from 115 to 300 K or by fission neutrons (E > 10 keV) at 273 to 300 K. The damage was thermally annealed at temperatures up to 673 K.

B. Study of Three Specific Defects

The introduction of three specific defects by 30-MeV electron irradiation and their subsequent thermal anneal were investigated using electron spin resonance or infrared absorption techniques. Specifically, the oxygen-vacancy (Si-B1), divacancy (Si-G7), and phosphorus-vacancy (Si-G8) centers have been studied. The results of these studies have been previously reported elsewhere (Refs. 7, 8) but may be summarized as follows.

The oxygen-vacancy and phosphorus-vacancy centers were studied by ESR techniques. In QC silicon, the Si-B1 center introduction rate is the same as in nondiffused silicon (~15 m^{-1} = 0.15 cm^{-1}) as long as the lithium density is much less than the oxygen density. When the lithium and oxygen densities are comparable, and B1 center introduction rate is significantly reduced (~2.5 m^{-1} = 0.025 cm^{-1}). This can be attributed to the lithium-oxygen pairing, reducing the number of oxygen atoms available to form oxygen-vacancy (Si-B1) centers, or to competition between oxygen and the positively charged lithium or lithium oxide donors for the vacancies. The B1 center in lithium-diffused silicon is found to anneal below 400 K instead of near 600 K, as in nondiffused silicon. The LiO^+ density and conductivity decreased as the Si-B1 center annealed.

Electron spin resonance was also used to study the phosphorus-vacancy (Si-G8) center. In phosphorus-doped lithium-diffused silicon (10^{22} P/m^3 = 10^{16} P/cm^3, ~10^{22} Li/m^3 ≅ 10^{16} Li/cm^3), 30-MeV electron irradiations of 10^{21} e/m^2 (10^{17} e/cm^2) below 150 K are found to produce Si-G8 (phosphorus-vacancy) defects at a rate comparable to nondiffused silicon. Production and annealing studies on the Si-G8 center at these densities and fluence levels indicate that the presence of lithium had little or no effect on the creation or annealing of that center. It is possible that at these high fluences, relative to the initial lithium density, the active lithium has been depleted.

The divacancy (Si-G7) was observed by monitoring the introduction and anneal of the 1.8-μm optical absorption band. In this investigation, it was found that for 30-MeV electron irradiations at less than 150 K to fluences of 10^{21} e/m^2 (10^{17} e/cm^2), the introduction rate of the Si-G7 center (divacancy) is comparable in electron-irradiated lithium-diffused (5×10^{22} Li/m^3 = 5×10^{16} Li/cm^3) and nondiffused silicon. The divacancy anneals at or below 300 K in diffused silicon compared with ~325 to 575 K in nondiffused silicon. As the 1.8-μm divacancy band disappears, new bands near 1.4 and 1.65 μm appear, and these anneal near 600 K. These bands have been observed by other investigators (Ref. 9) and attributed to the divacancy plus one or two lithium atoms.

C. Minority-Carrier Lifetime Measurements

The introduction and anneal of recombination centers were determined from minority-carrier lifetime measurements. Minority-carrier lifetime was determined from measurements of the decay of photoconductivity or by steady-state techniques. These measurements are described in detail elsewhere (Refs. 3, 8). The present results were at injection levels ($\Delta n/n_0$) of less than 1%. Interpretation of the results is based on Shockley-Read recombination theory (Ref. 10). Capture cross-section temperature dependence as estimated by Lax (Ref. 11) or Leadon (Ref. 12) was assumed. The temperature dependence of minority-carrier lifetime was measured before and after irradiation and again after thermal anneal. Figure 1 shows minority-carrier lifetime versus inverse temperature for a lithium-diffused quartz-crucible and a lithium-diffused float-zone sample. The minority-carrier lifetime temperature dependence of the QC silicon can be attributed to recombination centers further than about 0.3 eV from either band edge, but the lifetime of FZ silicon has a more severe temperature dependence and a discontinuity near $1000/T = 4.5\ K^{-1}$. This can be attributed to recombination centers about 0.17 eV below the conduction band, which were not observed in QC silicon, in addition to centers further than 0.35 eV from either band edge. The lines drawn through the data represent the low injection-level lifetimes calculated by Shockley-Read theory, assuming the temperature-dependent capture cross sections of Lax. The presence of a recombination center near E_c - 0.17 eV in FZ silicon and its absence in QC silicon suggests that this center is not the oxygen-vacancy (Si-B1) center, which is known to have an energy level in this range.

The minority-carrier lifetime degradation rate is defined in terms of lifetime τ and electron fluence ϕ to be

$$K = \Delta\frac{(\tau^{-1})}{\Delta\phi}$$

compared with phosphorus-doped silicon, and was found to increase with increasing lithium donor density. The degradation constant was found to be essentially independent of oxygen content. This shows that the 30-MeV electron-induced defects either contain lithium or are affected in their production by lithium. The minority-carrier lifetime degradation constant was found to vary with temperature in a way which could be attributed to the temperature dependence of the capture cross section.

Both isothermal and isochronal annealing experiments have been performed on a variety of lithium-diffused samples. The unannealed fraction of annealable defects for isothermal annealing is given by

$$\frac{1/\tau_t - 1/\tau_f}{1/\tau_0 - 1/\tau_f}$$

where τ_0 is the lifetime after irradiation and before anneal, τ_f is the fully annealed lifetime, and τ_t is the lifetime at the annealing temperature after time t. Linearity of the isothermal annealing data implies first-order annealing kinetics (Ref. 13) in which the number of recombination centers is given by

$$N = N_0 \exp(-Rt)$$

where N_0 is the initial number of annealable defects and R is the rate constant, which is given by

$$R = \nu \exp(-E/kT)$$

where E is the activation energy and ν is the effective frequency factor. In every case, our isothermal anneals indicated first-order annealing kinetics were appropriate.

For isochronal anneals, the unannealed fraction of annealable defects is given by

$$\frac{1/\tau_T - 1/\tau_f}{1/\tau_0 - 1/\tau_f}$$

where τ_T is the lifetime observed at 300 K after anneal at temperature T, and τ_0 and τ_f are the pre- and post-anneal lifetimes.

Analysis of isochronal and isothermal anneals, using first-order kinetics, yields the activation energy and frequency factor of the rate constant. Figure 2 shows the results of five separate isochronal annealing experiments on lithium-diffused QC silicon. A single first-order annealing stage at 380 ±10 K is readily apparent. Similar results were obtained on fission-neutron-irradiated silicon.

Table 1 summarizes our experimental findings for the annealing of radiation-induced recombination centers in lithium-diffused silicon exposed to 30-MeV electron and fission neutrons (E > 10 keV). The activation energies compare with the 0.65 ± 0.05 eV energy for lithium diffusion in oxygen-lean FZ silicon, and with 1.07 ± 0.05 eV energy of lithium-oxygen dissociation and diffusion in oxygen-rich QC silicon (Refs. 14-16). This data supports the supposition that radiation-induced damage, including the clustered damage attributed to fission neutrons, is annealed by the diffusion of lithium to the defect.

In addition, the effective frequency factors are much less than the atomic frequency factor of about 10^{13} s^{-1} and scale with the lithium donor density. This is consistent with a process involving the long-range migration of one annealing species to another (Ref. 13), which we take to be the migration of lithium to the damage site.

A more detailed discussion of our experimental findings and theoretical interpretations is presented elsewhere (Ref. 8), and a considerable body of additional data, provided by us and other investigators using other techniques, is available on bulk silicon. The following section of this paper describes one means of applying this body of data to the problem of predicting the response of a solar cell to various radiation and environmental conditions.

III. CODE FOR PREDICTING PERFORMANCE OF SOLAR CELLS

The purpose of this presentation is to describe a computer program that can be used for predicting the output performance of solar cells. This code was developed under Defense Atomic Support Agency contract and applied to solar cells under the JPL contract. Briefly, this code, which is fully operational at the present time, solves the complete equations for a one-dimensional P-N junction. The code starts with the current and continuity equations for electrons and holes, Poisson's equation for the electric field inside the cell, and appropriate equations for the generation and recombination of excess carriers. Arbitrary one-dimensional space profiles of doping density, mobilities, recombination lifetimes, and ionization densities are inputs to the code. The partial differential equations are converted to finite difference approximations, which are then solved by iteration. In principle, there are no adjustable parameters in the code. If one had accurate values for all of the material properties, the code would predict the absolute magnitudes of the current and voltage for selected values of load resistance. Thus, the accuracy of the results is primarily determined by how well one can measure or estimate the important physical parameters of the cell.

This code could be useful both in the design of new devices and in the analysis of radiation effects to solar cells. For example, if a cell manufacturer is designing a new type of cell, perhaps with an unusual doping profile, he could estimate the performance of the new device relative to a conventional cell and optimize its parameters before he goes through the expense of constructing it. Similarly, the radiation-effects physicist could use such a code to help him analyze his solar cell data in terms of kinds and densities of defects created by the radiation and to extrapolate the results to other radiation environments.

The three basic equations of the code are the one-dimensional continuity equations for holes (p) in the valence band and electrons (n) in the conduction band, and Poisson's equation for the electric field (E).

$$\frac{\partial p(x,t)}{\partial t} = g(x,t) - R(x,t) - \frac{\partial J_p(x,t)}{\partial x} \qquad (1)$$

$$\frac{\partial n(x,t)}{\partial t} = g(x,t) - R(x,t) - \frac{\partial J_n(x,t)}{\partial x} \qquad (2)$$

$$\frac{\partial E(x,t)}{\partial x} = \frac{q}{K}[p(x,t) - n(x,t) + \Delta N(x)] \qquad (3)$$

In the above equations, the dimension x is normal to the face of the cell and g(x, t) is the time- and space-dependent ionization rate of electron-hole pairs by the external radiation. This quantity is calculated ahead of time, using the spectral distribution of the incident light and the attenuation coefficients for the particular material, and is then an input into the code. The quantity q is the magnitude of the electronic charge, K is the dielectric constant in MKS units, $\Delta N(x)$ is the net doping of the semiconductor (positive for n-type, negative for p-type), and J_p and J_n are the particle current densities given by

$$J_p = p\mu_p E - D_p \frac{\partial p}{\partial x} \tag{4}$$

$$J_n = -n\mu_n E - D_n \frac{\partial n}{\partial x} \tag{5}$$

In Eqs. (4) and (5), the first terms are the drift components of the currents with mobilities μ_p and μ_n, while the second terms give the diffusion currents with diffusion coefficients D_p and D_n.

The term R(x, t) is the rate of recombination of excess carriers via recombination centers. There are several different options available to a user, depending on the sophistication he wishes to use in describing the recombination process. In many situations, it is adequate to use a Shockley-Read-type recombination rate for a single recombination level:

$$R = \frac{np - n_i^2}{\tau_{O_n}(p + p_F) + \tau_{O_p}(n + n_F)} \tag{6}$$

where n_i is the intrinsic carrier density, p_F and n_F are the values of p and n when the Fermi level coincides with the level of the recombination center that is being considered, and τ_{O_n} and τ_{O_p} are the recombination lifetimes of electrons in heavily p-type material and of holes in heavily n-type material, respectively.

This recombination equation does have the limitation that it only simulates the simultaneous annihilation of a free electron and a free hole. It does not consider the trapping of carriers on defect centers and, therefore, carrier removal. Since the latter phenomena can be important when the details of the trapping kinetics affect the carrier lifetimes or removal rates, the code also has the capability of simulating both single-level and double-level traps. This could be important, for example, if the radiation produces a high-density region of defect centers which significantly depletes the majority carriers and creates a p-n junction effect.

For a single-level trap with density N_1 and two possible charge states, negative (N_1^-) and neutral (N_1^o), the (-R) term in Eq. (1) would be replaced by

$$-R_p^- = \alpha_p^-\left(pN_1^- - N_1^o p_F\right) \tag{7}$$

and the (-R) term in Eq. (2) would be replaced by

$$-R_n^o = \alpha_n^o\left(nN_1^o - N_1^- n_F\right) \tag{8}$$

The quantity α_p^- is the product of the thermal velocity of a hole in the valance band and the cross section α_p^- for capture of a hole by a negatively charged defect, and α_n^o is a similar term for capture of an electron by a neutral defect. In addition to modifying Eqs. (1) and (2), the density of the negatively charged center (N_1^-) must be included in the summation of charges in Eq. (3). Furthermore, additional equations are required for the rate of change of N_1^- and N_1^o. For constant total N_1,

$$\frac{dN_1^-}{dt} = -\frac{dN_1^o}{dt} = R_n^o - R_p^- \tag{9}$$

Similar equations are available in the code for a double-level defect with three charge states, N_2^-, N_2^o, and N_2^+, but, for brevity, they are not presented here.

To obtain a solution to the above equations, they are converted to finite difference form for some prescribed mesh distribution. The distribution of the meshes can be chosen arbitrarily by the user to most judiciously utilize the permissible number of meshes. On the Univac 1108, core storage limits the number of meshes to about 230, which is an adequate number to simulate a three-layer planar transistor, and is certainly enough for a two-region solar cell.

Since this code was originally developed to study time-dependent processes in semiconductor devices, the finite difference equations are solved by iteration for finite time steps. Under conditions of steady illumination and circuit load, the code quickly goes to the steady-state solution. The resulting steady voltage and current form one point on the I-V curve. Additional points are obtained by changing the external load resistance and again allowing the problem to run to equilibrium.

Since Eqs. (1), (2), and (3) are time-dependent partial differential equations, one must specify boundary conditions at the two ends of the device and self-consistent initial distributions on n, p, and E. The self-consistent initial distributions could have been specified in any number of ways. To simplify the task of the user, a new problem is started from a condition of zero electric field and charge neutrality everywhere. This is usually a physically unrealistic, but mathematically correct, starting point. The code then does the work of proceeding to the correct solution. For a subsequent run, with the same device, it is usually possible and economical to restart from any previous cycle.

Two types of boundary conditions are available. The first, called "bulk," forces the carrier densities at the two ends of the device to have zero slopes. This is the condition that would apply if the p-n junction were far from the contacts

and the densities have a chance to approach their bulk values far from the junction (hence the name "bulk"). This boundary condition is suitable when the details of the contact are not important in the problem.

On the other hand, when the details of the contact between the semiconductor and the metal are important, the contact potential between the two materials can be simulated in the second type of boundary condition. A large surface recombination velocity can be simulated by defining a narrow region at the surface with a very short recombination lifetime. Of course, an additional requirement is that the current through the exterior circuit must equal the current through the device, including the displacement current in time-dependent problems. Detailed descriptions of the starting and operating procedures for the code can be found in Refs. 17 and 18.

Since this code solves the complete equations for the solar cell, the answers that it provides should be as good, within the accuracy of the finite difference method of solution, as the input data supplied to the code. For comparative design studies, the theoretical device characteristics can be specified exactly and the effect of varying one or more parameters individually can be evaluated. For the analysis of radiation effects in an actual device, the problem is somewhat different because the parameters for the undamaged test device, such as doping profile and lifetimes, are usually not accurately known. For the best results, it is always desirable to avail oneself of all possible nondestructive tests to determine the device parameters, such as capacitance-voltage measurements and resistivity for the doping density profile and diffusion lengths for the lifetimes.

However, in the final analysis, it may be necessary to adjust these parameters somewhat by trial and error to obtain acceptable agreement with the preirradiated test data. Once these characteristics are determined for the undamaged cell, the change in the bulk parameters due to radiation damage can then be estimated and included in the code. If the test data on radiation effects in the bulk material are sufficiently good so that the model for the radiation damage and the change per unit dose can be correctly determined, the predicted results for the irradiated cell should be in acceptable agreement with the post-irradiation test data. If there is significant disagreement, it must mean that the model for the radiation damage or the magnitude of the radiation effects is different from that estimated. In this way, the code can be used as a tool for analyzing and interpreting radiation effects test data. After agreement has been obtained between the experimental and calculated results for a number of test conditions, the code can then be used to extend the test results to other test or operating conditions.

As an example of the results from this code, Fig. 3 shows predicted I-V curves for a particular solar cell for several fluences of 300-keV protons impinging on the illuminated surface. The parameters for the undamaged cell were adjusted to give agreement with the performance curve supplied by the manufacturer. The proton damage was simulated by a distribution of recombination centers, concentrated mainly in the region of the maximum range of the protons. If adequate test data for the proton fluences were available, the validity of the model for the proton damage could be tested by comparing experiment to prediction.

REFERENCES

1. Naber, J. A., Horiye, H., and van Lint, V. A. J., "Radiation Effects on Silicon," Final Report GA-8668, Gulf General Atomic, Inc., Aug. 20, 1968.

2. Naber, J. A., Horiye, H., and Berger, R. A., "Production and Annealing of Defects in Lithium-Diffused Silicon After 30-MeV Electron Irradiation at 300°K," Proceedings of the Conference of Effects of Lithium Doping on Silicon Solar Cells, held at the Jet Propulsion Laboratory, May 9, 1969, Technical Memorandum 33-435. Jet Propulsion Laboratory, Pasadena, Calif., Aug. 15, 1969.

3. Naber, J. A., Passenheim, B. C., and Berger, R. A., "Study of Radiation Effects in Silicon Solar Cells," Report No. GA-9909, Annual Report for Contract No. NAS 7-100, Gulf General Atomic, Inc., Jan. 23, 1970.

4. Naber, J. A., Passenheim, B. C., and Horiye, H., "Introduction and Annealing of Damage in Lithium-Diffused Silicon," Proceedings of the Third Annual Conference on Effects of Lithium Doping on Silicon Solar Cells, held at the Jet Propulsion Laboratory April 27 and 28, 1970, Technical Memorandum 33-467. Jet Propulsion Laboratory, Pasadena, Calif., April 1, 1971.

5. Passenheim, B. C., and Naber, J. A., Radiation Effects, Vol. 2, p. 229, 1970.

6. Passenheim, B. C., Naber, J. A., and Berger, R. A., "Production and Annealing of Defects in Lithium-Diffused Silicon After Irradiation With 30-MeV Electrons and Fission Neutrons at 300°K," Conference Record of the 8th IEEE Photovoltaic Specialists Conference, Seattle, Wash., Aug. 4-6, 1970, IEEE Catalog No. 70C-32 ED, pp. 260-266.

7. Naber, J. A., Horiye, H., and Passenheim, B. C., "Lithium-an Impurity of Interest in Radiation Effects in Silicon," to be published in Radiation Effects (1971).

8. Passenheim, B. C., et al., "Study of Radiation Effects in Silicon Solar Cells," Report No. Gulf-RT-10482, Annual Report for Contract No. NAS 7-100, Gulf Radiation Technology, Jan. 20, 1971.

9. Young, R. C., et al., J. Appl. Phys., Vol. 40, p. 271, 1968.

10. Shockley, W., and Read, W. T., Jr., Phys. Rev., Vol. 87, p. 835, 1952.

11. Lax, M., Phys. Rev., Vol. 119, p. 1502, 1960.

12. Leadon, R., and Naber, J. A., J. Appl. Phys., Vol. 40, p. 2633, 1969.

13. Damask, A. C., and Dienes, G. J., Point Defects in Metals, Gordon and Breach, Science Publishers, New York, 1963.

14. Pell, E. M., J. Appl. Phys., Vol. 31, p. 291, 1960.

15. Fuller, C. S., and Severiens, J. C., Phys. Rev., Vol. 96, p. 21, 1960.

16. Maita, J. P., J. Phys. Chem. Solids, Vol. 4, p. 68, 1958.

17. Leadon, R., and Vaughn, M., "Short-Pulsed Radiation Effects on Dynamic Electronic Components," Final Report on Contract DASA01-68-C-0123, DASA Report No. 2358 Defense Atomic Support Agency; also Gulf General Atomic Report GA-9397, June 5, 1969.

18. Leadon, R. E., et al., "Radiation Effects on Dynamic Electronic Components," Final Report on Contract DAOSA01-69-C-0113, DASA Report No. 2546 Defense Atomic Support Agency; also Gulf Radiation Technology Report GA-9775, July 1970.

Table 1. Summary of the results of isochronal and isothermal annealing experiments on electron- and neutron-irradiated lithium-diffused float-zone and quartz-crucible silicon

Sample type	Float zone			Quartz crucible		
Lithium donor density, Li/m^{-3}	2.5×10^{22}	4.5×10^{20}	2×10^{21}	2.5×10^{21}	4.5×10^{20}	2.5×10^{21}
Fluence (particles/m^2)	$\sim 10^{17}$	10^{16} to 10^{17}	5×10^{14}	1.5×10^{16} to 8×10^{16}	10^{16}	4×10^{14}
Radiation	30-MeV electrons	30-MeV electrons	Fission neutrons	30-MeV electrons	30-MeV electrons	Fission neutrons
Activation energy, eV	0.85 ±0.10	0.60 ±0.10	0.67 ±0.05	1.0 ±0.2	0.75 ±0.10	1.2 ±0.6
Frequency factor, sec^{-1}	$\sim 10^{10}$	Unknown	$\sim 10^{7}$	10^{8} to 10^{10}	10^{7} to 10^{8}	Unknown

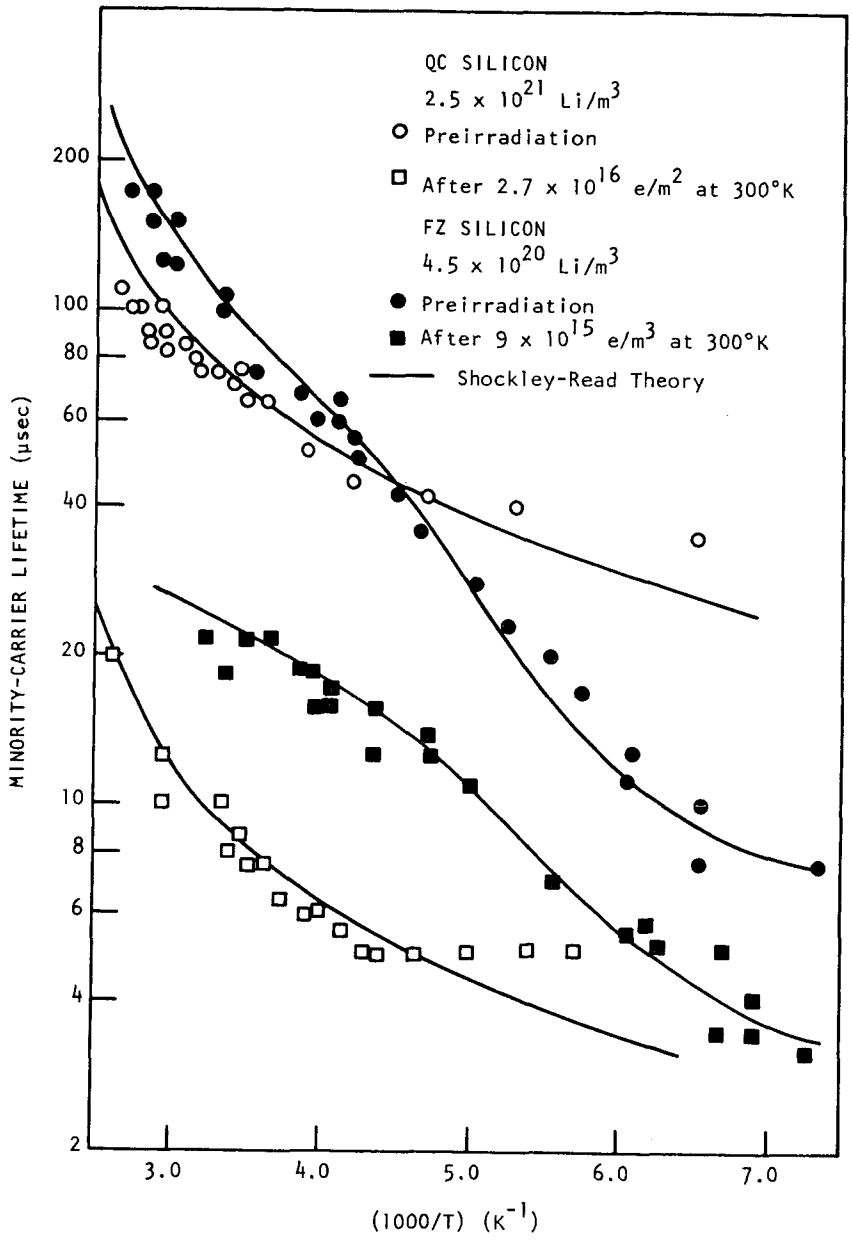

Fig. 1. Inverse temperature dependence of minority-carrier lifetime of lithium-diffused float-zone and quartz-crucible silicon before and after irradiation with 30-MeV electrons at room temperature

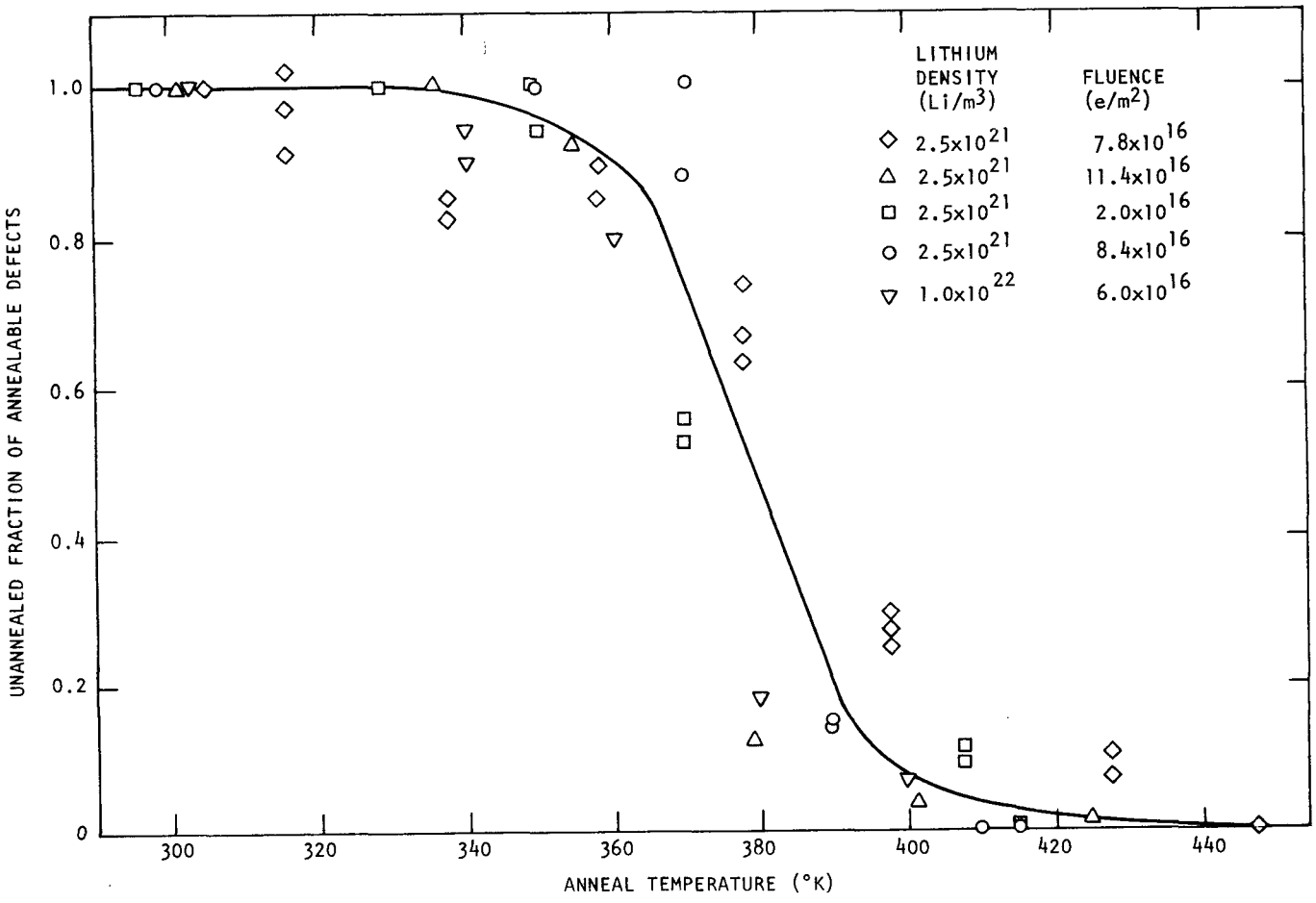

Fig. 2. Unannealed fraction of annealable defects after 5-min isochronal anneals at indicated temperatures after 30-MeV irradiation of lithium-diffused N-type QC silicon irradiated at 300 K

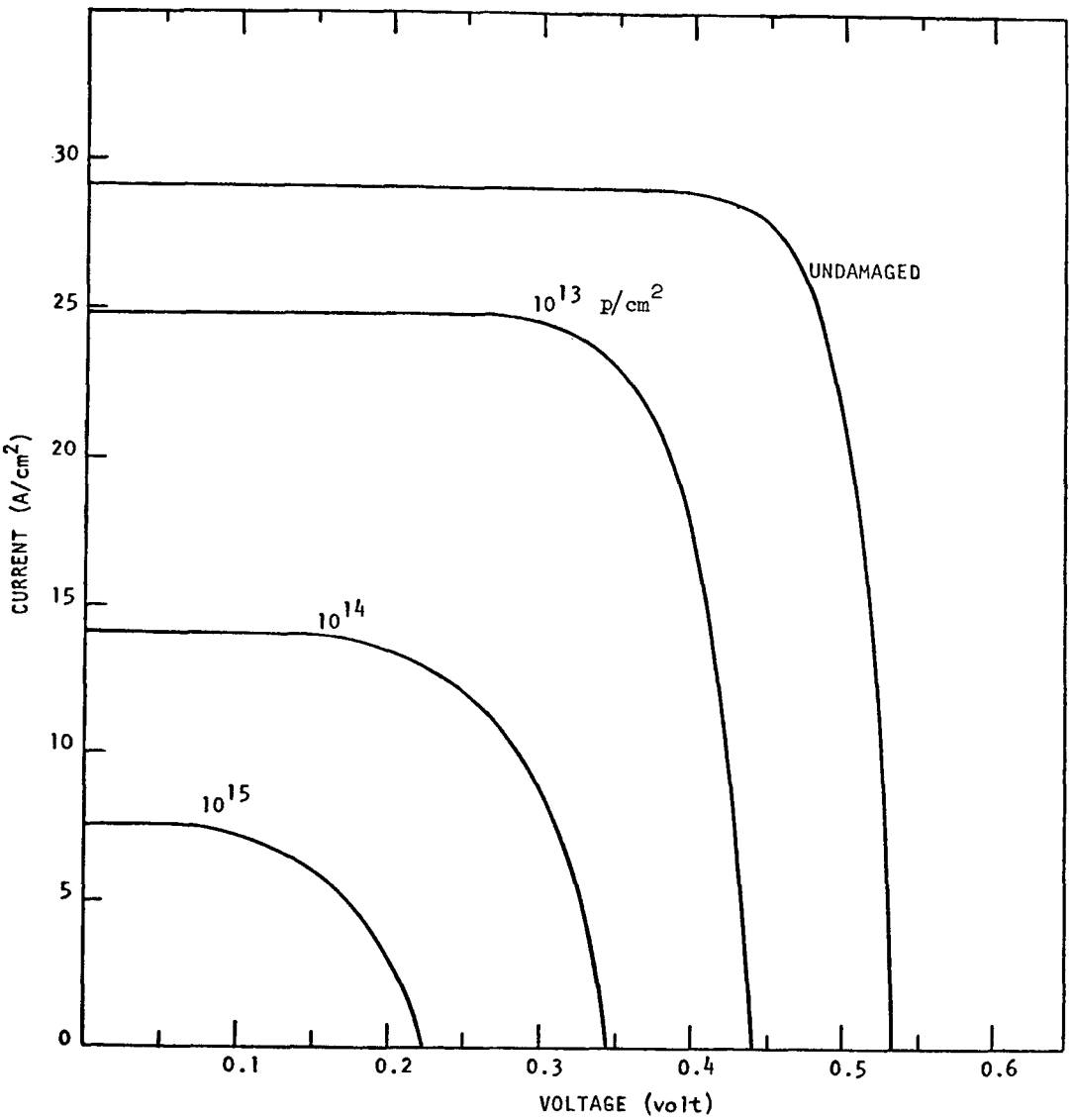

Fig. 3. Current-voltage curves of a graded-junction cell degraded by 300-keV protons to various fluences

N72-10062

HALL EFFECT STUDY OF ELECTRON IRRADIATED Si (Li)*

J. Stannard
Naval Research Laboratory
Washington, D.C.

I. INTRODUCTION

Measurement of the Hall coefficient as a function of temperature between 15 and 300 K allows the separate determination of donor and acceptor concentrations in silicon. In this experiment these concentrations were monitored in samples which were irradiated at 240 K by 1-MeV electrons and then thermally annealed at 300 K. Presumably in both lithium- and phosphorus-doped silicon one would expect irradiation to increase the acceptor concentration and decrease the donor concentration due to the formation of vacancy donor pairs. Annealing should not change either concentration in phosphorus-doped silicon and should cause both concentrations to decrease in silicon doped with moderate amounts of lithium. In addition to this, in both lithium- and phosphorus-doped silicon the concentration and energy level of the A center can be measured at each point in the sample's history. This experiment was limited to float-zoned silicon doped with less than 6×10^{14} donors/cm^3.

II. THE A CENTER

Before going into the details of this experiment some evidence will be given concerning the anomalous activation energy previously reported for the A center. Measurements made on a variety of samples indicated a level at E_c -0.14 eV, instead of at E_c -19 eV as expected for the A center (Ref. 1). All of these samples were cut from one of two boules made by Dow Corning. A sample of Semi-element's pulled silicon was irradiated and the A center energy measured to be 0.19 eV. Another sample of 14 Ω-cm float-zoned Si(P) made by Dow Corning was then lightly irradiated and the production rate and energy of the A center measured. Then the same sample was irradiated much more heavily so that enough deep centers would be created to depopulate the level at 0.14 eV and indicate the presence of any deeper levels. The results of this experiment were as follows:

Dose, e/cm^2	Concentration, cm^{-3}	Energy, eV	Production rate, cm^{-1}
2×10^{14}	2.5×10^{13}	0.14	0.13
1.3×10^{15}	1.5×10^{13}	0.19	0.01

This data resolves the problem. In this boule centers at 0.14 eV and 0.19 eV are both being formed as a result of irradiation. However, the center at 0.14 eV is being formed with a much higher production rate than the usual A center at 0.19 eV. When the sample was heavily irradiated the Hall effect ceased to count the level at 0.14 eV and also began to indicate the presence of a level at E_c -0.19 eV. The level at E_c -0.14 eV may be related to the level at E_c -0.13 eV seen by Stein in pulled silicon (Ref. 2). If so, the only unusual property of this Dow Corning material is that the formation rates of these two levels are reversed

*Work performed for the Jet Propulsion Laboratory (Contract WO-8056) and supported by the National Aeronautics and Space Administration under Contract NAS7-100.

in their normal order of importance. Since oxygen does form a number of different complexes in silicon, it is most likely that the 0.14 eV center is the usual A center but with perhaps an additional oxygen present in a nearby interstitial site. The possibility that another impurity such as carbon may be involved cannot be discounted, however.

III. LITHIUM AND THE A CENTER

The experiment to be described was designed to study the interaction of lithium with the A center. In order to determine what effects were due to the presence of lithium it was necessary to use a sample and a control cut from the same boule and having similar resistivities. The presence of both phosphorus and lithium in the sample reduced somewhat the variety of information obtainable, i.e., it was not possible to demonstrate that the LiV complex is formed during irradiation. A separate experiment would be necessary to investigate this question.

Two samples were prepared from the same boule of float-zoned 14 Ω-cm Dow Corning silicon containing 3.5×10^{14} donors/cm^3. Into one sample an additional 3.4×10^{14} lithium donors/cm^3 were introduced from a lithium in oil suspension using a tack-on and redistribution of 5/60/425°C. Measurements of the Hall effect versus temperature were made; (1) before irradiation, (2) after irradiation at 240 K by 1.7×10^{14} 1 MeV e/cm^2, (3) after 2 h, (4) and after 17 h at 300 K. The electrical contacts degraded due to thermal cycling after 17 h thereby terminating the experiment. Irradiation was performed at 240 K so that lithium could be considered immobile during irradiation. As a result the effects of irradiation could be separated from those due to lithium mobility. Donor and acceptor concentrations were obtained by least squares analysis of the data using Fermi statistics for silicon containing two kinds of donors and two kinds of acceptors. These calculations assumed the values of excited state splitting and ground state degeneracy obtained from optical experiments reported in the literature (Refs. 3-5).

Figure 1 shows the behavior of room temperature carrier concentration in the two samples as a function of annealing time and is the behavior expected. There was no measurable annealing in the phosphorus-doped sample and a decreasing carrier concentration in the sample containing lithium.

Figure 2 shows the change in donor concentration in these samples caused by annealing at 300 K. The most apparent difference between the two samples for annealing times longer than 2 h is that the donor concentration decreases in the lithium-doped sample and is constant in the phosphorus-doped sample. This change in the lithium-doped sample was clearly caused by radiation damage, since such samples do not show a change in resistivity with time prior to irradiation. From the data shown here it is not possible to show that the LiV complex forms during irradiation. From the pre-irradiation and post-irradiation points it is clear that there is more donor loss during irradiation in the sample containing both lithium and phosphorus than in the sample doped only with phosphorus. Unfortunately, several samples doped only with phosphorus showed a range of values for carrier removal rate. An experiment similar to this one, but using a sample doped only with lithium, would demonstrate the formation of LiV.

Comparison of the data before annealing and after 2 h of annealing indicates a decrease in donor concentration caused by bringing the sample up to room temperature from 250 K. This was not expected in the phosphorus-doped sample and represents a short-term thermal annealing in the direction of increased damage. Other samples containing phosphorus were irradiated at 250 K but were held at 250 K for 2 h before making any measurements. This was found to decrease the magnitude of the annealing stage, indicating that annealing occurs at 250 K as well as 300 K. In studies of unannealed Si(Li), data should be taken after substantial annealing at 250 K, which will remove this stage without allowing the lithium to be mobile. This short-term annealing is even more striking in Fig. 3, which shows the acceptor concentration.

The total measured acceptor concentration and A center concentration are represented by A_t and 0.14, respectively. For the phosphorus-doped sample the value indicated for the E-center concentration is the measured decrease in donor concentration caused by irradiation. Inspection of this data indicates that this annealing may be caused by thermal release of trapped vacancies which then form additional damage complexes. Such vacancies would have to be much more tightly bound than the vacancy-interstitial close-spaced pair, as the observed annealing temperatures are very high (Ref. 2). This behavior may also be a characteristic peculiar to these boules of silicon. As was expected, the behavior of acceptor concentration with continued annealing was very different in the two samples. Whereas annealing causes acceptor concentration to decrease in the lithium-doped sample, it has no effect in the phosphorus-doped sample. It is evident from this figure that A centers interact much more strongly with lithium than does the E center. Comparing the changes in total acceptor concentration with those in A center concentration it is apparent that almost 80% of those centers that are neutralized within 17 h were A centers. Since there were probably as many E centers in the lithium-doped sample as there were in the control sample, it is clear the A centers completely monopolized the neutralization process despite the fact there were more E centers than A centers.

By comparing the changes in donor and acceptor concentrations seen in Figs. 2 and 3 an idea can be obtained as to how many lithium ions are required to neutralize the A centers. The concentration changes between 2 and 17 h are:

$$\Delta Li^+ = -4.5 \times 10^{13}\ \text{cm}^{-3}$$

$$\Delta A_t = -1.3 \times 10^{13}$$

$$\Delta 0.14 = -1.0 \times 10^{13}$$

Since the total acceptor concentration (A_t) includes the A center concentration (0.14) it is apparent that 80% of the annealed centers were A centers. Comparing this change to the much

larger loss in lithium concentration it seems that as many as four lithium atoms may be required to neutralize this A center.

REFERENCES

1. Sonder, E., and Templeton, L., J. Appl. Phys., Vol. 31, p. 1279, 1970.
2. Stein, H., and Vook, F., Phys. Rev., Vol. 163, p. 790, 1967.
3. Aggarwal, R., et al., Phys. Rev., Vol. 138, p. A882, 1965.
4. Long, D., and Myers, J., Phys. Rev., Vol. 115, p. 1107, 1959.
5. Aggarwal, R., and Ramdas, A., Phys. Rev., Vol. 137, p. A602, 1965.

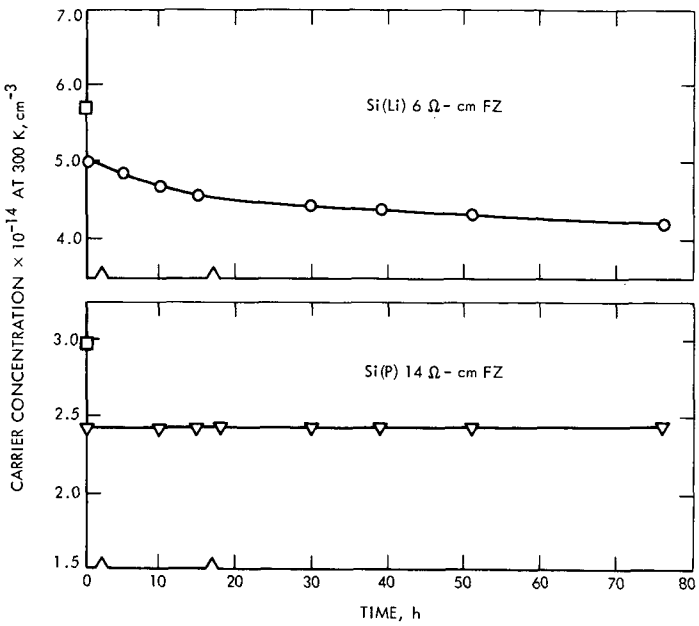

Fig. 1. Annealing of room-temperature carrier concentration, irradiated at 240 K by 1.7×10^{14} 1-MeV e/cm^2

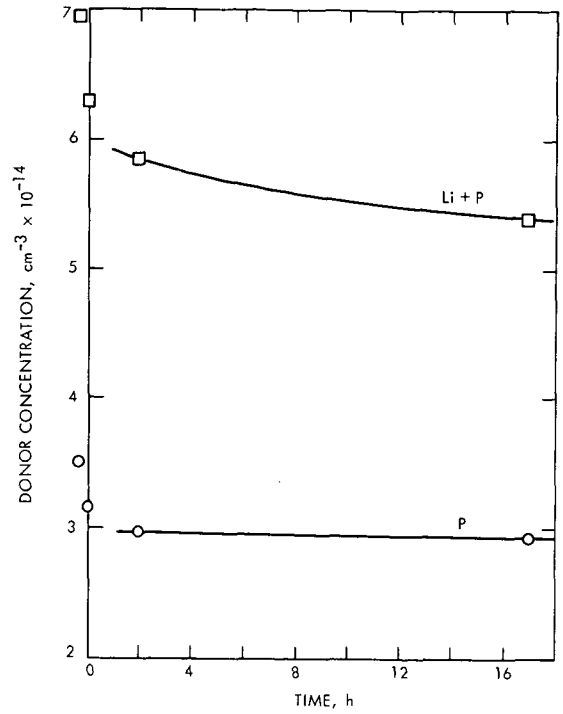

Fig. 2. Room temperature annealing of donor concentration in lithium and phosphorus-doped silicon

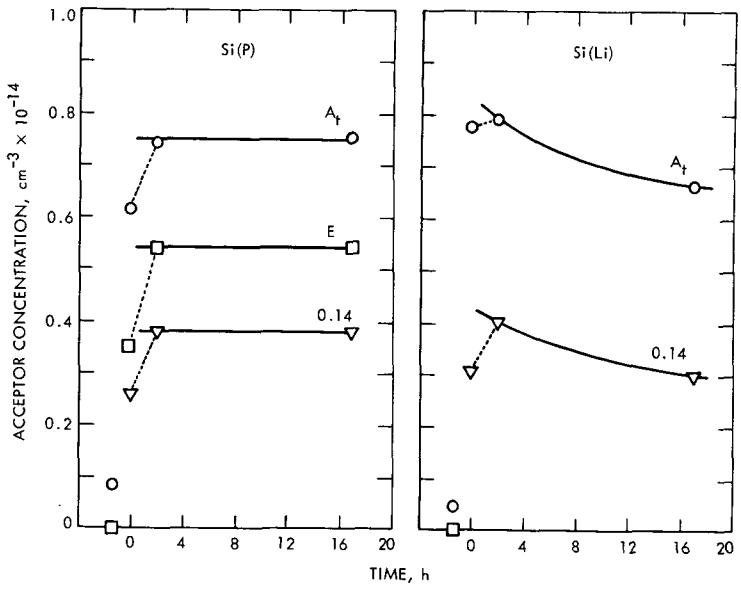

Fig. 3. Room temperature annealing of acceptor concentration in lithium and phosphorus-doped silicon

THE OBSERVATION OF STRUCTURAL DEFECTS IN NEUTRON-IRRADIATED LITHIUM-DOPED SILICON SOLAR CELLS

G. A. Sargent
Department of Metallurgical Engineering and Materials Science
University of Kentucky
Lexington, Kentucky

ABSTRACT

Electron microscopy has been used as a technique to observe the distribution and morphology of lattice defects introduced into lithium-doped silicon solar cells by neutron irradiation. Upon etching the surface of the solar cells after irradiation, crater-like defects are observed that are thought to be associated with the space charge region around vacancy clusters. The crater defect density was found to increase with increasing irradiation dose and increasing lithium content; however, the defect size was found to decrease with increasing dose and lithium.

Thermal annealing experiments showed that the crater defects were stable in the temperature range 300 to 1200 K in all of the lithium-doped samples. Some annealing of the crater defects was observed to occur in the undoped cells which were irradiated at the lowest doses.

I. INTRODUCTION

It is now generally accepted that a localized cluster of lattice defects may be produced by a recoil from a single collision between an energetic neutron and a lattice ion (Refs. 1-5). The energy of the recoil is dissipated by creating lattice disorder. Subsequent rapid quenching of the lattice should freeze a large concentration of lattice defects into the neighborhood.

Until recently, the behavior of irradiated semiconductors has been interpreted on the basis of isolated Frenkel defects in terms of the model of James and Lark-Horovitz (Ref. 6). However, Gossick (Ref. 7) and Crawford and Cleland (Ref. 8) have proposed a model of disordered regions that is more applicable to neutron-irradiated semiconductors and predicts the existence of regions of highly localized damage. Their model assumes that a region of lattice disorder is produced upon irradiation which may contain a high concentration of defects such as vacancies. Surrounding the disordered region is a potential well that arises because the position of the Fermi level relative to the energy band is different within the disordered region compared to that outside. Crawford and Cleland have estimated the size of the defect region to be of the order of 15 to 20 nm. For P-type silicon the dimensions of the space-change region surrounding the defect region due to the potential well is predicted to be about 200 to 250 nm in diameter.

The measurement of electrical properties by Closser (Ref. 9) and Stein (Refs. 10-12) have subsequently provided direct evidence for the existence of damage regions as predicted by the theoretical models of Gossick and Crawford and Cleland.

Until recently little work has been carried out to determine the exact structural nature of the lattice disorder created by irradiation damage. X-ray diffraction (Ref. 13) techniques and direct observation of thin foils by electron microscopy (Refs. 14-16) met with limited success in this respect. However, an alternative method for observing defects in semiconductors using surface replication electron microscopy has been

perfected by Bertolotti and his coworkers (Refs. 17-20).

Bertolotti found that upon etching the surface of neutron-irradiated silicon samples craters were produced, the dimensions of which were found to compare with the dimensions of the space-charge regions as predicted by the theory of Gossick (Ref. 7) and Crawford and Cleland (Ref. 8). Within the craters a small well-defined region could also be observed, the size of which compared well with the theoretical estimates for the size of the defect clusters.

The main objective of the work to be described in this present paper was to make use of the technique developed by Bertolotti to determine the effects of neutron irradiation on the structural characteristics of undoped and lithium-doped silicon solar cells. The overall objective was to obtain a better understanding of the morphology of the defects produced by irradiation damage and their interaction with dopants such as lithium. Such knowledge could lead to the development of solar cells which are more radiation resistant.

II. EXPERIMENTAL TECHNIQUE

The work was carried out on commercial undoped and lithium-doped silicon solar cells prepared by Heliotek. The cells were produced from float-zone melted single crystals of phosphorus-doped N-type silicon. Boron was diffused into the slice to give a junction depth of 0.5 μm. Lithium was diffused in using the paint-on technique to produce three types of cells: 10^{15}, 10^{16} and 10^{17} lithium atoms/cm^3. In addition, a fourth type of cell was produced with no lithium.

Samples of the undoped and lithium-doped cells were irradiated with monoenergetic 14.7-eV neutrons produced by a Cockroft-Walton generator. The irradiation was carried out at room temperature, and the dose was controlled by varying the distance of the samples from the target.

After irradiation the surface of the solar cells was prepared for replication by mechanically grinding and polishing and then by etching with CP4A etchant. A carbon replica of the surface was obtained by evaporation. The replica was shadowed with chromium and was observed in an electron microscope at 75 kV.

To study the recovery of the irradiation damage a number of samples were annealed at temperatures of 293, 593, 700, 900 and 1200 K for 10 min in a vacuum furnace (10^{-6} torr).

III. RESULTS AND DISCUSSION

Figure 1 shows a photograph obtained in the electron microscope of a surface replica taken from the etched surface of an unirradiated sample which contained no lithium. This photograph shows a finely etched uniform structure without any additional significant features. In contrast, Fig. 2 shows a surface replica from a sample which contained no lithium but was irradiated with 10^{11} neutrons/cm^2. This is a typical example of the appearance of the etched surfaces of the samples after neutron irradiation. The area shows a finely etched background structure on which many crater-like depressions can be observed.

According to the Gossick theory (Ref. 7), the dimensions of the craters revealed by the above techniques actually correspond to the size of the space-charge region which surrounds a cluster of lattice defects formed during the irradiation. Therefore, the density of the craters should relate to the total defect volume produced at a given irradiation dose.

The average density and diameter of the craters were measured as a function of dose and lithium content. Values of the average crater defect density and diameter as functions of irradiation dose and lithium content are presented in Figs. 3 and 4, respectively. It can be seen that the average defect density increases with increasing irradiation dose and increasing lithium content. On the other hand, however, it can be seen from Fig. 4 that the average defect diameter decreases with increasing dose and lithium content. It was found from these results that, for a given irradiation dose, the total defect volume is essentially constant. It appears that the presence of lithium provides more nucleation sites for the defect clusters to form, and as a result the average defect diameter is smaller. Under comparable irradiation conditions, 14.7-MeV neutrons at a dose of 10^{12}/cm^2, the present results are in good agreement with those reported by Bertolotti, et al., (Ref. 19). Therefore, the present results support the theories of Gossick (Ref. 7) and Crawford and Cleland (Ref. 8).

From the annealing experiments it was found that no change could be detected in either the average defect density or the average size over the temperature range 300 to 1200 K, with the exception of those samples which were undoped and irradiated at the two lowest doses, i.e., 10^{10} and 10^{11} n/cm^2. These results are shown in Figs. 5 and 6 where the average defect density and size are plotted, respectively, as a function of annealing temperature. In these samples annealing was found to be significant at a temperature of about 800 K and was reflected in both an increase in defect density and a decrease in defect diameter.

It would appear from these results, therefore, that the defect structure which is formed during the irradiation at room temperature of either the undoped or doped material, at the highest doses, represents the most stable defect structure. The large defect clusters which are formed at the low doses in the undoped material have a tendency to collapse upon annealing to form smaller defects at a higher density.

The results of the annealing experiments carried out in the present work appear to be significantly different from those observed previously from recovery of electrical properties in neutron irradiated silicon, by Stein (Ref. 21) and Passenheim and Naber (Ref. 22). However, it is not possible at the present time to make direct correlation with these results as the irradiation conditions and annealing times were significantly different.

It is not apparent from the present results exactly what role lithium plays in the nucleation and stabilization of the irradiation-induced defects. At the high temperatures used in the annealing experiments it is unlikely that lithium would remain in the bulk lattice. There is some evidence (Refs. 23, 24), however, that at the temperature

at which the irradiation is carried out the irradiation-induced defects are trapped at precipitated metallic lithium and form stable clusters. The subsequent annealing of the defect cluster, once it has reached a stable configuration or critical size, could be quite independent of the presence of lithium. Hence, the presence or mobility of lithium at the higher annealing temperature would not necessarily influence the annealing kinetics of the defect clusters.

REFERENCES

1. Seitz, F., Disc. Faraday Soc., Vol. 5, p. 271, 1949.
2. Seitz, F., and Koehler, J. S., in Solid State Physics. Edited by F. Seitz and D. Turnbull, Academic Press Inc., Vol. 2, 1956.
3. Siegel, S., Phys. Rev., Vol. 75, p. 1823, 1949.
4. Billington, D. S., Nucleonics, Vol. 14, p. 54, 1956.
5. Brooks, H., Am. Rev. Nuclear Sci., Vol. 6, p. 215, 1956.
6. James, H. M., and Lark-Horovitz, K., Z. Physick Chem., Vol. 198, p. 107, 1951.
7. Gossick, B. R., J. Appl. Phys., Vol. 30, p. 1214, 1959.
8. Crawford, J. H., and Cleland, J. W., J. Appl. Phys., Vol. 30, p. 1204, 1959.
9. Closser, W. H., J. Appl. Phys., Vol. 31, p. 1693, 1960.
10. Stein, H. J., J. Appl. Phys., Vol. 31, p. 1309, 1966.
11. Stein, H. J., Phys. Rev., Vol. 163, p. 801, 1967.
12. Stein, H. J., J. Appl. Phys., Vol. 39, p. 5283, 1968.
13. Fujita, F. E., and Gonser, U., J. Phys. Soc. Japan, Vol. 13, p. 1968, 1958.
14. Parsons, J. R., Balluffi, R. W., and Koehler, J. S., Appl. Phys. Letters, Vol. 1, p. 57, 1962.
15. Hemment, P. L. F., and Gunnersen, E. M., J. Appl. Phys., Vol. 37, p. 2912, 1966.
16. Pankratz, J. M., Sprague, J. A., and Rudee, M. L., J. Appl. Phys., Vol. 39, p. 101, 1968.
17. Bertolotti, M., et al., Nuovo Cimento, Vol. 29, p. 1200, 1963.
18. Bertolotti, M., et al., J. Appl. Phys., Vol. 36, p. 3506, 1965.
19. Bertolotti, M., et al., J. Appl. Phys., Vol. 38, p. 2645, 1967.
20. Bertolotti, M., Radiation Effects in Semiconductors, p. 311, Plenum Press, 1968.
21. Stein, H. J., J. Appl. Phys., Vol. 37, p. 3382, 1966.
22. Passenheim, B. C., and Naber, J. A., Radiation Effects, Vol. 2, p. 229, 1970.
23. Sargent, G. A., Research Study of Damage Produced in Silicon Semiconductors by Neutron Irradiation, Technical Report UKY 31-70-Met 13, University of Kentucky, 1970.
24. Berger, R. A., et al., Radiation Effects in Silicon Solar Cells, Quarterly Report by Gulf General Atomic to Jet Propulsion Laboratory, October 1969.

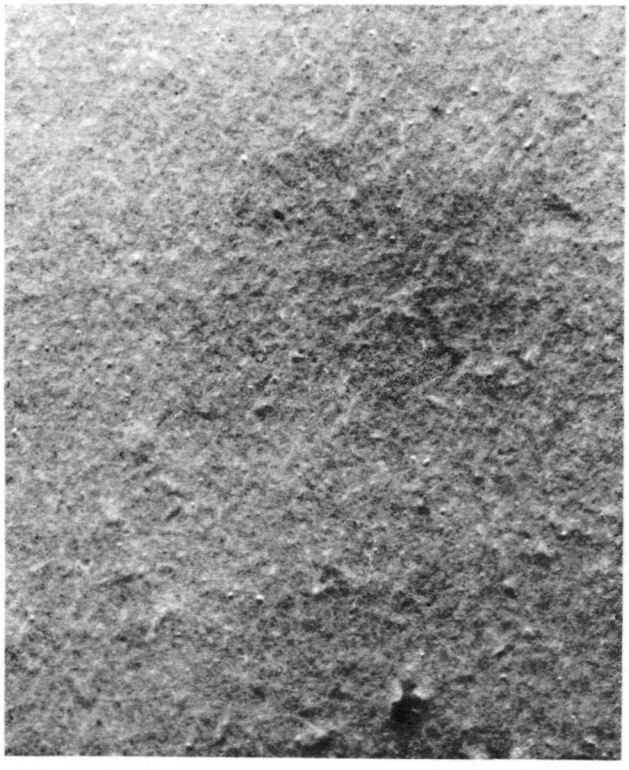

Fig. 1. Surface replica of an undoped and unirradiated solar cell

Fig. 2. Surface replica of an undoped solar cell irradiated with 10^{11} neutrons/cm^2

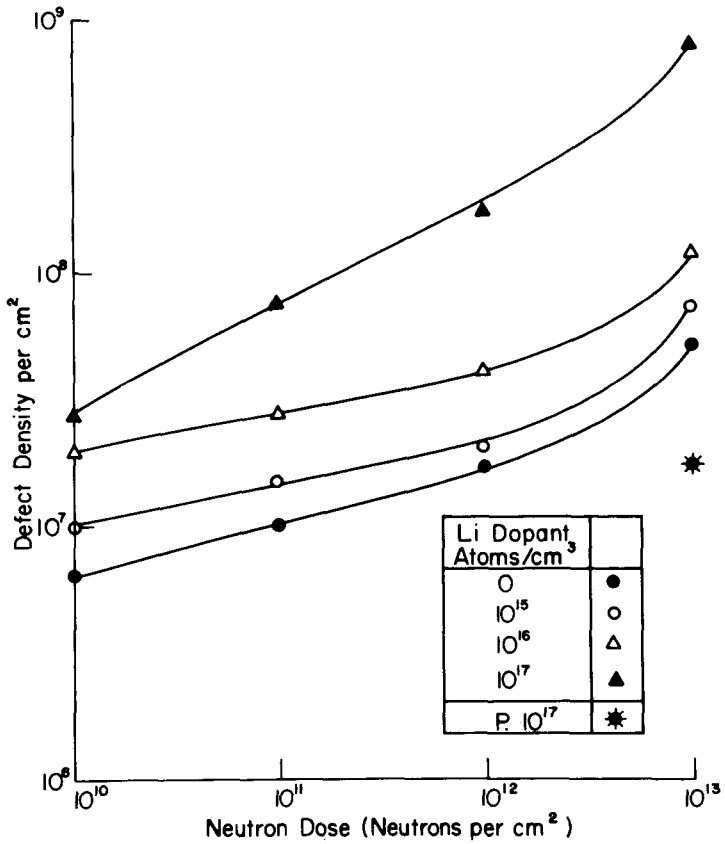

Fig. 3. Average defect density as a function of irradiation dose and lithium dopant

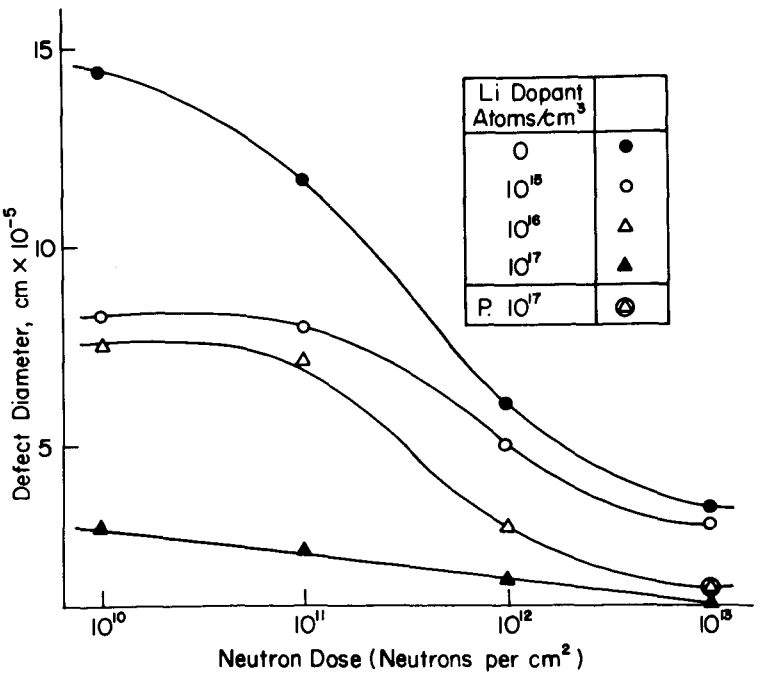

Fig. 4. Average defect diameter as a function of neutron dose and lithium dopant

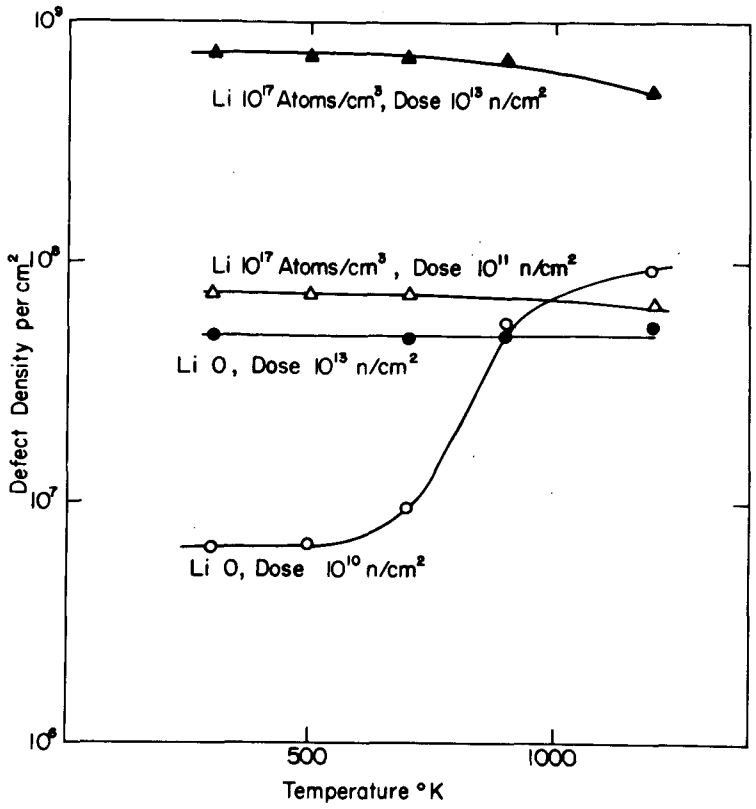

Fig. 5. Effect of thermal annealing on defect density

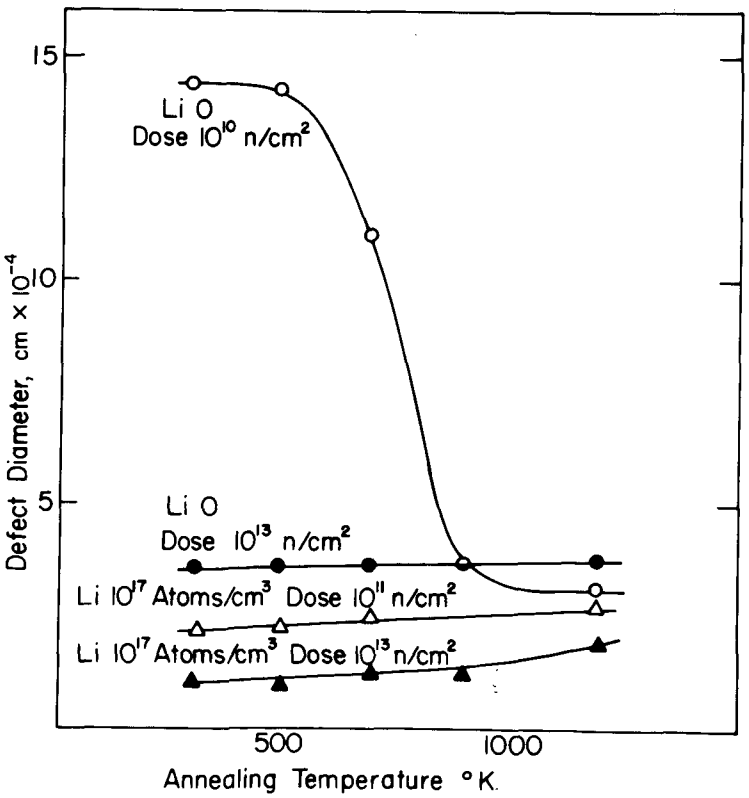

Fig. 6. Effect of thermal annealing on defect diameter

RADIATION DAMAGE AND ANNEALING OF LITHIUM-DOPED SILICON SOLAR CELLS*

R. L. Statler
Naval Research Laboratory
Washington, D. C.

I. INTRODUCTION

The origination of the lithium-doped radiation-hardened silicon solar cell in 1966 (Ref. 1) has been followed by an intensive effort to study the specifics of the radiation damage and recovery processes. As one step in the direction toward optimizing the chemical and physical parameters of the cell for maximum radiation hardness, it is essential to determine the performance of this solar cell in various radiation environments. The amount and rate of this recovery process have been shown to depend on the oxygen impurity in the silicon, the type of irradiating particle, the fluence, and the temperature of the cell following the irradiation. In addition, low-flux rate irradiation as contrasted with Van de Graaff bombardment, have provided valuable information on the behavior of these cells in a simulated space environment. A part of this paper will discuss the recent results of a continuing real-time-rate irradiation (Ref. 2) which was begun in September 1969. Since that time, better lithium-doped cells have been made, and placed into the study. We shall also discuss the results of 1-MeV electron and 4-MeV proton Van de Graaff irradiation and annealing of a solar cell made from crucible-grown silicon which has been lithium-diffused for 8 h at 325°C.

II. EXPERIMENTAL

Three modes of radiation were used to study damage and recovery in the lithium solar cells. They comprised 1.2-MeV gamma photons from the Naval Research Laboratory (NRL) Cobalt 60 source, 1-MeV electrons from a Van de Graaff, and 4-MeV protons from a Van de Graaff. The damage caused by the 1.2-MeV gamma photon comes about from energized electrons which are produced in the chamber walls, in the solar cell holder, and within the solar cell by means of Compton interactions of the gamma ray with electrons in the material (Ref. 3). These electrons have a spectrum of energies ranging upward to 0.8 MeV. These energetic electrons create lattice vacancies in the silicon, followed by the formation of defects and recombination centers similar to those occurring in 1-MeV electron irradiated silicon. A first approximation for equivalency of damage in solar cells from Cobalt 60 gammas, as compared with electrons, can be made by determining the number of gamma photons that will produce the same number of lattice displacements as a 1-MeV electron. If values (Ref. 4) are used for the total number of displaced silicon atoms per unit of incident flux of 10^{-2} for 1-MeV gamma photons and 4.6 for 1-MeV electrons, the equivalent electron dose corresponding to 1 rad (Si),

*This work was performed for the Jet Propulsion Laboratory, sponsored by the National Aeronautics and Space Administration under Contract No. NAS7-100.

which is 2.22×10^7 photons/cm^2, is 4.35×10^6 e/cm^2. This equivalency factor is applicable only when the gamma environment is one of electronic equilibrium for the irradiated sample. In this case, this condition is essentially satisfied.

The flux values, in units of particles/cm^2-s, varied widely. In the case of gamma flux, the value was 5×10^6 e/cm^2-s, later increased to 2.7×10^7 e/cm^2-s. For the electron Van de Graaff irradiations the flux was 5×10^{11} e/cm^2-s, and for the proton Van de Graaff, 3×10^9 particles/cm^2-s.

The solar cells discussed here are five types. There are four groups of Heliotek lithium-doped P/N cells, one of Centralab lithium-doped P/N c cells, and a group of Centralab 10-Ω-cm N/P flight-quality solar cells. Table 1 shows the experimental matrix for the gamma ray portion of this study.

The experimental apparatus for the gamma irradiations consisted of three stainless-steel cylindrical cans about 7.6 cm in diameter, 24 cm long, with a 0.51-cm-thick wall. The solar cells were held in contact with temperature-controlled brass plates by means of spring clips. Each cell was loaded with a 10-Ω resistor, with pressure contact made through the spring clips and brass plate.

Illumination was provided during irradiation by means of five 12-V automobile lamps in each can. Replacement of lamps was required about every 3 mon because of radiation darkening of the glass bulbs. Then cans were evacuated after sealing, and back-filled with 0.7 N/cm^2 (1 psi) of argon to provide for thermal conduction of the heat from the lamps to the chamber walls. (Under vacuum, the bulbs failed in a few hours.)

The cell temperatures were controlled by means of a combination of electrical strip heaters and water-carrying copper tubing fastened to the rear of the solar cell mounting plates. One can was held at 30°C, and two cans at 60°C with a variation of ±1°C. For measurements of the I-V curves, the solar cells were removed from the cans and placed under a Spectrosun X-25L solar simulator calibrated for 140 mW/cm^2 air mass zero. Solar cell temperature was 25°C for all measurements at the simulator. During the times the cells were out of the irradiation chambers, they were held at dry-ice temperature to prevent annealing, except for the actual measurement time.

The irradiations at the NRL 2-MeV electron Van de Graaff were carried out on solar cells at room temperature, with forced-air cooling on the sample. The fluence obtained was 5×10^{14} 1-MeV e/cm^2. All of the solar simulator measurements were performed with cell temperatures of 25°C. The annealing of the solar cells after irradiation was done in forced-draft laboratory ovens at 60 and 30°C with solar simulator measurements being performed at intervals throughout the recovery period.

The 4-MeV proton bombardment was performed at the NRL 5-MeV proton Van de Graaff to a fluence of 2.2×10^{11} p/m^2, with the two solar cells in a vacuum of 6.7×10^{-3} N/m^2 during the irradiation. As in the case of the electron-irradiated cells, these samples were measured at the solar simulator at 25°C at intervals throughout their 60°C annealing period.

III. RESULTS

The results of Cobalt 60 gamma irradiations over a period of 18 mon will be discussed. During this time the solar cells were removed from the source 12 times for measurements. A total gamma exposure of 1.4×10^8 R was received by the cells, equivalent to a 1-MeV electron fluence of 6.1×10^{14} e/cm^2. It should be mentioned that the dose rate was increased from 5×10^6 e/cm^2-s to 2.7×10^7 e/cm^2-s after a fluence of 2×10^{14}. The trend of the data show that the results were not affected by this increase. Figure 1 is a plot of the power output of the cells as they are irradiated at 60°C in a continuous gamma ray environment. The power is measured with a cell temperature of 25°C at one sun of illumination. It can be seen from Table 2 that the four types of lithium cells were much lower in initial efficiency than the N/P 10 Ω-cm cell which was used for comparison. The results of the 30°C irradiation showed slightly more damage than these at high fluences, although up to 1×10^{14} e/cm^2 there was generally little difference between the 30 and 60°C data (Ref. 2). The groups H2 and H5 were designated generally to be low lithium content. In fact, junction capacity measurements on H5 indicated no lithium concentration near the junction. The poor radiation hardness attests to this finding. On the other hand, the more heavily doped H6 and H9 were also so low in efficiency that they were never competitive to the H2 and N/P cells in the course of the experiment.

A quite different picture of the performance of a lithium cell is given in Fig. 2. The maximum efficiency shown here for the C11A cell is 11.2% compared with 10.4% for the N/P cell. However, the rapid decrease in power brings the lithium cell performance exactly to the level of the N/P cell at 60°C irradiation temperature. The results of the 30°C irradiation show that the C11A cell output is definitely lower. One might assume that the increased mobility of lithium at the higher temperature causes a more rapid annealing rate for the damage centers which are being produced. The most important point of this figure is that the power level of the C11A cell ultimately stays above the N/P cell at fluences beyond 4×10^{14} e/cm^2, with an improvement of about 5%. In terms of long exposures in an electron environment, it appears that the lithium cell will offer an advantage over the conventional N/P cell.

The next part of the study was to investigate the annealing rate of rapidly damaged solar cells as a function of temperature and cell type. The C11A lithium-doped cell was chosen because of its good characteristics, and was compared with the same type of N/P cell used throughout this work. Figure 3 depicts the post-irradiation annealing of the power lost through 1-MeV electron irradiation in C11A and N/P solar cells. The N/P cell shows a slight recovery immediately after the irradiation, then quickly saturating and even slightly declining. The C11A cell shows additional damage occurring within the first few hours following the

irradiation. The 30°C annealing does not regain any of the power lost during the irradiation. However, annealing at 60°C produces a large recovery of the lost power. This result can be seen more quantitatively in Fig. 4 where the percentage of recovered power is shown. Percentage recovery is defined as

$$\frac{P_a - P_r}{P_0 - P_r} \times 100$$

where P_0 is the original power, P_r is measured after the irradiation, and P_a after annealing. In Fig. 4 one observes that the lithium cell has recovered 42% of its power after 200 h at 60°C, while the N/P cell has recovered only 10%. In actual power level, the lithium cell is about 5% greater at 200 h (Fig. 3).

All of the previous results, for 60°C gamma radiation and 60°C annealing after electron radiation are summarized in Fig. 5. The maximum annealing time for this data is 100 days, whereas the time to gamma irradiate cells to this dose is about 200 days. With this fact in mind, we observe that more damage is produced during the slow irradiation with simultaneous annealing than is left in the cells when they are rapidly damaged, then allowed to anneal for an equivalent length of time. Some of the Heliotek lithium cells used in the first part of the gamma experiment were removed after a fluence of 2×10^{14} e/cm^2 and placed in a 60°C annealing temperature with and without illumination. No recovery of these cells was observed; indeed, many cells degraded somewhat further. Thus it is unlikely that the gamma-irradiated C11A cells would show recovery if the radiation were removed. It is interesting to note that in both experimental situations, the lithium-doped solar cells demonstrate a power margin of about 5% over the N/P cell.

The final portion of the experiment consisted of a 4-MeV proton bombardment of two C11A cells to a fluence of 2.2×10^{11} p/cm^2. The cells were allowed to anneal in an oven at 60°C for 800 h, with I-V measurements made at intervals throughout. This data is summarized in Fig. 6, along with the electron-damage annealing data from Fig. 3. In both electron and proton Van de Graaff bombardment, the P/N lithium cells are degraded much more than the N/P cell. This difference between radiation hardness in P-type and N-type silicon solar cells has been established for many years (Refs. 5, 6). During the annealing, the lithium cell recovers to a higher power level than the N/P cell after 800 h at 60°C. Carter and Downing (Ref. 7) report like behavior in similar solar cells irradiated to 3×10^{15} 1-MeV e/cm^2 and annealed at 100°C. In their case, the lithium cell power recovered to the value for the N/P cell in 2 h. Since recovery rate depends on irradiation fluence and annealing temperature (Ref. 8), these two results are not necessarily conflicting. The recovery from proton damage follows a different behavior. There is no additional damage found during the first few hours after irradiation; recovery begins at once and proceeds more rapidly and to a higher degree than for electron damage. The percentage recovery at 800 h is 38% for electron damage and 68% for proton damage. The proton data shown for the N/P cell is a typical value extrapolated from a previous experiment (Ref. 6). No annealing data was available for the N/P cell.

IV. SUMMARY

Very conclusive evidence has been presented that a lithium-diffused crucible-grown silicon solar cell can be made with better efficiency than the flight-quality N/P 10 Ω-cm solar cell. When this lithium cell is exposed to a continuous radiation environment at 60°C (electron spectrum from gamma rays) it has a higher power output than the N/P cell after a fluence of 4×10^{14} e/cm^2 (equivalent 1 MeV).

A comparison of annealing of proton- and electron-damage in this lithium cell reveals a decidedly faster rate of recovery and higher level of recoverable power from the proton effects. This fact strongly suggests that the lithium cell in a low-rate continuous proton flux would have even greater superiority over the N/P cell than it has in the case of electrons. Therefore, the lithium cell shows a good potential for many space missions where the proton flux is a significant fraction of the radiation field to be encountered. This is the case for many specified earth-orbit trajectories as well as interplanetary missions.

The need for additional proton radiation studies is obvious, in view of the superior performance of the lithium cells. Such work will be carried out utilizing various other proton energies of interest.

REFERENCES

1. Wysocki, J. J., "Lithium-Doped Radiation Resistant Silicon Solar Cells," IEEE Trans. Nucl Sci., NS-13, p. 168, 1966.
2. Statler, R. L., "Real-Time Irradiation of Lithium-Doped Solar Cells," Proceedings of the Third Annual Conference on Effects of Lithium-Doping on Silicon Solar Cells, Technical Memorandum 33-467, pp. 81-84, April 1971.
3. Price, B. T., and Horton, C. C., Radiation Shielding, Pergamon Press, New York, pp. 24-30, 90-92, 1957.
4. Transient-Radiation Effects on Electronics Handbook, DASA 1420, edited by R. K. Thatcher, Battelle Memorial Institute, Columbus, Ohio, August 1967.
5. Statler, R. L., "Electron Bombardment Damage in Silicon Solar Cells," NRL Report 6091, Naval Research Laboratory, Washington, D. C., October 1964.
6. Statler, R. L., "Radiation Damage in Silicon Solar Cells From 4.6-MeV Proton Bombardment," NRL Report 6333, Naval Research Laboratory, Washington, D. C., November 1965.
7. Carter, J. R., and Downing, R. G., "Behavior of Lithium in Irradiated Solar Cells," Colloque International Sur Les Cellules Solaires, Toulouse, France, July 1970.
8. Berman, P. A., "Effects of Lithium Doping on the Behavior of Silicon and Silicon Solar Cells," Technical Report 32-1514, Jet Propulsion Laboratory, Pasadena, Calif., February 1971.

Table 1. Co^{60} Experiment sample matrix

Cell group	Type	Li diffusion parameters	Quantity of samples		
			Irradiated		Control
			Illuminated 30°C	Illuminated 60°C	Illuminated 60°C
H-2	Li P/N crucible	90 min, 425°C-60 min, 425°C	5	5	3
H-6	Li P/N crucible	90 min, 450°C-60 min, 450°C	5	5	3
H-5	Li P/N FZ	90 min, 350°C-60 min, 350°C	5	5	3
H-9	Li P/N FZ	90 min, 425°C-60 min, 425°C	5	5	3
C11A	Li P/N crucible	480 min, 325°C	2	2	1
Centralab	N/P crucible 10 Ω-cm	NA	5	5	3

All cells are illuminated with tungsten light and are individually loaded with a 10-Ω resistor developing a load voltage of 0.21 to 0.24 V. The cells are removed from the chambers for measuring the electrical performance at 25°C under a solar simulator.

Table 2. Photovoltaic parameters of experimental cells

Cell group	Type	I_{sc}, mA	P_{max}, mW	Efficiency, %
H-2	Li CG	64.5	27.8	9.9
H-6	Li CG	60.0	24.7	8.8
H-5	Li FZ	70.0	27.4	9.8
H-9	Li FZ	61.0	25.1	9.0
C11A	Li CG	71.6	31.0	11.1
N/P	10 Ω-cm	71.5	29.2	10.4

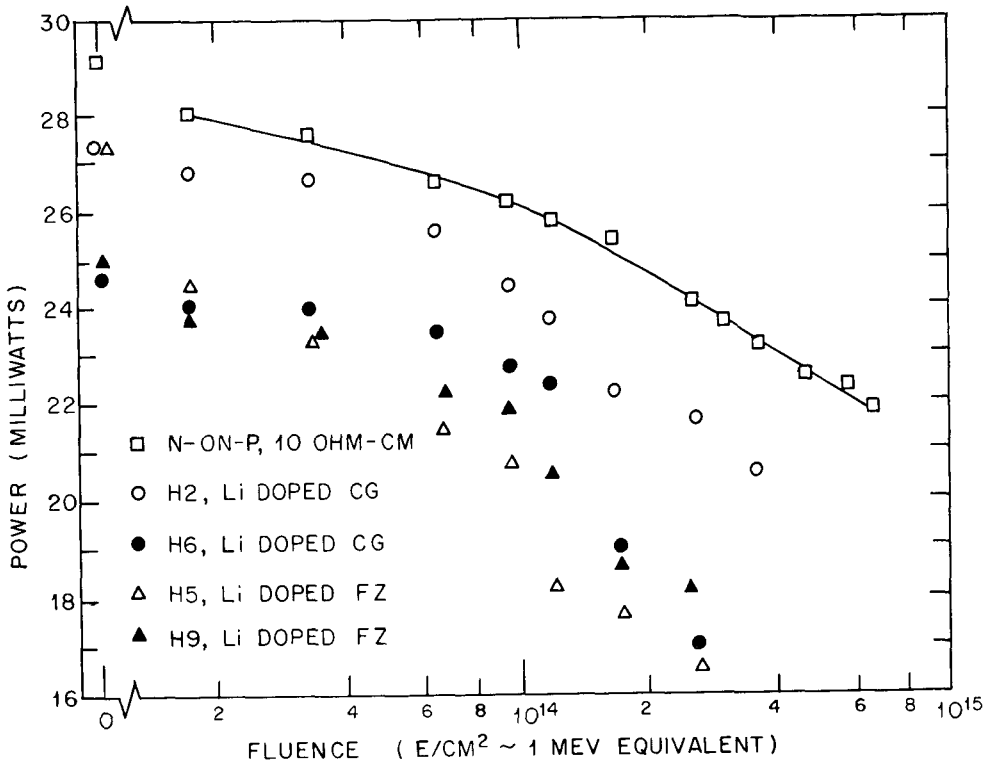

Fig. 1. Power loss in lithium-doped P-on-N solar cells compared to an N-on-P 10 Ω-cm solar cell irradiated by Co^{60} gamma flux at 60 °C

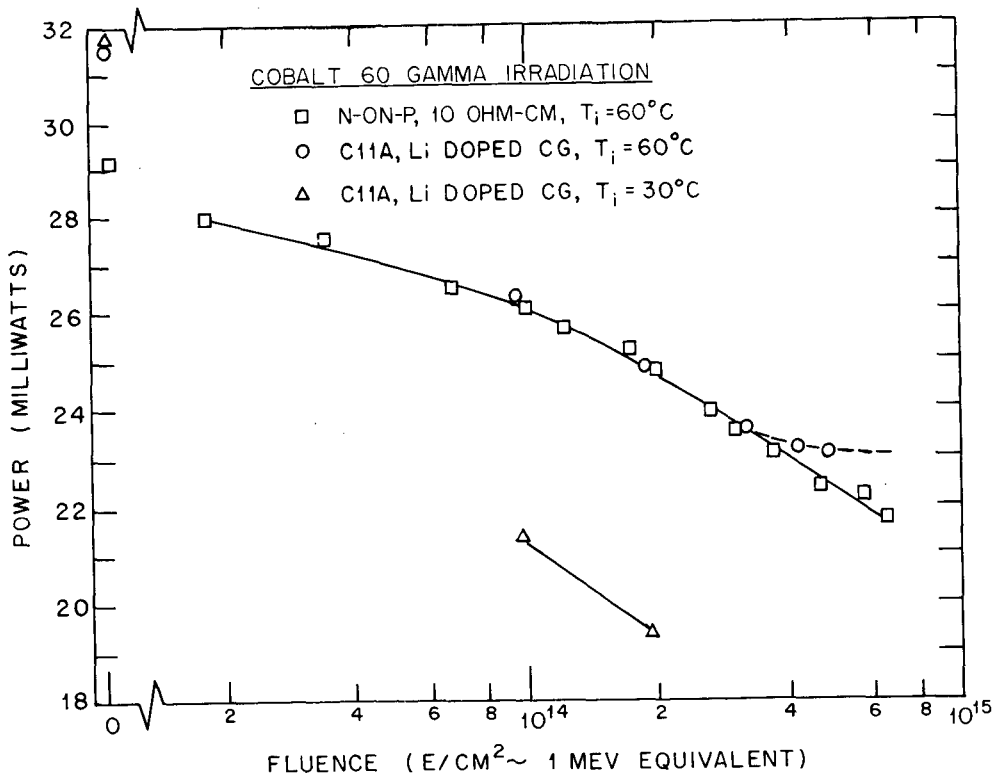

Fig. 2. Power loss in lithium-doped P-on-N solar cells and 10 Ω-cm N-on-P solar cells irradiated at 30 and 60 °C by Co^{60} gamma flux

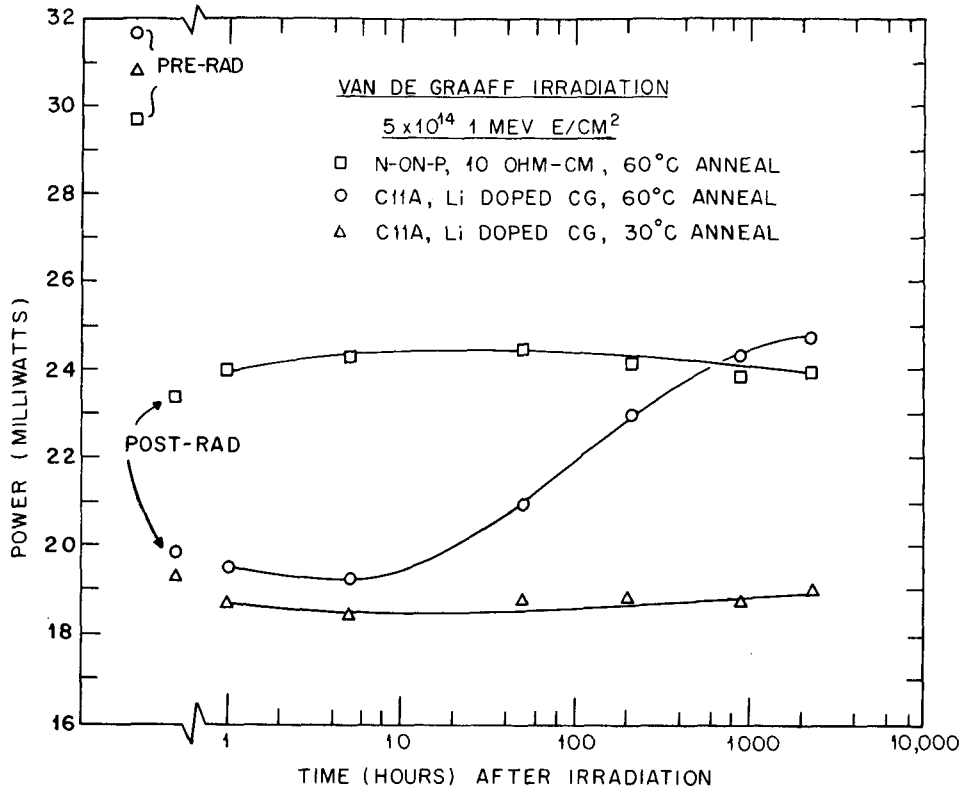

Fig. 3. Post-radiation annealing of power lost through 1-MeV electron irradiation in lithium-doped P-on-N solar cells and N-on-P 10 Ω-cm solar cells

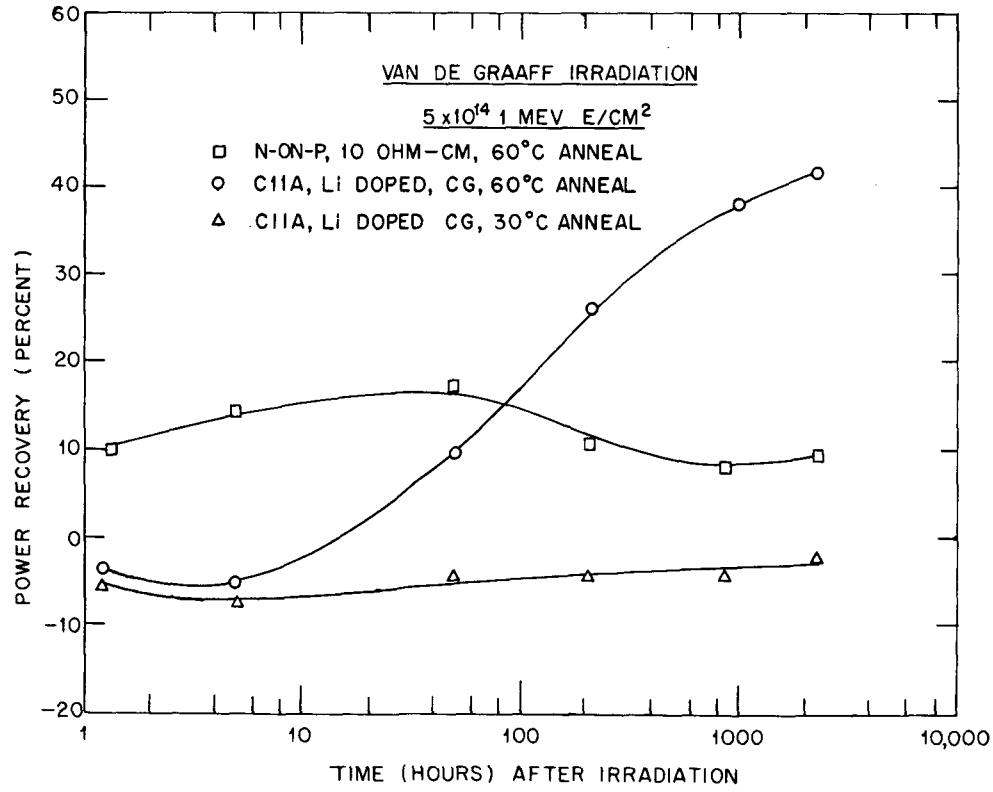

Fig. 4. Percentage of power recovered through post-radiation annealing in solar cells irradiated by 1-MeV electrons

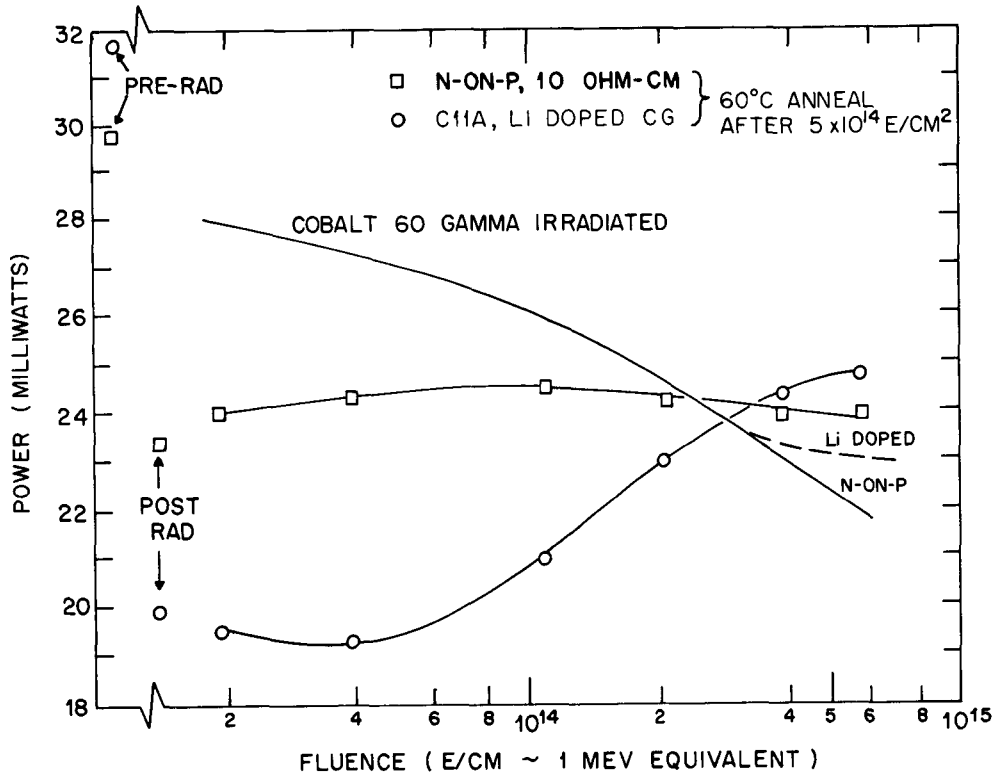

Fig. 5. Comparison of power recovery by annealing following a 1-MeV electron radiation, and the power lost in a real-time Co^{60} gamma radiation for lithium-doped P-on-N solar cells and N-on-P 10 Ω-cm solar cells. The annealing time extends to 2300 h, whereas the time to gamma irradiate to 5×10^{14} is 200 days

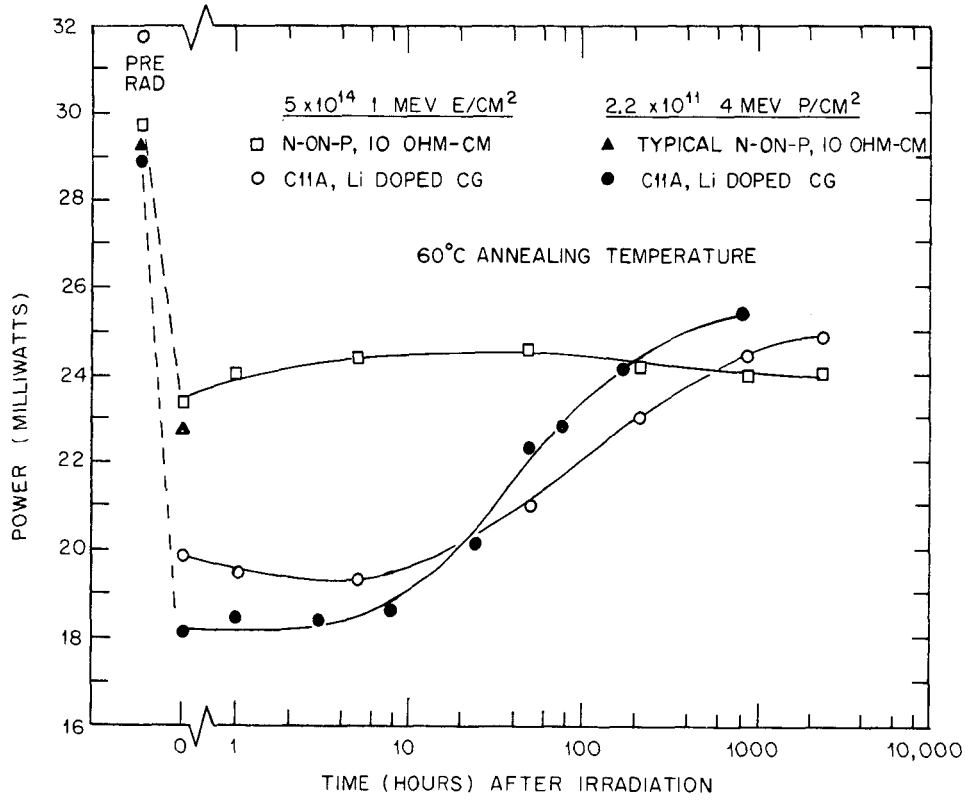

Fig. 6. Comparison of power recovery following a 1-MeV electron radiation and a 4-MeV proton radiation for lithium-doped P-on-N solar cells

LOW FLUX IRRADIATION OF LITHIUM-DOPED SOLAR CELLS

D. L. Reynard
Philco-Ford Corporation
Palo Alto, Calif.

LOW FLUX IRRADIATION OF LITHIUM-DOPED SOLAR CELLS

W. Krull
Lockheed-Georgia Company
Marietta, Ga.

The above papers were not available at time of publication.

Page intentionally left blank

N72-10065

RADIATION DAMAGE ANNEALING KINETICS

M. S. Dresselhaus
Department of Electrical Engineering,
Center for Materials Science and Engineering,
Massachusetts Institute of Technology, Cambridge, Mass.

I. INTRODUCTION

Our primary task is to understand how the presence of lithium assists in the recovery process of irradiated silicon solar cells. Although lithium is more effective in accelerating the recovery rate from neutron and proton bombardment, lithium has also proved useful in the recovery process from electron irradiation. Since neutron irradiation is not especially important for typical NASA space missions involving solar cells, and, furthermore, since it is relatively easy to provide protection against proton damage, our efforts have been mainly directed toward the study of recovery from electron irradiation.

II. BACKGROUND

To see how to tackle the problem let us start at the beginning and consider the solar cell as a p-n junction where for our case, the base region is the n-region, as is illustrated in Fig. 1. Light incident on this base region produces electron-hole pairs, with the holes capable of surmounting the potential barrier at the p-n junction and reaching the collecting electrode. We are accustomed to thinking of typical carrier diffusion lengths in crucible-grown quartz as $L \sim 1.2 \times 10^{-4}$ m so that collection can result from electron-hole pairs formed far from the junction. It is this long diffusion length that encourages us to think that the kinetics in bulk silicon might be the crucial factor in determining solar cell behavior. We shall now show why, on one hand, the consideration of bulk effects might by themselves lead to erroneous conclusions and, on the other hand, why it is nevertheless important to consider the kinetics of bulk silicon.

Any kinetics modeling based on a first-principles approach requires the observation of: (1) the defects that are formed during irradiation, (2) how these defects are annealed out in the recovery process, and (3) how these defects affect the diffusion length, minority carrier lifetime, carrier removal rate, etc. In dealing with this problem, we must classify the defects into various categories, and since each category tends to have a rather different cross section for minority carrier removal, different concentration ranges could significantly affect the minority carrier diffusion length.

In the first category we have the shallow donor and acceptor levels. These defects do not represent a major perturbation to the periodic potential characteristic of the host silicon lattice and consequently offer just a small cross-section for minority carrier removal. Typical concentrations of such defects have little effect on the minority carrier transport problem. On the other hand, the deep defect levels represent appreciable perturbations to the periodic potential and offer large cross-sections for a number of carrier removal processes. For such defects (e.g., gold), a concentration as low as $\sim 10^{19}/m^3$ (which is merely a trace concentration) can appreciably affect the minority carrier diffusion length (Ref. 1). Some deep defect levels act like traps and are important in minority carrier removal processes associated with transient phenomena. But in the steady state, once a trap is filled, it will remain filled.

On the other hand, a single recombination center can continuously remove minority carriers by combining them with majority carriers in either a radiative or a non-radiative recombination process. If the process is radiative, it is, in principle, observable by radiation recombination measurements; on the other hand, non-radiative processes are very difficult to study experimentally.

The types of defects most prevalent in the base region before irradiation are: (1) the shallow donor defects which are present in concentrations as large as $10^{21}/m^3$, and (2) deep impurity defects which are present in trace concentrations. Before irradiation, it is these trace quantities of deep impurity recombination centers which control the minority carrier diffusion length. The types of defects introduced by irradiation with electrons in the energy range of ~1 MeV are predominantly in the deep defect level classification, since the radiation-induced defects (such as the vacancy) represent a major perturbation to the periodic lattice of the host crystal. For fluences typical of the space environment of a synchronous orbit mission of 5-yr duration, the radiation-induced deep defect concentrations will generally exceed the native deep-defect concentrations. Upon annealing, the radiation-induced defects tend to form complexes which are also associated with deep level states but generally represent less of a perturbation to the periodic potential of the host crystal. In both the irradiation and recovery processes, majority carriers are removed when they become bound to the various defect centers. This carrier removal results in a degradation of the junction.

To consider the kinetics problem from first principles, we must identify the primary radiation-induced defects and determine their effect on the minority carrier lifetime. We must then identify the centers that result upon annealing of the primary centers and determine the effect of these new centers on the minority carrier lifetime. In this connection it would be desirable to carry out measurements of both the minority carrier lifetime and the energy level spectrum of the defects. Such joint measurements should be made on samples that are well-characterized with regard to both material parameters and radiation environment.

III. EXPERIMENTAL TECHNIQUES

A number of experimental techniques are available for the study of defect levels. The infrared absorption technique is one of the most useful techniques for establishing the energy levels associated with defects. We must remember here that there are many different species of defects present in the base region of an irradiated solar cell. Furthermore, each defect can be found in any one of a number of energy states as shown in Fig. 2. This figure shows the energy levels of the divacancy, one of the common defects occurring in irradiated float-zone silicon (Ref. 2). If the photon energy of the infrared radiation is just sufficient to excite electrons from the singly charged (-1) occupied level, 0.4 eV below the Fermi level, to the conduction band, there is an absorption of power from the incident beam. An experiment closely related to the infrared absorption is the photoconductivity experiment whereby we look at the current of the photoexcited electrons rather than at the power absorbed from the incident beam. These experiments are not actually equivalent insofar as the final state in the photoconductivity experiment must be a band state, while a bound state is an acceptable final state in the infrared absorption process. At any rate, both types of experiments have, in fact, been carried out under our program and some results of the photoconductivity studies by Corelli are shown in Fig. 3. In interpreting such curves, the maxima in the photocurrent are identified with the resonant absorption from or to a defect level. These measurements by themselves do not identify the nature of the defect centers; to make such identifications it is necessary to study concentration dependences, temperature dependences, effects of stress or possibly magnetic fields. To study the effect of these centers on solar cell characteristics, measurements of the minority carrier lifetimes should be made on the same samples and correlated with the optical data.

There are, however, some more fundamental difficulties with these data: in order to observe these defects optically, it was necessary to irradiate the samples with fluences which create defect densities far in excess of the lithium concentration. These fluences are larger than are of practical interest for space missions. Since the benefits of lithium donors are realized primarily when the lithium concentration exceeds the damage center concentration (Ref. 3), these experiments are only of limited utility for our kinetic modeling program. Furthermore, this difficulty would not be resolved by increasing the lithium concentration, since the lithium concentrations used in this work were already as high as might be of interest to possible solar cell applications. In order for optical techniques to be useful to us, the sensitivity of the technique must be increased by perhaps two orders of magnitude. To accomplish this, a modulation technique could be exploited to advantage.

To study defect centers in bulk material some rather elegant recombination luminescence studies have been carried out by the University of Illinois group. In recombination luminescence, one measures the spectrum of the radiation emitted when, for example, an electron associated with a particular defect level combines with trapped hole or with hole in the valence band. An example of such a spectrum is shown in Fig. 4. Because recombination luminescence in silicon is not an efficient process, these experiments have also been plagued with the same difficulties as the optical experiments insofar as it has been necessary to employ high irradiation fluences in order to observe recombination luminescence signals. Recently, increased sensitivity has been achieved in silicon through use of a laser source to achieve the initial excitation (Ref. 4). Perhaps such techniques could also be employed in the luminescence recombination work in our program. In the luminescence studies made under our program, considerable success has been achieved in the identification of the nature of the observed defects. For example, the structure at 0.97 eV is identified with the divacancy 0.19 eV below the conduction band and the structure at 0.79 eV is identified with a two-oxygen defect complex. To make such studies valuable to a kinetic modeling effort, it will be necessary to correlate the luminescence studies with minority carrier lifetime measurements in order to understand the role of such defects in the solar cell degradation upon irradiation and subsequent recovery.

The difficulty with the bulk measurements made under conditions of intense irradiation can also be understood in terms of Fig. 5, where the dependence of the minority carrier diffusion length L is plotted as a function of fluence for 1-MeV electron irradiation on standard n/p solar cells, made from crucible grown silicon (Ref. 5). While L is $\sim 1.20 \times 10^{-4}$ m for the pre-irradiated cells, we see a rapid decrease in L with increasing fluence so that for a fluence $\sim 10^{20}/m^2$ the diffusion length is already below 10^{-5} m. This figure tells us that if we are considering fluences in excess of $\sim 10^{20}/m^2$, the solar cell current generation in the base region will become less important compared with the behavior in the vicinity of the junction. Since the impurity concentrations and defect densities tend to be rather different near the junction as compared with the bulk behavior, the kind of data on bulk silicon that is of primary interest for kinetic modeling is that for low fluence levels corresponding to typical space environments. On the other hand, we should not conclude from this figure that measurements on bulk silicon are irrelevant. We shall soon see why it is important to consider both the data on the devices and data on the bulk material.

Another powerful technique that has been applied to the study of radiation-induced defects and their subsequent annealing in the presence of lithium is the electron spin resonance (ESR) technique. This technique is applicable to the study of defects in a singly charged state; for these states, the ESR technique provides a microscopic and detailed probe. With this technique, it has been possible to identify resonances associated with the oxygen-vacancy, the divacancy, the phosphorus-vacancy, the lithium-oxygen, as well as many other centers. The interpretation of these experiments indicates that for oxygen-lean silicon, the presence of lithium favors the formation of lithium-vacancy complexes rather than phosphorus-vacancy complexes and that in the annealing process, lithium can help to neutralize phosphorus in the phorphorus-vacancy complexes that happen to be present (Ref. 6). For the oxygen-rich silicon, the presence of lithium tends to favor formation of LiOV centers rather than the OV center itself. The fluences necessary for observation of ESR signals are still rather large (like 10^{20} to 10^{21} electrons/m^2) but somewhat smaller than are required for the optical measurements.

We have, however, encountered several difficulties in utilizing some of the ESR data: (1) The measurements employ 30-MeV rather than 1-MeV electrons, the lower energy matching more closely other work in the program as well as the environmental conditions in space. Since the production and annealing rates for a given defect are strongly energy dependent, it would be desirable to have ESR data on similar samples as a function of electron irradiation energy. (2) The lithium concentration tends to be higher than the range of interest for solar cell applications and yet the lithium concentration is often less than the density of irradiation defects. Thus, the parameters do not really fall into the desired range for solar cell modeling. (3) Not all centers can be studied by the ESR method because they have the wrong charge state or are unoccupied.

From the point of view of cell modeling, our most useful data have come from less microscopic and perhaps less elegant techniques, but nevertheless capable of yielding information on the defect production and annealing in the parameter range of interest to solar cells and the type of space environment where the cells will be utilized. Such techniques are the bulk Hall and resistivity measurements, minority carrier lifetimes in bulk silicon and in solar cell devices, and capacitance measurements. We will have more to say about relating such data to the kinetic modeling later. From the temperature dependence of the Hall effect and from analysis of the temperature dependence of the minority carrier lifetime data, it is also possible to deduce defect levels. Such techniques have been widely exploited for this purpose in our program by the RCA, TRW, and Gulf-Atomic groups. If we now consider all the defect levels that have been reported in the literature to date we get the typical representation shown in Fig. 6. This diagram shows that a large number of defects have been identified and that a given defect can exist in various energy states. Not only is the number of defect levels overwhelmingly large, but the quantity of reliable and necessary information on each level is discouragingly small. From this situation, we must conclude that it is not feasible at this time to construct a first-principles kinetic model for the annealing of electron radiation damage in lithium-diffused silicon solar cells.

IV. KINETICS MODELING

We have, therefore, looked toward a phenomenological approach whereby a parametric model is developed to predict lifetime damage constants and carrier removal rates relevant to the operation of the solar cell. In dealing with the kinetics problem, we divide it into two parts: (1) a determination of the minority carrier lifetime as a function of the material and environmental parameters, and (2) the deduction of solar cell performance from the minority carrier lifetime, and from doping profiles in the n- and p-material and of the diffused lithium in the solar cell. The second part of the problem has been dealt with by the Exotech and Gulf-Atomic groups. For this reason, we have mainly concerned ourselves with the determination of minority carrier lifetimes. (We have recently learned that the Gulf-Atomic group has also been successful in modeling minority carrier lifetimes under a variety of material and environmental parameters).

Almost all lifetime data is analyzed in terms of the Shockley-Read-Hall theory for recombination processes. According to this theory, the lifetime for a single level defect is given by the expression,

$$\tau = \tau_{p_0}\left(\frac{n_0 + n_1 + \Delta n}{n_0 + p_0 + \Delta n}\right) + \tau_{n_0}\left(\frac{p_0 + p_1 + \Delta n}{n_0 + p_0 + \Delta n}\right)$$

where the lifetimes in heavily p-type and n-type material are given by

$$\tau_{p_0} = \frac{1}{N_R v_{th}(T)\sigma_p(T)}$$

and

$$\tau_{n_0} = \frac{1}{N_R v_{th}(T) \sigma_n(T)}$$

In these expressions

N_R = recombination center density

v_{th} = thermal velocity

$\sigma_{p,n}$ = cross sections for recombination of holes or electrons

n_0, p_0 = thermal equilibrium carrier concentration

$\Delta n = \Delta p$ = concentration of excess carriers

T = temperature

$$n_1 = N_c e^{[(E_R - E_C)/kT]}$$

$$p_1 = N_v e^{[(E_V - E_R)/kT]}$$

where N_c and N_v are integrals over the density of states for the conduction and valence bands, respectively, and

$$N_c = \int \rho_c(E)\, e^{[-(E-E_C)/kT dE]}$$

$$N_v = \int \rho_v(E)\, e^{[-(E_V-E)/kT dE]}$$

In order to interpret lifetime versus temperature data, an explicit temperature dependence of the cross sections and of the thermal velocity v_{th} must be assumed. The temperature dependence of σ is complicated but has been treated theoretically (Ref. 8). Although there exist divergent opinions on the temperature dependence of σ, there is general agreement that the temperature dependence of v_{th} goes as $T^{1/2}$. Most interpretations of lifetime data consider $\sigma(T) \sim T^{-1/2}$ so that σ_{p_0} and σ_{n_0} are temperature independent. If temperature dependences for v_{th} and $\sigma(T)$ are introduced, then it is possible to fit the experimental lifetime measurements as a function of temperature and thereby to deduce the energy of the defect level E_R.

We are at present trying to understand how to use the Shockley-Hall-Read theory to find this effective defect level in an unambiguous way. It is our hope that the minority carrier lifetime is controlled by one or two dominant defects, e.g., the divacancy in oxygen-lean silicon and the oxygen-vacancy complex in oxygen-rich silicon. If this is the case, then we might expect the effective defect level E_R to be correlated with an important defect level that has been identified by more direct measurements on bulk material, e.g., optical, luminescence, ESR, temperature dependence of the Hall effect, etc. In this context, it would be most desirable to make measurements on the same samples by different techniques.

The application of the Shockley-Read-Hall approach to the minority carrier lifetime problem is itself beset with complications. To illustrate these complications, Fig. 7 displays the various energy levels identified with radiation defects produced by 1-MeV electrons in n-type silicon. In all cases, the levels were obtained from Shockley-Read-Hall analysis of the temperature dependence of lifetime data. The two most important reasons for the variety of effective levels in this diagram are: (1) differences in material parameters in the n-type silicon, and (2) differences in the use of the Shockley-Read-Hall theory. Differences in the material parameters are difficult to handle because it has not been customary to give a complete characterization in the literature of the material and environmental parameters. This lack of information has made it exceedingly difficult to compare the work of different groups. This lack of sample characterization may also be responsible for the tendency on the part of some workers to ignore past work and to report their findings with little or no attempt to correlate their results with previous measurements. Because of the collaborative aspect of the JPL program, we have a unique opportunity to correlate lifetime measurements in a more significant way. Differences in the use of the Shockley-Read-Hall theory arise largely through differences in the assumptions for the temperature dependence of the cross sections. As can be seen in Fig. 7, the upper energy level is relatively less sensitive than is the lower level to these two classes of differences.

As a first stab at the annealing problem, we have decided to use the Shockley-Read-Hall approach and to consider the recombination center density N_R to be time dependent. The determination of N_R then is governed by a rate equation, such as has been developed by Fang and others (Ref. 9).

Although we have given some thought to radiation annealing in the presence of lithium, we are still developing techniques for handling the kinetics problem for non-lithium-diffused irradiated silicon. We are trying to understand such questions as the presence of multiple competing defects and defects with more than one important recombination level. The introduction of lithium donors suggests a need for such a generalization to multilevel Shockley-Read-Hall models.

Because of the complexity of the annealing process itself, it will be necessary to develop some physical insight into the problem in order to know what type of approximations can be made. The first problematical fact about lithium is its rather low solubility in silicon: $\sim 10^{20}/m^3$. Yet, it is customary for us to unconcernedly characterize our materials with Li concentrations as high as $10^{23}/m^3$. Electron microscopy studies such as those shown in Fig. 8 show a precipitation of lithium metal in oxygen-lean silicon having nominally a $10^{23}/m^3$ lithium concentration. Substantive evidence for such precipitation comes from the identification of body-centered cubic electron diffraction patterns with the lattice constant of metallic lithium. We have not yet understood how this property can be incorporated into the kinetic model.

A second property that must be considered is the fact that the lithium profile in a solar cell

exhibits a linear concentration gradient across the junction, as well as concentration gradients far into the base region, as is seen in Fig. 9. Since the minority carrier diffusion lengths for irradiated material become comparable to a few junction widths, this lithium gradient is important in analysis of lifetime data. The presence of lithium gradients introduces electric fields. Since the minority carrier drift to the collecting electrodes is assisted by these electric fields, the interpretation of the minority carrier lifetime measurement in solar cell devices becomes more complicated. The effective minority carrier diffusion lengths now become an average over the lithium concentration profile and thus we cannot now write simply $L = \sqrt{D\tau}$.

One promising technique for studying the minority carrier diffusion lengths in just such a situation is the spectral response curve. For incident light with photon energies in excess of the indirect gap, absorption will occur. As the photon energy is increased above the band gap, the absorption will increase and the effective length for the penetration of the light will decrease, as can be seen in Fig. 10, showing the frequency dependence of the optical absorption coefficient in silicon. The presence of impurities and radiation defects has no important effect on such a curve, which is characteristic of the valence and conduction band states. Therefore, we can use the wavelength of the light to control the dimensions of the active region of the solar cell, i.e., minority carrier generation will proceed only up to the penetration depth of the light.

In the spectral response curve itself shown in Fig. 11, we measure the short-circuit current as a function of the wavelength (or photon energy) of the light. In the long wavelength region, where the absorption coefficient is small and the light penetrates far into the base of the cell, the spectral response is dominated by the base region minority carrier lifetime or diffusion length. At shorter wavelengths where the optical penetration depth is somewhat larger than the junction depth, the effect of concentration gradients near the junction become important. At yet shorter wavelengths where the optical penetration depth is confined to the diffused layer, the spectral response will be sensitive to the minority carrier lifetime in the diffused layer and to the front surface recombination velocity. Our main interest in this work is to study the spectral response curves for optical penetration depths traversing the base region of the cell. It should be noted that the spectral response curve rises for photon energies above the indirect band gap even though the optical penetration length decreases; this is because the optical absorption is increasing with increasing photon energy. For sufficiently high photon energies the effect of the decreased penetration depth begins to dominate over the effect of increasing optical absorption.

Spectral response studies have been made in non-lithium solar cells covering a variety of environmental parameters, though very little has so far been done on lithium-diffused solar cells. The spectral response of a solar cell with uniform doping in the base region and in the front diffused layer can be analyzed relatively simply. In addition, exponential carrier concentration gradients and their resulting electric fields can also be included in the analysis.

The spectral response method is complementary to the short-circuit current determination of the damage constant where one measures some effective diffusion length characteristic of the entire base region of the cell. On the other hand, in the analysis of spectral response measurements it will be necessary to include the effect of: (1) lithium concentration gradients, and (2) the electric field resulting from such gradients. This analysis will involve a fairly complicated computer program. We aim to correlate these spectral response measurements with diffusion length measurements made on the same samples.

A spectral response apparatus has been built and tests are being made on a preliminary batch of cells. Here we measure the wavelength dependence of the collection efficiency, $Q = I_{sc}/qN_{ph}$ where I_{sc} is the short-circuit current produced by the incident photon flux N_{ph} and q is the electronic charge.

A block diagram of the appartus is shown in Fig. 12. Here the monochromator is a double-pass Perkin-Elmer prism monochromator with a resolution of better than 1 cm $\times 10^{-8}$, and the light source is a flat filament tungsten lamp. The output of the monochromator is chopped and imaged uniformly over the active area of the cell by a toroidal section mirror. In these measurements, the cell is loaded to short-circuit conditions. In the first mode of operation, the measurements will be made first using only the illumination of the monochromator. In the second mode of operation, spectral response will be probed by the low intensity light from the monochromator while the cell is simultaneously illuminated by the solar simulator (a powerful tungsten source). The simulated sunlight will allow observation of injection level dependence in the recombination mechanisms. In the second mode of operation, high power output will be obtained from the solar cell and, consequently only a small load will be needed to keep the voltage low. The ac signal from the appropriately loaded cell is amplified, synchronously rectified, and recorded.

As a first step in our experimental program, we will develop a reliable technique for spectral response measurements using non-irradiated (i.e., undamaged) standard n/p solar cells.

The next step will involve the extensions of the spectral response measurements to non-irradiated lithium solar cells. In this work, we will determine values of the same set of characteristic parameters for the lithium-doped cells as for the non-lithium-doped cells.

As a third step, we will irradiate both standard cells and the lithium diffused cells with 1-MeV electrons and measure the spectral response at several fluence levels. This procedure is important for the identification of the particular parameters which are being degraded by the irradiation and in ultimately determining the damage constants for minority carrier lifetime degradation. If the kinetic modeling of the lifetime damage mechanism is to be successful, it is imperative that the cell degradation be attributed to the

appropriate degraded parameters. If, for example, the electric field changes in a lithium-doped cell due to radiation damage, then there will be consequent changes in the short-circuit current which of course must not be attributed to changes in lifetime. Such misinterpretation of the cell degradation could lead to a seriously distorted model of the damage mechanism. It is this kind of separation of the radiation damage effects which makes the spectral response method a valuable tool for studying the complexities of the annealing kinetics in lithium-diffused solar cells.

REFERENCES

1. Tkachev, V. D., Plotnikov, A. F., and Vavilov, V. S., Fiz. Tverd. Tela, Vol. 5, p. 3188, 1963; [Soviet Phys. -Solid State, Vol. 5, p. 2333, 1964].

2. Cheng, L. J., et al., Phys. Rev., Vol. 152, p. 761, 1966.

3. Carter, J. R., Jr., J. Phys. Chem. Solids, Vol. 31, p. 2405, 1970.

4. Cherlow, J., (private communication).

5. Rosenzweig, W., Bell System Tech. J., Vol. 42, p. 1573, 1962.

6. Passenheim, B. C., Naber, J. A., and Berger, R. A., "Production and Annealing of Defects in Lithium-Diffused Silicon After Irradiation With 30-MeV Electrons and Neutrons at 300°K," paper presented at the Eighth IEEE Photovoltaic Specialists Conference, Seattle, Wash., August 1970.

7. Shockley, W., and Read, W. T., Jr., Phys. Rev., Vol. 87, p. 835, 1952.

8. Lax, M., Phys. Rev., Vol. 119, p. 1502, 1960

9. Fang, P. H., J. Appl. Phys., Vol. 41, p. 3453, 1970.

10. Corelli, J. C., Final Report on JPL Contract 952456, Rensselaer Polytechnic Institute, Troy, N. Y., October 1970.

11. Compton, W. D., Semiannual Progress Report on JPL Contract 952383, University of Illinois, July 1970.

12. Glaenzer, R. H., and Wolf, C. J., J. App. Phys., Vol. 36, p. 2197, 1965.

13. Baicker, J. A., Phys. Rev., Vol. 129, p. 1174, 1963.

14. Wertheim, G. K., Phys. Rev., Vol. 10, p. 1086, 1958.

15. Carter, J. R., Downing, R. G., and Flicker, H., TRW final Technical Report 4161-6023-R000, May 25, 1966.

16. Sargent, G. A., Final Report on JPL Contract 952561, University of Kentucky, July 1970.

17. Iles, P., Proceedings of the Third Annual Conference on Effects of Lithium Doping on Silicon Cells, Technical Memorandum 33-467, pp. 3-6, Jet Propulsion Laboratory, Pasadena, Calif., April 1, 1971.

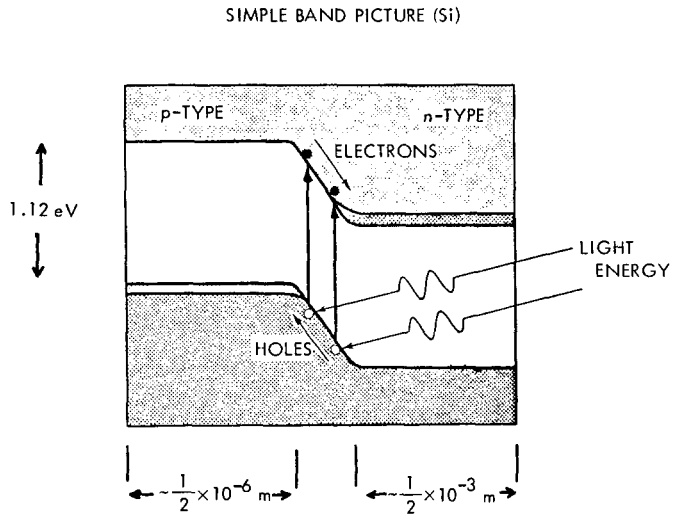

Fig. 1. The P/N junction as a photovoltaic device in silicon

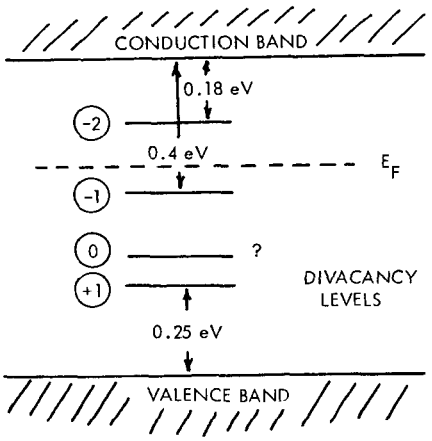

Fig. 2. Energy levels of the divacancy defect in silicon

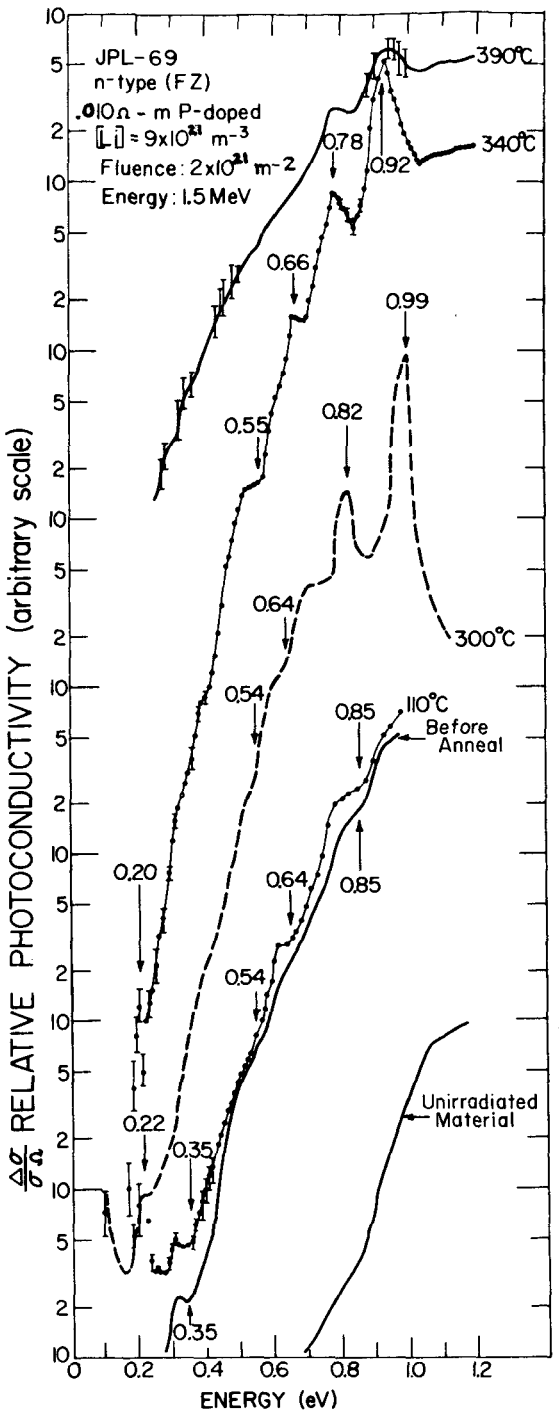

Fig. 3. Relative photoconductivity as a function of photon energy (Ref. 10).

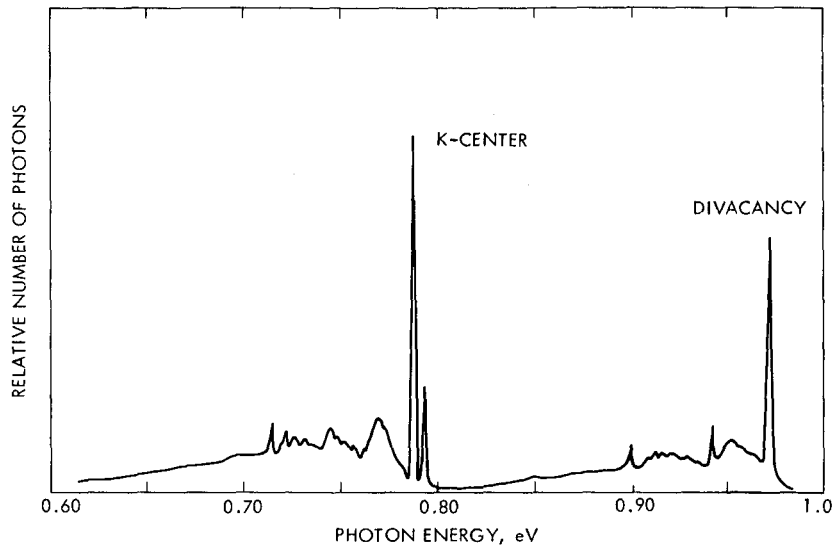

Fig. 4. Luminescence spectrum of n-type pulled silicon, phosphorous doped, irradiated with 10^{21} electrons/m^2 at 2.5 MeV. Here the indirect energy gap is 1.164 eV (Ref. 11)

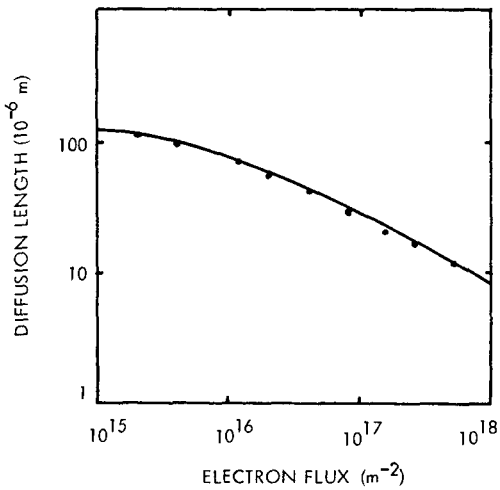

Fig. 5. Minority carrier diffusion length as a function of fluence for 1-MeV electron irradiation on standard N/P solar cells made from crucible-grown silicon (Ref. 5)

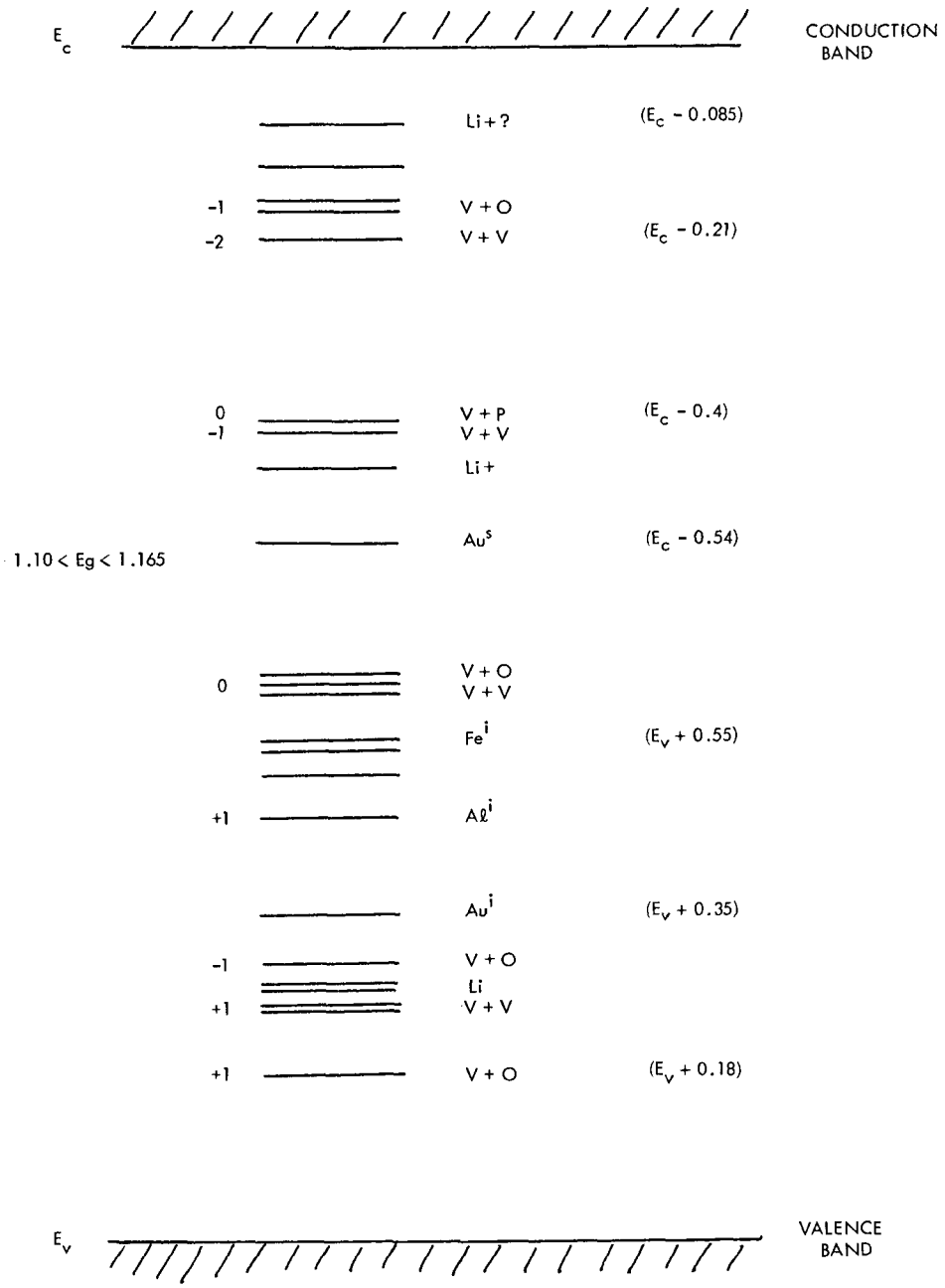

Fig. 6. Energy levels of various defect levels in silicon given in units of electron volts

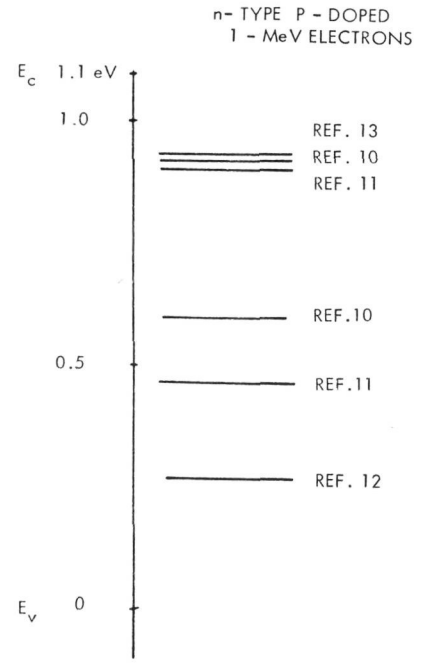

Fig. 7. Energy levels of radiation defects produced by 1-MeV electrons in n-type silicon as obtained from analysis of Shockley-Read-Hall lifetime data

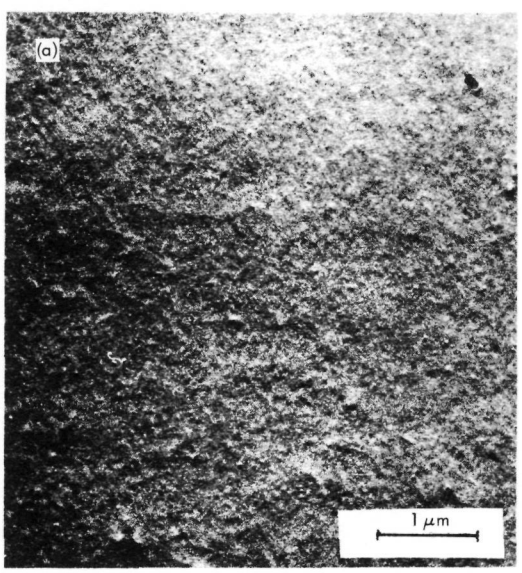

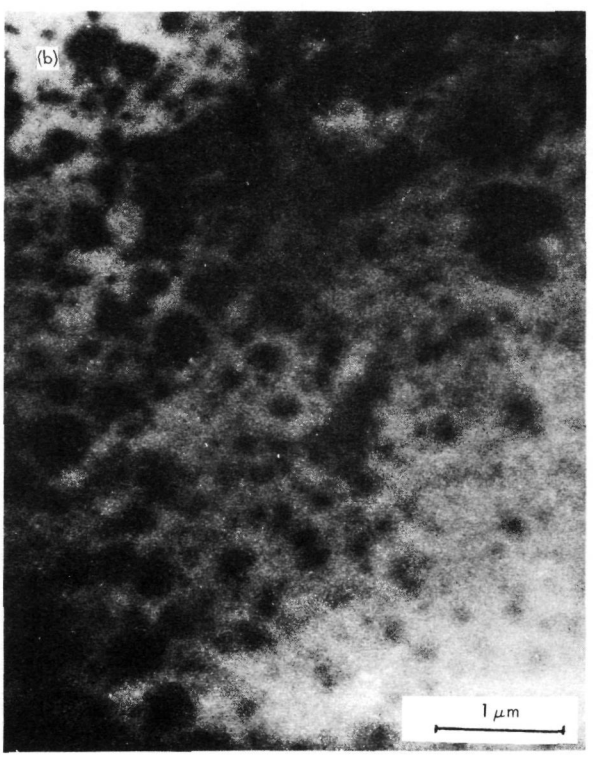

Fig. 8. Electron microscopy studies of unirradiated float-zone silicon: (a) no lithium, (b) with 10^{23} lithium atoms/m^3, and showing lithium precipitation (Ref. 16)

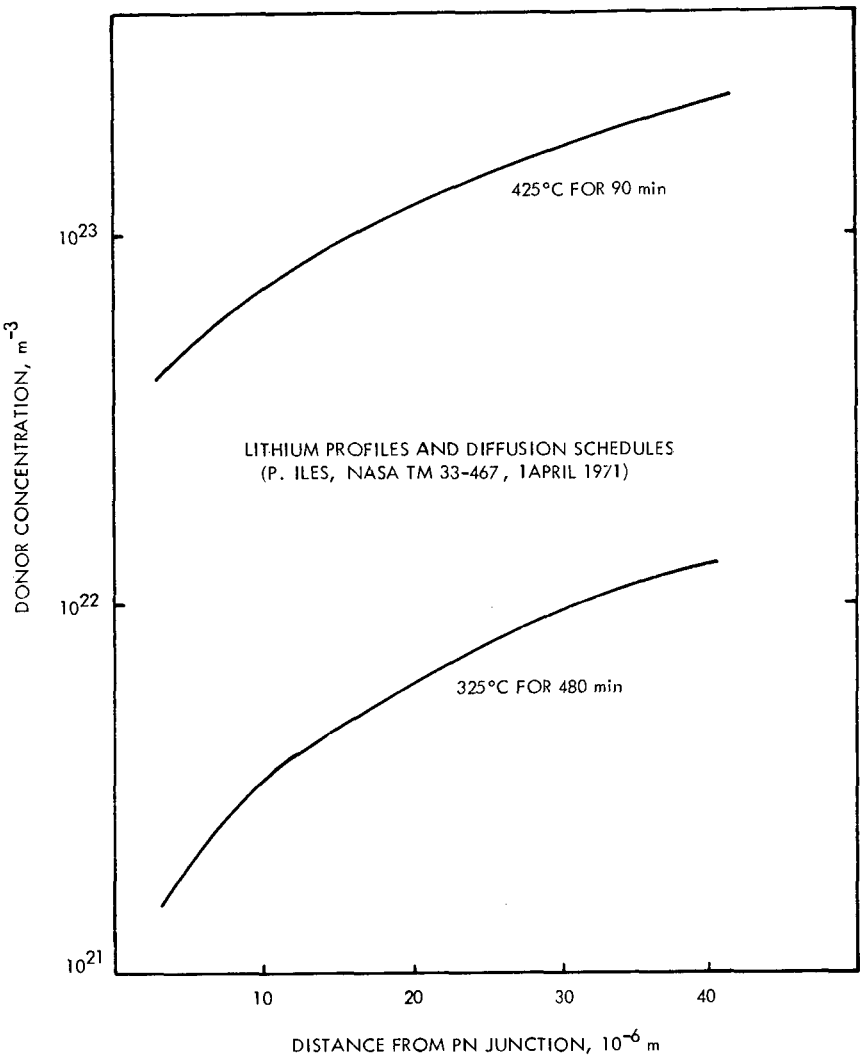

Fig. 9. Lithium profiles and diffusion schedules (Ref. 17)

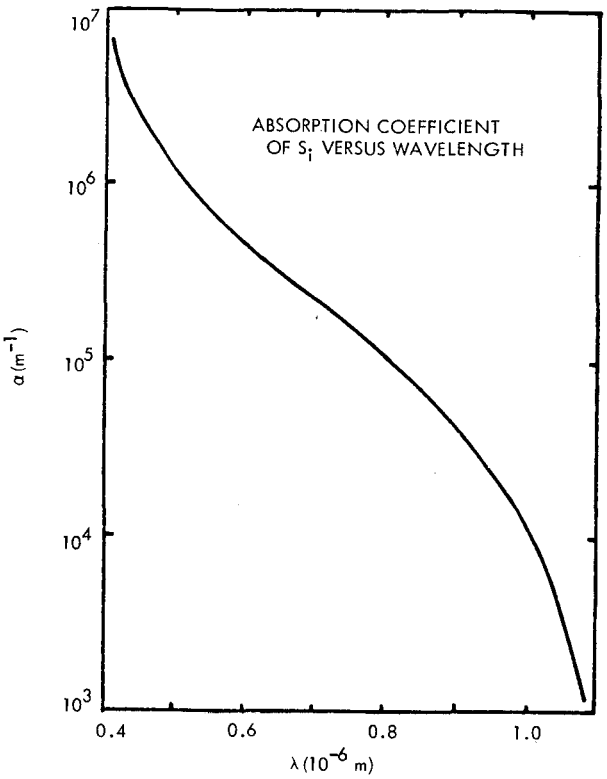

Fig. 10. Optical absorption coefficient of silicon versus wavelength

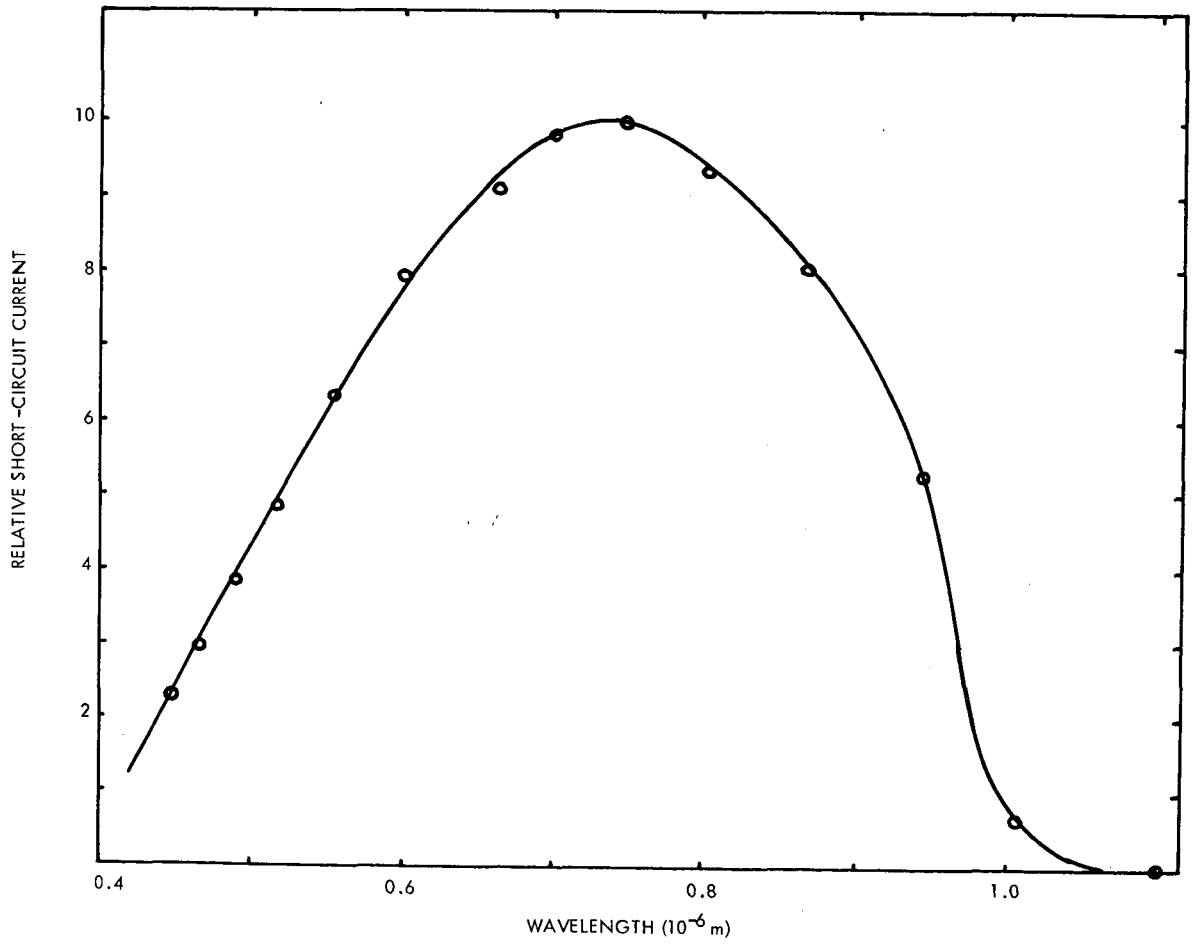

Fig. 11. A spectral response curve for a silicon solar cell exposed to a tungsten light source

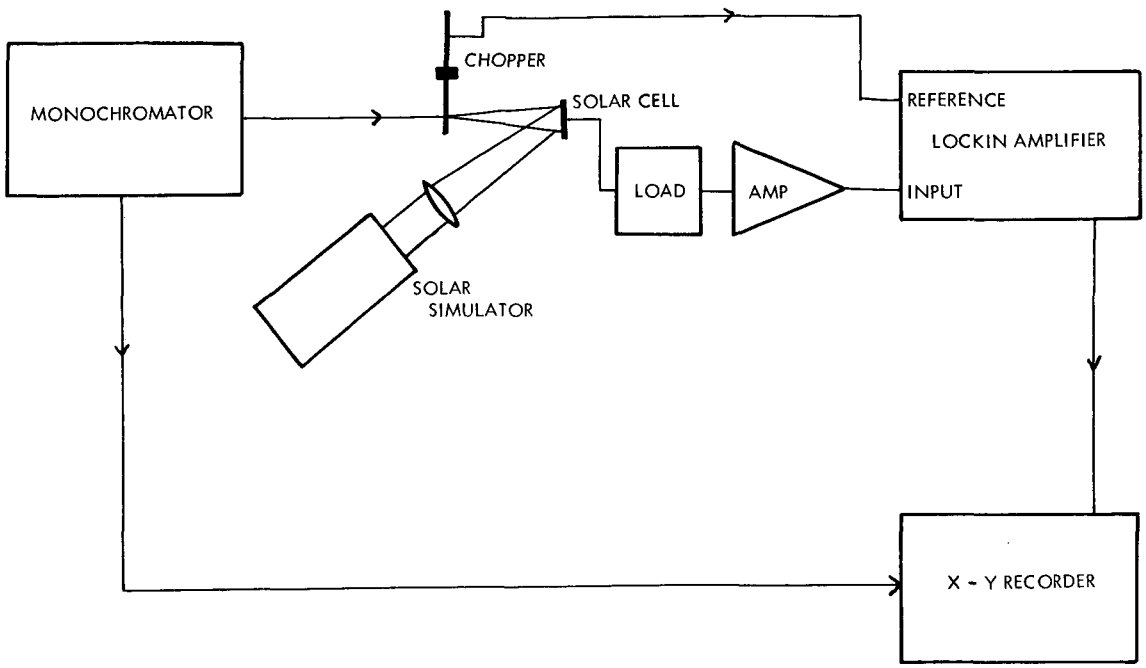

Fig. 12. Block diagram for spectral response measurements